universität wien

MASTERARBEIT / MASTER'S THESIS

Titel der Masterarbeit / Title of the Master's Thesis

„Synthesis of fatty acid-amino acid conjugates (FACs) and investigation of their impacts on plants“

verfasst von / submitted by

Joanna Karolina Matek, BSc

angestrebter akademischer Grad / in partial fulfilment of the requirements for the degree of

Master of Science (MSc)

Wien, 2022 / Vienna 2022

Studienkennzahl lt. Studienblatt / degree programme code as it appears on the student record sheet:	UA 066 862
Studienrichtung lt. Studienblatt / degree programme as it appears on the student record sheet:	Masterstudium Chemie
Betreut von / Supervisor:	Univ.-Prof. Dipl.-Chem. Dr. Lothar Brecker, Privatdoz.

"[..] we have just begun to eavesdrop on what are likely to be very complex insect–plant dialogs. The opportunities to contribute to our mechanistic and ecological understanding of these communications are immense, but will require the concerted and combined efforts of chemists, entomologists, molecular biologists, plant biologists and microbiologists, in order to fully appreciate the biological complexity found in these plant–herbivore interactions."

Gary Felton & James Tumlinson (2008)

Abstract

The work presented herein describes the investigation of the impact of diverse fatty acid-amino acid conjugates (FACs) on plant biosynthetic processes to draw the conclusions about the plant defence strategies against herbivores.

A plethora of external factors have caused the plants as sessile organisms to develop different survival strategies. In general, a broad spectrum of plant defensive tactics encompasses particularly mechanical and chemical protection. Besides the trichomes and thorns, a vast number of complex chemical structures such as secondary metabolites also take part in the plant-predator dialog. It is worth noting at this stage that in order to activate the cascade of biochemical processes, the plant first needs to be physically injured, followed by chemical elicitor propagation at the plant-herbivore interface. One of the prominent triggers of plant defensive strategies is the FAC volicitin. Since the biochemical efficacy of this compound is beyond question, as it has already been investigated in previous studies, other volicitin-like compounds were synthesized in the present work and their potential impact in inducing biosynthetic pathways was investigated.

To examine the alterations of specialized metabolite pattern of *Vinca minor* plants and *Populus* hybrids (*Populus alba* × *Populus tremula*), eleven FACs not strongly differing from each other in their chemical structure were synthesized: *N*-(10-hydroxyundecanoyl)-L-glutamine (**1d**), (S)-*N*-α-undec-10-enoyl-L-glutamine (**2b**), *N*-((9Z)-octadec-9-enoyl)-L-glutamine (**3b**), (S)-*N*-α-octadecanoyl-L-glutamine (**4b**), *N*-(heptanoyl)-L-glutamine (**5c**), *N*-(pent-2-enoyl)-L-glutamine (**6c**), *N*-(hept-2-enoyl)-L-glutamine (**7c**), *N*-(9-(1´´-oxooctadecanoyl)-octadec-10-enoyl)-L-glutamine (**8c**), *N*-(10-(1´´-oxooctadecanoyl)-octadec-8-enoyl)-L-glutamine (**8d**), *N*-(12-oxononacosa-9-enoyl)-L-glutamine (**9b**), (S)-*N*-α-octanoyl-L-glutamine (**10b**) and *N*-(12-hydroxynonadec-9-enoyl)-L-glutamine (**11e**). In the succeeding experiment, FACs-associated molecular patterns addressing monoterpenoid indole alkaloid (MIA) vincamine in *V. minor* and two salicinoids tremulacin and tremuloidin in *Populus* hybrids were examined in more detail with the aid of high-pressure liquid-solid chromatography (HPLC) method.

Treatment with *N*-(pent-2-enoyl)-L-glutamine (**6c**) extensively altered the content of vincamine in *V. minor* plants. A twofold increase in vincamine levels in contrast to other FACs or even caterpillars demonstratively confirmed the postulated induction of MIAs pathway in periwinkle. Moreover, the investigation of temporal alterations in the vincamine concentration after the application of the **6c** visualized immediate changes in MIA level in *V. minor* 24 h after application of the FAC candidate, whereas on the sixth day the lowest vincamine concentration was monitored. Consequently, less and less vincamine was detected in the course of time. Therefore, it was suspected that the available MIA was converted into other compounds, might even be alkaloids.

In the current work observations could also be made concerning the biosynthesis of two significant salicinoids tremulacin and tremuloidin after application of FACs *N*-(10-hydroxyundecanoyl)-L-glutamine (**1d**), *N*-(heptanoyl)-L-glutamine (**5c**), *N*-(9-(1´´-oxooctadecanoyl)-octadec-10-enoyl)-L-

glutamine (**8c**) and *N*-(10-(1′′-oxooctadecanoyl)-octadec-8-enoyl)-L-glutamine (**8d**) as well as (S)-*N*-α-octanoyl-L-glutamine (**10b**) to the *Populus alba* × *Populus tremula* hybrids. *Populus tremula*-like individuals indicated higher values of relative tremulacin and tremuloidin concentrations than *Populus alba*-like species, which confirmed causal relationship between the genomic ancestry of the poplars and concentrations of the two phenyl glycosides.

In a nutshell, the current work has revealed new perspectives for FACs synthesis research, which is associated with the study of plant defensive strategies in the form of induction of the still enigmatic biosynthetic pathways of alkaloids and phenyl glycosides.

Zusammenfassung

Die vorliegende Masterarbeit beschreibt die Untersuchung der Auswirkungen verschiedener Fettsäure-Aminosäure-Konjugate (FACs) auf pflanzliche Biosyntheseprozesse, um Rückschlüsse auf pflanzliche Abwehrstrategien gegen Fressfeinde zu ziehen.

Eine enorme Anzahl äußerer Faktoren hat Pflanzen als immobile Organismen veranlasst, verschiedene Überlebensstrategien zu entwickeln. Das breite Spektrum pflanzlicher Verteidigungstaktiken umfasst generell mechanischen und chemischen Schutz. Neben Stacheln und Dornen ist auch eine Vielzahl komplexer chemischer Strukturen wie Sekundärmetabolite an der Interaktion zwischen Pflanzen und Herbivoren beteiligt. Erwähnenswert ist, dass die Pflanze zunächst physisch verletzt werden muss, gefolgt von einer Ausbreitung chemischer Auslöser an der Kontaktstelle zwischen Pflanze und Pflanzenfresser, um eine Kaskade biochemischer Prozesse zu aktivieren. Einer der wichtigsten Initiatoren pflanzlicher Verteidigungsstrategien ist das FAC Volicitin. Da die biochemische Wirksamkeit dieser Verbindung außer Frage steht, weil sie bereits in früheren Studien untersucht wurde, wurden in der vorliegenden Arbeit andere dem Volicitin ähnliche Verbindungen synthetisiert und es wurde ihre potenzielle Fähigkeit biosynthetische Wege zu induzieren untersucht.

Um die Konzentrationsveränderungen von bestimmten sekundären Inhaltsstoffen von *Vinca minor*-Pflanzen und *Populus*-Hybriden (*Populus alba* × *Populus tremula*) zu untersuchen, wurden elf FACs synthetisiert, die sich in ihrer chemischen Struktur nicht stark voneinander unterscheiden: *N*-(10-Hydroxyundecanoyl)-L-glutamin (**1d**), (S)-*N*-α-Undec-10-enoyl-L-glutamin (**2b**), *N*-((9Z)-Octadec-9-enoyl)-L-glutamin (**3b**), (S)-*N*-α-Octadecanoyl-L-glutamin (**4b**), *N*-(Heptanoyl)-L-glutamin (**5c**), *N*-(Pent-2-enoyl)-L-glutamin (**6c**), *N*-(Hept-2-enoyl)-L-glutamin (**7c**), *N*-(9-(1′′-Oxooctadecanoyl)-octadec-10-enoyl)-L-glutamin (**8c**), *N*-(10-(1′′-Oxooctadecanoyl)-octadec-8-enoyl)-L-glutamin (**8d**), *N*-(12-Oxononacosa-9-enoyl)-L-glutamin (**9b**), (S)-*N*-α-Octanoyl-L-glutamin (**10b**) und *N*-(12-Hydroxynonadec-9-enoyl)-L-glutamin (**11e**). Im anschließenden Experiment wurden die FAC-assoziierten Molekülmuster des monoterpenoiden Indolalkaloids (MIA) Vincamin in *V. minor* und der beiden Salicinoide Tremulacin und Tremuloidin in *Populus*-Hybriden mit Hilfe einer Hochdruck-Flüssig-Fest-Chromatographie (HPLC) näher untersucht.

Die Behandlung mit *N*-(Pent-2-enoyl)-L-glutamin (**6c**) veränderte den Gehalt an Vincamin in *V. minor*-Pflanzen erheblich. Hier wurde im Gegensatz zu den erhaltenen Ergebnissen nach der Auftragung der anderen FACs oder der ägyptischen Baumwollblattwürmer (*Spodoptera littoralis*) ein zweifacher Anstieg des Vincamingehalts identifiziert. Dies bestätigte nachweislich die postulierte Induktion des MIAs-Biosyntheseweges im Kleinen Immergrün. Darüber hinaus wurden bei der Untersuchung der zeitlichen Veränderungen der Vincaminkonzentration nach der Anwendung von **6c** sofortige Veränderungen des MIA-Spiegels in *V. minor* 24 h nach der Anwendung des oben erwähnten FAC-Kandidaten sichtbar, während am sechsten Tag die niedrigste Vincaminkonzentration

beobachtet wurde. Folglich wurde im Laufe der Zeit immer weniger Vincamin nachgewiesen, da es sich möglicherweise um eine sukzessive Umwandlung der vorhandenen MIAs in andere Alkaloide handelte.

Des Weiteren konnten im Rahmen dieser Masterarbeit auch Beobachtungen zur Biosynthese der beiden bedeutenden Salicinoide Tremulacin und Tremuloidin nach Anwendung der FACs *N*-(10-Hydroxyundecanoyl)-L-glutamin (**1d**), *N*-(Heptanoyl)-L-glutamin (**5c**) *N*-(9-(1′′-Oxooctadecanoyl)-octadec-10-enoyl)-L-glutamin (**8c**) und *N*-(10-(1′′-Oxooctadecanoyl)-octadec-8-enoyl)-L-glutamin (**8d**) sowie (S)-*N*-α-Octanoyl-L-glutamin (**10b**) auf die *Populus alba* × *Populus tremula* Hybriden gemacht werden. *Populus tremula*-ähnliche Individuen wiesen höhere Werte von relativen Tremulacin- und Tremuloidin-Konzentrationen auf als *Populus alba*-ähnliche Arten, was einen kausalen Zusammenhang zwischen der genomischen Abstammung der Pappeln und den Konzentrationen der beiden Phenylglycoside bestätigte.

Zusammenfassend lässt sich sagen, dass diese Masterarbeit weitere Perspektiven für die Erforschung der FAC-Synthese, die mit der Untersuchung pflanzlicher Verteidigungsstrategien in Form der Induktion der noch immer rätselhaften Biosynthesewege von Alkaloiden und Phenylglycosiden verbunden ist, eröffnet.

Acknowledgements

First of all, my deepest gratitude goes to Univ.-Prof. Dipl.-Chem. Dr. Lothar Brecker, Privatdoz., who supervised my master thesis. He gave me the opportunity to work in a very challenging and interesting field of research. Most of all, I am thankful for his constant professional support and patience throughout my work. My deepest thanks also go to Mag. Dr. Johann Schinnerl who also supervised this thesis. I am thankful for his good advice, personal guidance, and his willingness to answer an endless number of my questions.

Many thanks to my dear colleagues from our workgroup, Evelyn Fülöp, B.Sc. MSc and Florian Traxler, BSc. MSc. for the friendly atmosphere in the lab and very helpful advice whenever I needed it. Dear Evelyn and Florian, thank you for your many brilliant suggestions and the ideas you had.

I would furthermore like to acknowledge support by the Mass Spectrometry Centre of the Faculty of Chemistry, University of Vienna (a member of Vienna Life-Science Instruments). Special thanks goes to Mag. Dr. Martin Zehl and Anna Fabisikova, MSc for their help with mass spectrometric measurements, which provided an important contribution to this work. Furthermore, dear Dipl.-Ing. Evelyn Rampler, Privatdoz. Bakk. techn. PhD and dear DI Dr. Elisabeth Varga, thanks to you I have discovered many interesting and exciting topics in the field of analytical and food chemistry. I was very inspired not only by your professionalism but also by your friendly and sincere personality.

I would especially like to thank all the amazing people I met during my master study. The time we spent together and the conversations we had were very precious for me. I want to mention Olivia Gatterbauer, BSc MSc; Matthias Glück, BSc MSc; Alexander Karbalei, BSc; Bojana Lukajic, BSc; Juliane Rumpelsberger, BSc; Lucia Schmidtbauer, BSc MSc; Aranka Tímea Szeredi, BSc MSc; Viktoria Wieser, BSc and Hao Qi Zhang, BSc MSc. A special thanks goes to Klaudia Tadus, BSc for always listening to whatever problems I had, gorgeously written annotations, with which I was able to learn better than with my own transcripts, funny moments we enjoyed together and especially her unlimited willingness to help. I am heartily thankful for Mag. Jakob Gabler for his accuracy and professionalism during the English proofreading of my master thesis.

I cannot begin to express my gratitude to my family who have accompanied me along this journey. Thank you, my sister Katarzyna, my brother Radosław, my mother Ewa and dear recently deceased father Artur who remains forever in my heart, for believing in me. To my daughter Susanne, you are my inspiration and without you I could not imagine my life. Thanks to you Susi I have pulled myself together and overcome difficult moments during this time. I would also like to say a big thank you to my partner's parents and his brother Thomas for support. And last but not the least, I would like to express my gratitude to my partner Matthias. As an organic chemistry enthusiast, I could only conclude that we have created a kind of a diamond C-C bond over the last decade, which is characterized not only by its extraordinary strength but also robustness against compression. Dear Matthias, you are the one who let me finish my degree and for that I am really grateful to you. I look forward to the beautiful moments that are still to come.

Table of contents

Abbreviations

16OMT	16-hydroxytabersonine-*O*-methyltransferase
1D-NMR	one-dimensional nuclear magnetic resonance
2D-NMR	two-dimensional nuclear magnetic resonance
6-HCH	6-hydroxy-2-cyclohexenone
AC	time-dependent potential
AMP	adenosine monophosphate
BAW	beet armyworm
CGA	chlorogenic acid
CI	chemical ionization
COSY	correlation spectroscopy
CS	catharanthine synthase
D4H	deacetoxyvindoline 4-hydroxylase
DAT	deacetylvindoline-*O*-acetyltransferase
DC	time-independent potential
DCM	dichloromethane
DMAPP	dimethylallyl pyrophosphate
DMSO	dimethyl sulfoxide
E4-P	erythrose 4-phosphate
ED_{50}	median effective dose
EI	electron ionization
ESI	electrospray ionization
Et_2O	diethyl ether
FAC	fatty acid-amino acid conjugate
FI	fluorescence detector
FID	free induction decay
FTC	forest tent caterpillar
FT-NMR	Fourier transfer- nuclear magnetic resonance
HCC	1-hydroxy-6-oxocyclohex-2-ene-1-carboxylic acid
HETP	height equivalent to a theoretical plate
HMBC	heteronuclear multiple-bond coherence
HPLC	high-performance liquid chromatography
HPLC	high-pressure liquid-solid chromatography
HRMS	high-resolution mass spectrometry
HSQC	heteronuclear single quantum coherence
IPP	isopentenyl pyrophosphate

JA	jasmonic acid
LC	liquid chromatography
LG	leaving group
MAPK	mitogen-activated protein kinase
MeJa	methyl jasmonate
MeOH	methanol
MIA	monoterpenoid indole alkaloid
miRNA	micro ribonucleic acid
MS	mass spectrometry
MS/MS	tandem mass spectrometry
NICI	negative-ion chemical ionization
NMR	nuclear magnetic resonance
NOESY	nuclear Overhauser enhancement spectroscopy
NPLC	normal phase liquid chromatography
PDA	photo diode array
PEEK	polyetheretherketone
PEP	phosphoenol pyruvate
PG	phenolic glycoside
PICI	positive-ion chemical ionization
PPO	polyphenol oxidizing enzyme
Q	quadrupole
RDA	retro Diels-Alder
RF	radio frequency
RPLC	reversed phase liquid chromatography
SLS	secologanin synthase
STR	strictosidine synthase
T16H	tabersonine 16-hydroxylase
T3O	tabersonine 3-oxidase
T3R	tabersonine 3-reductase
TDC	tryptophan decarboxylase
TEX1	tabersonine 6,7-epoxidase 1
THF	tetrahydrofuran
THW	tobacco hornworm
TLC	thin layer chromatography
TMS	tetramethylsilane
TOCSY	total correlation spectroscopy
TOF	time-of-flight

TPS	terpenoid synthase
TQMS	triple quadrupole tandem mass spectrometer
TS	tabersonine synthase
UDP	uridine diphosphate
UHPLC	ultrahigh pressure liquid chromatography
UV	ultraviolet
UV/Vis	ultraviolet-visible
V19H	vincadifformine 19-hydroxylase
VS1/2	vincadifformine synthase 1/2

1. Introduction

1.1. Plant defense system

A plethora of different external factors have caused the plants to develop different survival strategies. Regarding the fact that not only light, water, temperature, salinity or nutrients as abiotic factors but also herbivores, pathogens, other plants, endophytic fungi or mycorrhizal as biotic factors have an influence on the fitness of a plant, it is not easy to predict which of all these factors indeed trigger plant defense [1], [2].

Although the plant kingdom belongs to sessile organisms, they can effectively protect themselves both mechanically and chemically [3]. Generally, hardness, sharpness, and toughness as mechanical defense properties, are an effective weapon for deterring herbivores, especially mammals or insects. To achieve these features, certain plants possess for instance cell walls with microfibrils composed of cellulose and embedded in hemicellulose or lignin. The most common examples of physical barriers of plants represent thorns, spines and so called “leaf hairs”, trichomes [3]–[5]. In addition, based on tens of thousands of primary metabolites present in millions of plant species, it is estimated that as many as twenty times that number of secondary metabolites can be synthesized by plants. Part of this large number of specialized metabolites is used for defense against enemies [6]. Considering this chemical defense, if the secondary compounds are always present in a plant, it is a constitutive defense. This kind of defensive strategy can be represented by the plant glycoside avenacoside B, a saponin originating from *Avena sativa* which can effectively destroy cell membranes. Other examples representing constitutive toxins produced by plants are polyethyne cicutoxin from water hemlock *Cicuta virosa* or one of the many benzylisoquinoline alkaloids (BIA) accumulated by opium poppy (*Papaver somniferum*), analgesic morphine, which is able to influence the action potential in neurons as well as has narcotic properties, respectively. Due to the difficulty of tracking the constitutively direct mechanisms of plant defense, the focus in recent years has been primarily on induced chemical defense mechanisms [7]–[10].

In contrast, an induced resistance against herbivores appears only when the plant is attacked [11]. Both constitutive and induced defenses can be distinguished into direct and indirect strategies, whereby the first one means the plant's own defense and the second one, called tritrophic interaction, involves the intervention of organisms from higher levels of the nutritional pyramid to protect the attacked plant from the herbivore [3], [12], [13].

1.1.1. Overview of plant chemical defense strategies

1.1.1.1. Terpenoids

In general, a broad spectrum of plants’ specialized compounds encompasses terpenoids, phenolics and alkaloids. The terpenoids constructed from the smallest molecule containing five carbon atoms called isoprene are widespread in all plants [5]. Isoprene can act as a direct or indirect defender in a plant;

thus, it not only deters a species like a moth *Manduca sexta* but can even attract parasites such as *Diadegma semiclausum* helping in defense [14], [15]. Two isoprene units form monoterpenoids, which are represented, for example, by an insecticide pyrethrine as an ester with neurotoxic properties produced by pyrethrum plants (*Tanacetum cinerariifolium*, Asteraceae) [16]. Following this, triterpenoids containing six isoprene units such as phytoectysones from spinach (*Spinacia oleracea*) cause higher death rates for insects as it interferes with larval development. In contrast, terpenoids such as cardiac glycosides digoxin and digitoxin do not pose a threat to other herbivores such as the monarch butterfly larvae. Thus, larvae feeding on these toxic substances transform into a butterfly that is inedible to birds [5].

Generally, various monoterpenoids (C_{10}) and sesquiterpenoids (C_{15}), as volatiles released by plants, play an extremely important defensive role against herbivores. On one hand, the individual volatile substances, or a variation of these act as a deterrent to herbivores. On the other hand, they may attract some parasites or parasitoids, and therefore activate an indirect defensive mechanism[3]. It has been demonstrated for Arabidopsis plants that flowers can emanate a scent with different terpenoids, which allows interaction with the environment [17]. Since the whole Arabidopsis genome was sequenced, it was found there are putative genes expressed for the production of different terpenoid synthases (TPSs) [17]. Accordingly, it has been shown by Van Poecke *et al.* that the expression of certain genes plays a crucial role in stress-induced plant defensive mechanisms. *AtTPS10* gene was responsible for the encoding of β-myrcene synthesizing protein, following a response to *Pieris rapae* caterpillar attack [18]. The formation of (*E*)-β-ocimene in consequence of mechanical wounding and subsequent application of jasmonic acid has also been observed. An increased gen *AtTPS03* expression was the respond to these stress factors [19]. (*E*)-β-ocimene was also a target of studies on *Lotus japonicus* plants. Here, the plant showing herbivore-induced indirect defense response was infested with two-spotted spider mites (*Tetranycurticae*) [20].

Interestingly, monoterpenoids and sesquiterpenoids are not only synthesized in the previously mentioned plants but are also found in conifers. A conifer much larger than Arabidopsis or *Lotus japonicus* still needs a defense mechanism, as it can also be attacked by insects. Thus, in the resin from a wounded coniferous tree, there is a deterrent turpentine fraction containing mono- and sesquiterpene, which first evaporates enabling the polymerization of the compounds contained in the turpentine fraction. Subsequently, trapping of the insects and killing of those is the goal of the direct defense mechanism [3], [21], [22].

1.1.1.2. Phenolics

The second class of organic compounds dominating in the plant kingdom are phenolics. Plant phenolics consist of one or more aromatic ring to which different numbers of hydroxy groups can be attached. The compounds play an essential role in plant life, thus they can influence their development, take part in the recognition of microbes, regulate growth, participates in the

differentiation of the cells and the associated development of the organs, whereby it all depends on the plant species, biological process and the structural property of a phenolic compound [23]–[26]. Lattanzio *et al.* present evidence that phenolics as signal molecules are able to influence other species in a chemical way. Hence, phenolics, also defined as allelochemicals, are released into the soil through leaf leaching or root exudation into the rhizosphere, which affects the adjacent plants through, for example, chemical inhibition and associated displacement from these [27].

Both biotic and abiotic stress factors can trigger phenol production in plant tissue [23]. For instance, after infection with the pathogen, the plant stores phenolics in its cell walls [26]. The phenolic content also changes during drought, nutrition deficit or whenever the plant is exposed to radiation [28]–[30]. Moreover, Clé *et al.* published a study of the UV experiments on tomato *Solanum lycopersicum*, in which it was found that the leaves treated with UV-B light showed increased chlorogenic acid (CGA) accumulation. Consequently, they concluded that phenylpropanoid metabolism is influenced by environmental conditions and phenolic precursor flux is regulated accordingly [31].

Biotic stress factors for the plant represent insects or mammals. It has been evidenced that the constitutive phenolics inhibit the organisms and thus protect the plant from being eaten [27], [32]–[35]. Accordingly, plants exhibiting induced defense produce toxic phenolic substances that protect the host from further damage by the insects [27], [36], [37]. These antifeeding properties possess, for example, judaicin and maackiain, which act as a deterrent for *Spodoptera littoralis* and *Spodoptera frugiperda* larvae, respectively [27]. Nevertheless, in the saliva of sucking-piercing insects there are polyphenol oxidizing enzymes (PPO) enabling them to circumvent the toxicity of some phenolics by oxidizing and polymerizing of this class of organic compounds into non-toxic substances [38]. In addition, it has been demonstrated that plants also obtain PPO enzymes participating in the oxidation of phenolic. Regarding this, the expression of PPO was studied in mechanically wounded hybrid poplars, and the activity of this enzyme was found to increase, when the plants were exposed to feeding larvae. This can be explained by the fact that the plants through the use of such enzyme machinery make themselves inedible and indigestible, since the phenolic are converted into the polymers and the proteins are cross-linked. Finally, the defense of poplars against herbivores was confirmed [39], [40].

1.1.1.3. Alkaloids

Whilst phenolics and terpenoids are ubiquitous in many plant taxa, nitrogenous secondary constituents called alkaloids are found in about 20 % of all plant species, with plant families Solanaceae, Ranunculaceae, Apocynaceae, and Papaveraceae being a few prominent examples [3], [9]. These specialized metabolites can be accumulated in different parts of the plant and provide protection against herbivores or pathogens. Alkaloids originating from amino acids such as indole alkaloids, are

prominent examples in the combat against herbivores. Moreover, plants growing on nitrogen-rich soils are more robust after predator attack [41].

There are many alkaloid definitions, but here only two will be mentioned. Species from which these organic compounds originate are often used to define the alkaloids. Thus, alkaloids found in *Vinca rosea* were named vincristine and vinblastine. In addition, the second option for designating the class of organic compounds is to refer to the biosynthetic pathways from which the alkaloids originate [42]. Hence, a well-known and often studied defense alkaloid called nicotine originating as the name suggests from *Nicotiana tabacum* is synthesized mainly in a cascade of enzyme reactions starting from L-arginine and L-ornithine in response to a pest attack. An essential role is played here by phytohormones such as jasmonate, which act as signaling and regulatory molecules and stimulate the biosynthesis of nicotine. The synthesis takes place in roots, from which the alkaloid is transported into the leaf tissue and accumulated in this aerial part. Nicotine is one of the naturally occurring insecticides as it binds to insect postsynaptic receptors [43]–[45].

Furthermore, the purine alkaloid caffeine occurring particularly in *Coffea arabica* was shown to be effective in defense against herbivore such as larvae of tobacco horn moth (ED_{50}: 0.03 – 10 %; *Manduca sexta*) or mosquito (ED_{50}: 0.0007 %; Culex ssp). The mode of caffeine action based on inhibition of phosphodiesterase hydrolyzing a signal molecule adenosine monophosphate (AMP) [46], [47].

In the array of secondary metabolites playing an essential role in the chemical defense mechanisms of plants, pyrrolizidine alkaloids have been found as well. Hence, “pro-toxic free base” senecionine appear to have strong repellent properties on insects. In this molecular form, senecionine is bioactivated in insects with the help of cytochrome P450 oxidase and thereby converted into mutagenic pyrrolic intermediate [48].

1.2. Molecules indicating eliciting properties

These few examples indicate that plants are indeed able to produce an array of substances by multiple biosynthetic pathways that protect them from the biotic and abiotic factors. Knowledge of which substances triggered a defense mechanism in a plant is as important as understanding the phenomena described above. Owing to this, Alborn *et al.* have studied intensively to find the elicitors in oral secretion of beet armyworm (BAW; *Spodoptera exigua* Hübner) caterpillars. The substance they isolated and identified at that time was *N*-(17-hydroxylinolenoyl)-L-glutamine (volicitin), which has already been mentioned in many publications. Interestingly, a volicitin applied to wounded leaves of corn (*Zea mays* L.) caused the plant to emit a perfume mixture of various volatile terpenoids and indoles, thereby attracting natural enemy of caterpillars, parasitic wasps (*Cotesia marginiventris*) to it, which is termed to tritrophic interaction as stated above [49]–[51]. Three years later, Alborn *et al.* published results showing that not only volicitin, but also other substances were present in the oral secret of the same caterpillars. These have comprised 17-hydroxylinolenic, linolenic, 17-

hydroxylinoleic and linoleic acid. Nevertheless, the most active elicitor was still volicitin [52]. Volicitin is a prominent example of fatty acid amino acid conjugates (FACs) consisting of amino acid and nonpolar fatty acid moiety (**Figure 1**). FACs can show quite a large structural diversity as a result of the many possible combinations of the two classes of compounds. For instance, species specific FACs-composition of lepidopteran caterpillars salivary secretion can vary in the amino acid composition, in the fatty acid chain length as well as the number of double bonds of the fatty acid moiety. Additionally, it is important to point out that FACs consisting of L-glutamine as amino acid subunit are apparently the most effective in the herbal response [53], [54]. Among FAC elicitors, *N*-(18-hydroxylinolenoyl)-L-glutamine (18-OH-volicitin) isolated from lepidopteran species tobacco hornworm (THW; *Manduca sexta*) and applied on damaged leaves of solanaceous plants has shown a similar elicitor activity to volicitin [53]. Other trigger of the herbal response to stress and consisting of L-glutamine as amino acid moiety was *N*-linolenoyl-L-glutamine, which was found to be effective against maize cultivars [49].

Tremendous variability in plant responses to the elicitors such as above mentioned volicitin has caused the researchers to mimic nature. In fact, *Alborn et al.* have successfully synthesized 17-hydroxylinolenic acid and 17-hydroxylinoleic acid following by the synthesis of *N*-[17-hydroxylinolenoyl]-L-glutamine and *N*-[17-hydroxylinoleoyl]-L-glutamine, respectively [52]. To obtain the desired amides, a modified approach based on method implemented by Sheehan *et al.* was carried out [55]. The (17R)- and (17S)-isomers of volicitin could also be accomplished by semi-hydrogenation of alkynes and selective olefination, as shown in the Itoh *et al.* method [56]. Subsequently, the other group reported a formal synthesis of both enantiomers of volicitin *via* one-pot bis-Wittig reaction as a short stereoselective synthesis [57].

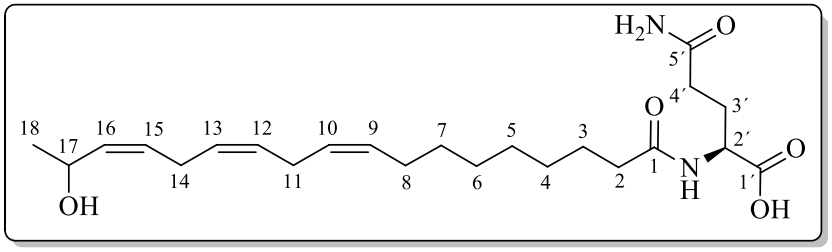

Figure 1: Chemical structure of *N*-(17-hydroxylinolenoyl)-L-glutamine (volicitine).

1.3. MIAs pathway modulation in *Vinca minor*

Vinca minor derived from the plant family Apocynaceae and also called periwinkle, evergreen perennial herbaceous plant, myrtle or vinca is a relatively slow growing plant that responds to environmental alterations [58]–[60]. *V. minor* is also the MIAs (monoterpenoid indole alkaloids) - rich source. According to this, eburnamine alkaloid vincamine seems to be the most important representative in leaves of periwinkle. In addition, young leaves of *V. minor* draw a higher metabolism

than the older tissues [58], [61]–[64]. The biosynthesis towards vincamine production derives from two important routes viz. shikimate and seco-iridoid biosynthetic pathways.

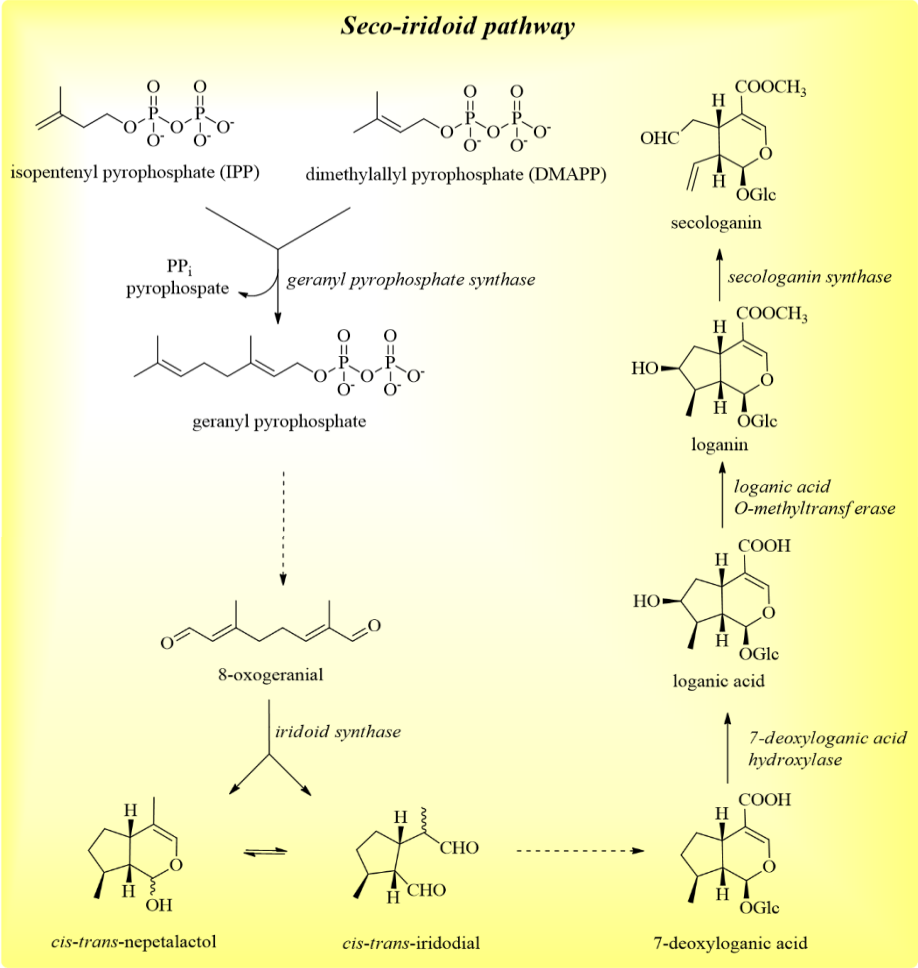

Figure 2: Seco-iridoid pathway operating in plants.

The biosynthesis of terpenoids does not start from isoprene but from the biochemically activated isomers isopentenyl pyrophosphate (IPP) and dimethylallyl pyrophosphate (DMAPP). Oxidation, reduction, methylation, and glycosylation reactions can take place with the aid of various enzymes involved in the biosynthesis of terpenoids (iridoids) as shown in **Figure 2**. In this way biosynthesized seco-iridoid secologanin can be further introduced into the indole alkaloid biosynthesis pathway [65].

One of the most important biosynthetic pathways in plants, leading to the substances with phenolic structures represents shikimic acid biosynthetic pathway (**Figure 3**) [23]. Since an important intermediate and at the same time a branching point of the shikimate pathway is a compound termed chorismate, the natural process is also known as the chorismate pathway [66]. The biosynthetic pathway plays an essential role in the production of aromatic amino acids from primary metabolites phosphoenol pyruvate (PEP) and erythrose 4-phosphate (E4-P). The three amino acids L-tryptophan, L-phenylalanine and L-tyrosine synthesized in this way, are intermediate compounds of great

importance for the biosynthesis of aromatic secondary metabolites such as lignins, flavonoids, alkaloids and phytoalexins [67].

Based on frontier metabolic and genetic studies of *Catharanthus roseus* as well as transcriptomics and gene co-expressions analysis of *V. minor*, it is now feasible to elucidate an almost complete vincamine biosynthetic pathway [68]. A putative MIAs biosynthetic pathway leading to the production of vincamine and operating in *V. minor* is displayed in the **Figure 5**.

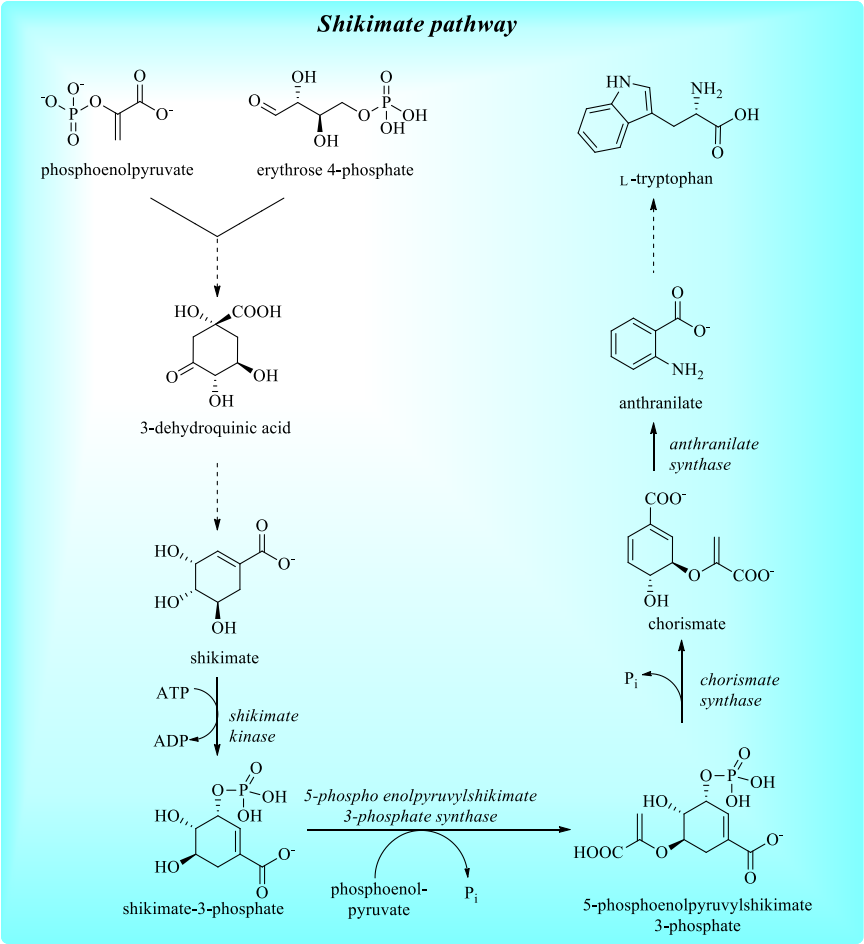

Figure 3: Shikimate pathway operating in plants.

A condensation of tryptamine and secologanin derived from seco-iridoid and shikimate pathway supplies strictosidine skeleton consisting of an indole ring and terpenoid subunit donor, respectively [69]. Starting from strictosidine, MIAs route proceeds via a few common intermediates such as cathenamine, 19*E*-geissoschizine and stemmadenine until it reaches a branching point, that is, *O*-acetylstemmadenine. If at this point an enzyme catharanthine synthase (CS) is involved, a precursor of two chemotherapeutic drugs vincristine and vinblastine is formed. Furthermore, *O*-acetylstemmadenine can also be converted into vincadifformine, following by enzymatic reaction of vincadifformine 19-hydroxylase (V19H) resulting finally in formation of minovincinine. Additionally, it was determined that the enzyme tabersonine 3-oxidase (T3O) presenting in *V. minor* plants is

responsible for the formation of vincamine. Moreover, it was found that, if the enzyme tabersonine 3-reductase (T3R), which is responsible for the synthesis of vindoline, is not present, the biosynthetic flux will proceed in the direction of vincamine skeleton production (**Figure 5** & **Figure 36**) [68], [70].

Almost at the same time, another study was undertaken on pathways operating in *V. minor*. Transcriptomics analyses based on identification of specific miRNA involved in MIAs pathway demonstrated a slightly deviating putative biosynthetic pathway from the one outlined above. The proposed biosynthesis of vincamine proceeds with the help of deacetylvindoline-*O*-acetyltransferase (DAT) and deacetoxyvindoline 4-hydroxylase (D4H), therefore the resulting intermediate is deacetylvindoline, following by vindoline type of alkaloid, which is finally converted into vincamine [71]. Biosynthesis of MIAs is generally controlled by gene expression and a number of enzymes. Thus, it has been reported that light, UV and mechanical wounding facilitate the production of MIAs by expressing genes responsible for enzymes involved in this pathway [72]. In addition, Stander *et al.* reported about the influence of light on the increased expression of the genes responsible for biotic and abiotic factors such as high temperature, salt concentration or herbivore attack [68].

If a plant is exposed to a deficit of constituent such as sulfur, what results in the absence of the sulfuric amino acids, other amino acid biosynthetic pathways are induced and consequently higher levels of especially L-tryptophan can be observed. In short, by increasing the biosynthetic flux and therefore L-tryptophan accumulation resulting from the sulfur amino acid losses, the plant manages to survive [73]. Furthermore, L-tryptophan production can be reflected in the modulation of the vincamine biosynthetic pathway, as this route originates from L-tryptophan and secologanin. In fact, over-production of this amino acid revealed in an increment of vincamine content in periwinkle [58]. An infestation of Madagascar periwinkle (*Catharanthus roseus*) by the herbivore *Manduca sexta* led to increased production of toxic alkaloids vindoline and catharanthine in newly developed leaves what caused the larvae to die [72]. Moreover, while the drought forced the same plant species to synthesize more vindoline in seedlings, high temperatures resulted in the induction of the biosynthetic pathway toward the production of vindoline in leaves [74], [75]. In contrast, low temperature resulted in decreasing production of vindoline, vinblastine and vincristine in *C. roseus* leaves as shown by Dutta *et al.* [76].

Not only wounding, UV radiation or pathogens can affect MIAs pathway, but also methyl jasmonate (MeJA) (**Figure 4**), seems to be a trigger of increased production of vinca alkaloids such as vindoline, thus the well-known plant stress hormone is able to induce certain biosynthetic pathways. This occurs due to the activation of enzymes such as the above-mentioned D4H, DHT enzymes, and even tryptophan decarboxylase (TDC) as well as strictosidine synthase (STR), which are the common enzymes of the MIAs pathway [77], [78]. Application of MeJA to *C. roseus* leaves triggered stress signal transduction. In this process, a specific mitogen-activated protein kinase (MAPK) such as CrMPK3 was induced, which revealed in the major MIAs accumulation as plant defense mechanism against this stress [79]. Furthermore, recent study on *C. roseus* have demonstrated that with increasing

concentration of foliar applied jasmonic acid (JA) (**Figure 4**), the content of alkaloids produced also tends to increase [80]. This leads to the conclusion that the factors listed above have an influence on the stimulation of the MIAs pathway.

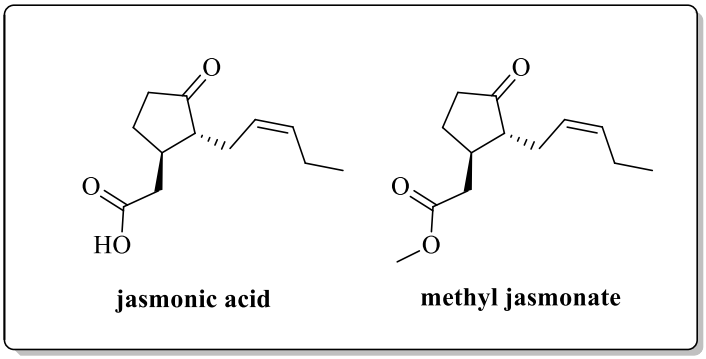

Figure 4: Chemical structures of jasmonic acid (JA) and methyl jasmonate (MeJA).

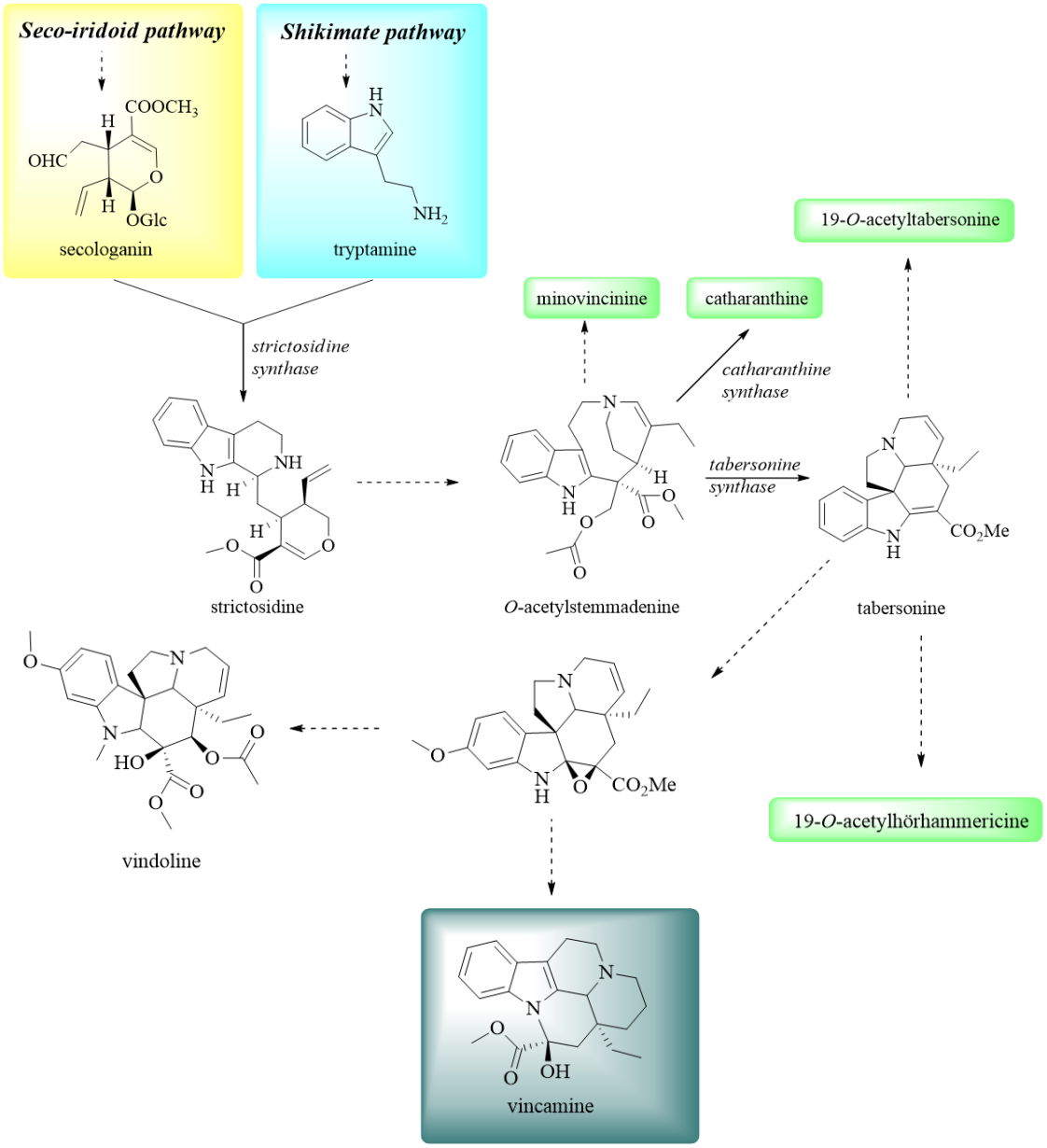

Figure 5: Putative MIAs biosynthetic pathway in Apocynaceae.

1.4. Specialized metabolites in *Populus*

Within the Salicaceous family there are trees of the genera *Populus* also known as poplar, which possess anti-herbivory properties [81], [82]. The substances being responsible for the way of defense are bioactive compounds referred to as salicylate-like phenolic glycosides (PGs) and originating from the above mentioned shikimate pathway **(Figure 3**) [82]. Apart from shikimate pathway, which has been well elucidated, the plant biosynthesis of substances such as PGs salicinoids has remained hypothetical to date [83]. Previous reports have shown that the complex PG structures are built on a basic structure salicin consisting of salicyl alcohol and β-D-glucopyranose units. The hydrophilic property of the saline structure is reduced by means of an esterification, in which the alcohol group of the salicyl alcohol moiety or two sugar positions (2′ and 6′) react with diverse organic acids. In this manner, for instance tremulacin (**Figure 6**) esterified with benzoic acid and 1-hydroxy-6-oxocyclohex-2-ene-1-carboxylic acid (HCC) is formed [84].

Recently, transcriptomics and co-expression analyses on *Populus tremula* × *Populus alba* hybrids have been approached to better follow the biosynthetic pathways of salicinoids such as salicortin, tremulacin and tremuloidin. Thus, knocking out of gene encoding the activity of the enzyme salicyl benzoate UDP-glycosyltransferase UGT71L1 has stopped synthesis of the three salicinoids, confirming that the enzyme is responsible in the biosynthesis of these specialized metabolites with anti-herbivore properties. Simultaneously, it was shown that salicin probably originates either from another branch of the biosynthetic pathway or from the same one. However, salicortin seems to be an intermediate in the biosynthesis of salicin [83].

Noteworthy, tremulacin seems to have a negative effect on insect herbivores, since there is a HCH group in its chemical structure [84]. There is a report evidence that poplar leaves attacked by herbivores release a toxic substance 6-hydroxy-2-cyclohexenone (6-HCH) [85]. The 6-HCH is formed by the cleavage of 1-hydroxy-6-oxo-2-cyclohexenone carboxylic acid anion from PGs such as tremulacin. The anion is first decarboxylated and the resulting 2-hydroxy-3-cyclohexenone is finally tautomerized to 6-HCH. The hydroxyketone is an intermediate compound that can also further oxidize to another toxic compound called catechol in the presence of the oxygen from the air [85]–[87].

Since poplars, like other species of the plant kingdom, are unable to escape herbivores, they have also developed defensive strategies against them. To cope with insect invasion, poplars can possess constitutive and induced defense strategies. For this, they need a rich set of specialized metabolites such as PGs, which they release locally, i.e. at the damaged site, or systemic ones, which are activated far from the wounded site [88]. A distribution of these specialized metabolites can vary not only between but also within poplar species [89], [90]. Hence, depending on genetic variations, nutrient accessibility, growing season and insect infestation, PGs concentrations may deviate [84], [91]–[93]. For example, while four major PGs (tremuloidin, tremulacin (**Figure 6**), salicin and salicortin) were present in all genotypes of *Populus tremula* studied by Abreu *et al.*, the other five novel PGs found at that time such as 2'-*O*-cinnamoyl-salicortin, 2'-*O*-acetyl-salicortin, 2'-*O*-acetyl-salicin, acetyl-

tremulacin, and salicyloyl-salicin were identified only in some genotypes [82]. It has also been shown that different clones of quaking aspen (*Populus tremuloides*) growing in Michigan can differ significantly in their tremulacin and salicortin concentrations. This also could affect the interaction between insects and poplars in the area [81]. The interaction of certain hybrids of poplars (*Populus trichocarpa* × *Populus deltoides*) and lepidopteran caterpillars such as forest tent caterpillar (FTC; *Malacosoma disstria*) have already been understood at the molecular level using gene expression analyses. Thus, regurgitant of FTC containing previously reviewed fatty acid-amino acid conjugate volicitin induced a specific set of genes involving in the herbivore response and secondary metabolism stimulation in the affected plant [94]. On the other side, studies on *P. tremuloides* genotypes have revealed correlations between high PGs levels and negative effects on development, fecundity, and growth of the gypsy moth *Lymantria dispar* larvae [95].

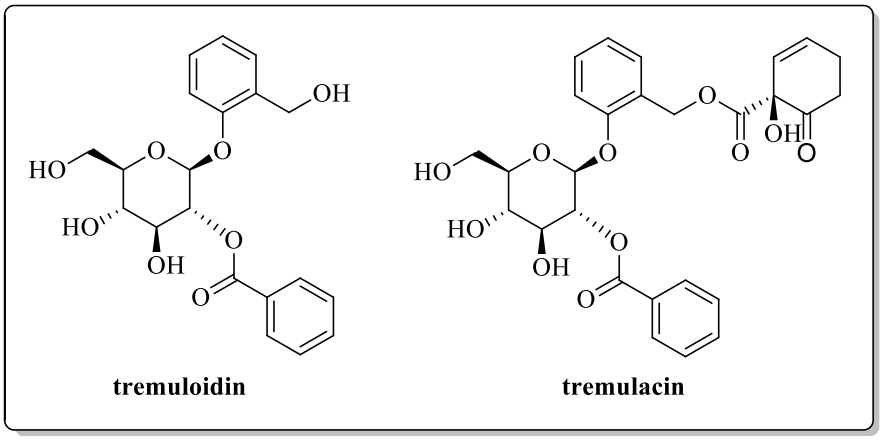

Figure 6: Chemical structures of tremuloidin and tremulacin.

1.5. Objectives

The main goal of this thesis was to draw the conclusions about the plant defense against herbivores. This work is a further development of the already existing study of Szeredi [96]. Thus, special focus was placed on the synthesis of *N*-(17-hydroxylinolenoyl)-L-glutamine (volicitin) analogs and the subsequent artificial wounding followed by an application of the synthesized substances to two plants derived from different plant families. The objects under study were *Vinca minor* derived from the plant family Apocynaceae as well as *Populus* hybrids (*Populus alba* × *Populus tremula*) belonging to the Salicaceous family.

Volicitin is the fatty acid – amino acid conjugate first identified in the oral secretion of beet armyworm (*Spodoptera exigua* Hübner) caterpillars and possesses plant response eliciting properties [49]–[51]. To investigate whether different chain lengths, chain branching, the number of double bonds, and the presence of a functional hydroxy- or keto-group in the fatty acid moiety affect plant biochemical processes, they were first synthesized and then attached to the amino acid L-glutamine to form a fatty acid – amino acid conjugate (FAC). The structures of the compounds obtained were verified using standard spectroscopic and spectrometric techniques including nuclear magnetic resonance spectroscopy (NMR) and mass spectrometry (MS), respectively.

In the second section of this thesis, the effects of the previously prepared analogs of volicitin on monoterpenoid indole alkaloid (MIA) vincamine and phenyl glycosides (PG) tremulacin and tremuloidin biosynthesis in plants were examined. For this purpose, the leaves of the above-mentioned plants were harvested after a certain time after treatment with previously synthesized volicitin analogs, dried, and the extracted substances under investigation were finally analyzed qualitatively as well as quantitatively by high-pressure liquid-solid chromatography (HPLC) method.

2. Methods

2.1. Synthesis and reaction mechanism

This chapter provides a comprehensive view of syntheses of the eleven compounds made in this work with the focus on reaction mechanisms. Herein, fundamental reaction mechanisms, for instance the nucleophilic attack on ketone or the formation of amides for the synthesis of **11c/11d** or all compounds respectively, are summarized. Moreover, an overview of well-known named reactions (e.g., the Friedel-Crafts acylation or Jones oxidation) providing a closer study of synthesis pathways of **8a**/**8b**, **9a**, **11a**, **5b**, **6b** and **7b**, is also visualized. Finally, it should be mentioned that this section also illustrated a significant reaction which was required in one case (**1b**); more specifically, oxymercuration-demercuration reaction was considered in more detail.

2.1.1. Carbonyl reduction by nucleophilic attack of hydride

The aim of this process, which can be carried out with $NaBH_4$ as a compound containing a hydrogen atom with a pair of electrons, is a reduction of a carbon atom of a carbonyl group to the corresponding alcohol. After the hydride transfer, an oxyanion is produced and added to the previously formed BH_3 molecule with the deficit of the pair of electrons. Therefore, boron anion resulted again, and the carbonyl group (ketone) undergoes the second nucleophilic attack by hydride (second hydride transfer). In this way, all four hydrogen atoms with a pair of electrons each, can be added to carbonyl groups resulting in the formation of appropriate alcohol groups (**Figure 7**). In this work, 12-oxononadec-9-enoic acid (**11a**) and 12-oxononadec-10-enoic acid (**11b**) as ketones (electrophiles) were attacked as described above using hydride donor ($NaBH_4$) as nucleophile. In this manner, the nucleophilic attack provided the formation of desired 12-hydroxynonadec-9-enoic acid (**11c**) and 12-hydroxynonadec-10-enoic acid (**11d**), respectively [97].

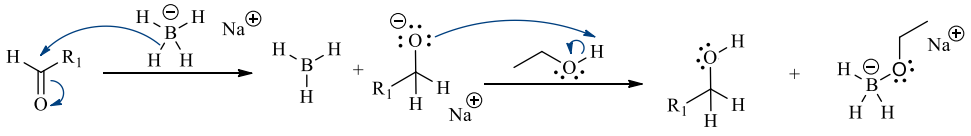

Figure 7: The first step of nucleophilic addition by sodium borohydride to the aldehyde group.

2.1.2. Friedel-Crafts acylation

Friedel-Crafts acylation is a well-known reaction of an acyl halide with aromatic reactant using a Lewis acid as catalyst [98]. The mentioned acylation can be also run with unsaturated carboxylic acids instead of aromatic compounds and an alkylaluminium chloride in catalytic quantities to achieve long or branched β,γ-unsaturated keto carboxylic acids as reported in 1993 by Metzger and Biermann [99].

Herein, ethylaluminium dichloride-induced Friedel-Crafts acylation was carried out with the acylating agent (octadecanoyl chloride (**4a**) or octanoyl chloride (**10a**)) together with the corresponding unsaturated fatty acid (octadecene-8-enoic acid (**3a**) or 10-undecenoic acid (**1a**)), to give various β,γ-unsaturated keto carboxylic acids such as branched fatty acids **8a**/**8b** and long chain fatty acids **9a** and **11a**. A closer look at the general reaction mechanism illustrates the formation of acylium cation *via* nucleophilic attack by a chlorine atom on a Lewis acid ($AlCl_3$) followed by an electrophilic substitution in the presence of an unsaturated organic compound (**Figure 8**) [100], [101].

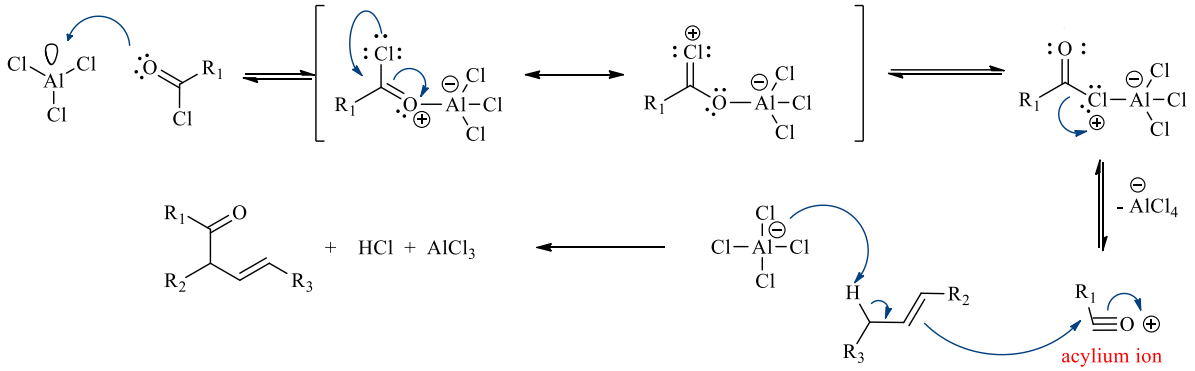

Figure 8: Lewis acid-induced Friedel-Crafts acylation mechanism.

2.1.3. Jones oxidation

There are many potential reagents applied for the selective oxidation of aldehydes to carboxylic acids. One of the most common reagents employed for this reaction and developed in 1949 by Sir Ewart Ray Herbert Jones is Jones reagent [102]. The most important reagents used for this approach are manganese dioxide, hexavalent chromium and other inorganic or organic oxidizing compounds [103]. Here, a reaction mechanism of the oxidation with CrO_3 is described, due to the application of this reagent for the synthesis of carboxylic acids such as heptanoic acid (**5b**), hept-2-enoic acid (**7b**) and pent-2-enoic acid (**6b**) starting from heptanal (**5a**), hept-2-enal (**7a**) and pent-2-enal (**6a**), respectively. The Jones oxidation mechanism starts with the protonation of the aldehyde and nucleophilic attack by water on the carbonyl group. Through the next nucleophilic attack on CrO_3, a chromate ester will be formed. Hence, Cr(VI) species participates in the oxidation of aldehyde to the carboxylic acid oxidation level as depicted in **Figure 9** below [101].

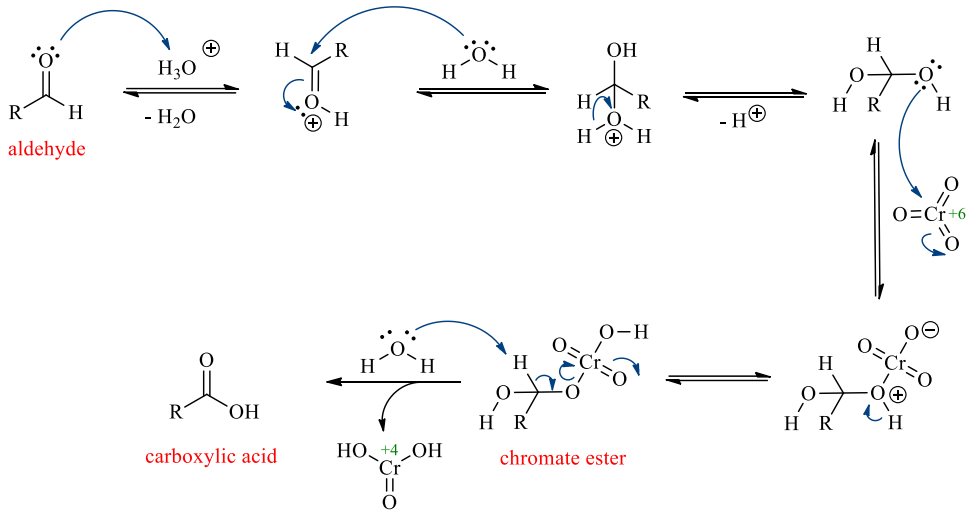

Figure 9: Synthesis of carboxylic acid starting from aldehyde *via* Jones oxidation.

2.1.4. Oxymercuration-demercuration

The oxymercuration-demercuration was first described by Seyferth and Kahlen in 1959 [104]. This reaction procedure illustrated an electrophilic addition to alkenes using soft metal cations such a Hg(II) cation [97]. Brown and Geoghegan reported study on the solvomercuration-demercuration in aqueous tetrahydrofuran system to obtain high yields of a Markovnikow product [105]. A reaction mechanism of the oxymercuration is depicted in the **Figure 10** and requires a mercuric salt, for example mercury (II) acetate, and an olefinic double bond to give a mercurinium ion. On one side, water or alcohols as solvents act as weak nucleophiles for attack on this ion. On the other side, sodium borohydride reduces the C-Hg bond (demercuration) to achieve a desired synthetic product. Accordingly, due to the high specificity of the oxymercuration-demercuration reaction mechanism, a mercuric(II) acetate salt, a sodium borohydride and an olefin (10-undecenoic acid, **1a**) in an aqueous THF system, were involved to obtain the desired Markovnikow alcohol (10-hydroxyundecenoic acid, **1b**) [105].

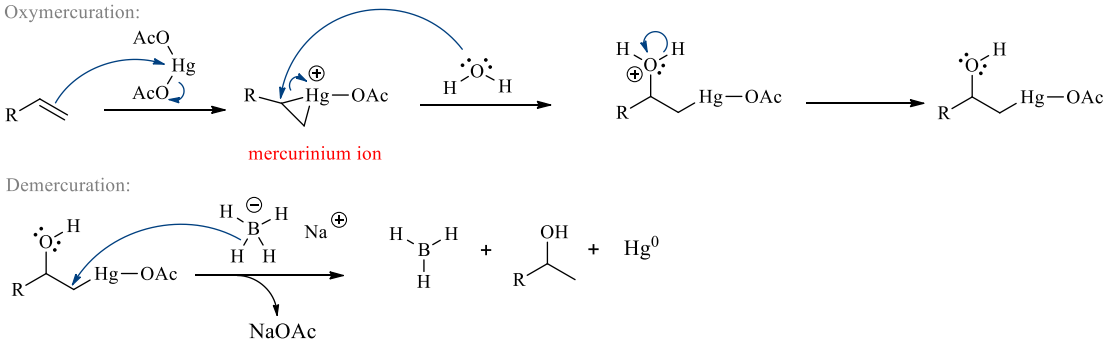

Figure 10: Oxymercuration-demercuration reaction mechanism.

2.1.5. Synthesis of amide

Amides can be generated through reaction of an α-amine group from amino acids with carboxylic acid derivatives such as acyl chlorides or acid anhydrides. Generally, this type of reaction is the well-known nucleophilic substitution and depends on the ability of the leaving group attached to the carbon atom of a carbonyl (C=O) group. Accordingly, the leaving group (LG) ability increases, if the pK_{aH} value decreases. Thus, acyl chlorides following by acid anhydrides are reagents of choice for the synthesis of amides. First, the amine group of an amino acid (nucleophile) reacts with the carbonyl group of acyl chloride or acid anhydride *via* nucleophilic substitution in the presence of a base to achieve an unstable intermediate. The tetrahedral intermediate collapses and the leaving group such as Cl^- or RCO_2^- cleaves *via* elimination reaction to give a desired amide (**Figure 11**) [97]. The reaction mechanism is the basis of all fatty acid-amino acid conjugates (FACs) syntheses in this work. Based on this, different amides (**1d**, **2b**, **3b**, **4b**, **5c**, **6c**, **7c**, **8c/8d**, **9b**, **10b** and **11e**) starting from the amino acid L-glutamine (**1c**) as nucleophile and fatty acid chlorides as well as fatty acid anhydrides (generated from fatty acids and pivaloyl chloride) as electrophile in the presence of a base such as KOH or TEA were successfully formed.

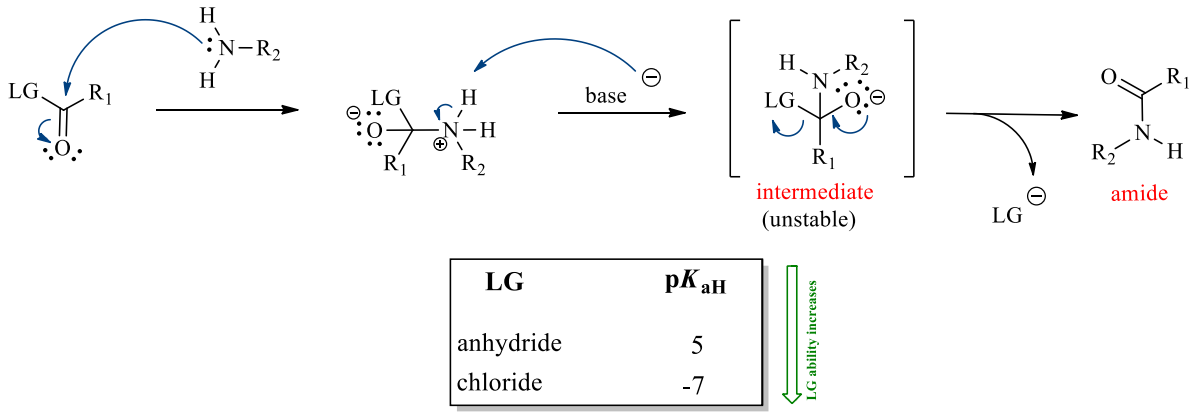

LG	pK_{aH}
anhydride	5
chloride	-7

Figure 11: Reaction mechanism of an amide formation, including a short information about leaving groups (LG) and their corresponding pK_{aH} values.

2.2. Analytical methods

2.2.1. Nuclear magnetic resonance spectroscopy

Over a number of years nuclear magnetic resonance (NMR) spectroscopy plays a crucial role in organic and analytical research environment. The information, which NMR gives, provides structure elucidation of different classes of complex organic molecules, and allows in combination with high-resolution mass-spectrometry, establishing structures of new organic molecules, too [106].

NMR technique uses an advantage of many atoms, for instance ^{1}H, ^{13}C, ^{31}P or ^{15}N, which relies on their positively charged spinning nuclei generating feeble magnetic fields. When a strong magnetic field is applied, atom spins start like a spinning top with the precession in a circular path (**Figure 12**). The frequency of this motion called Larmor frequency ν_0 (given in Hertz) is in direct proportion with the external magnetic field strength B_0 (given in Tesla) and the fundamental nucleus property, gyromagnetic ratio γ (given in rad $\cdot$ s^{-1} $\cdot$ T^{-1}) as shown equation (2.1) below [107]:

$$\boldsymbol{\nu_0 = \frac{\gamma B_0}{2\pi}} \tag{2.1}$$

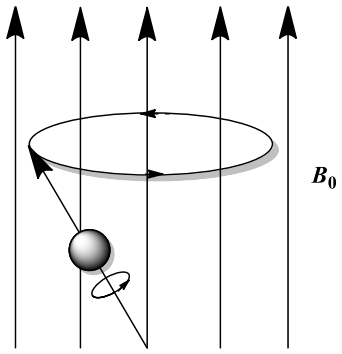

Figure 12: A classical model of the precession of an atom spin as a magnetization vector about the external magnetic field direction.

To make clear how NMR experiments really work, it is necessary to consider a quantum mechanical approach. Quantum mechanics tells us that spin-half nuclei (e.g., ^{1}H, ^{13}C, ^{31}P) can possess two quantum states with corresponding quantum numbers labelled by m. The state with $m = +\frac{1}{2}$ is described as "spin up". Accordingly, the state with $m = -\frac{1}{2}$ has the spin axis pointing down ("spin down" state) [108]. Both states take place on the same energy level. However, in the presence of an external magnetic field, there are two energy states available to a spin-half nucleus, and due to the quantum phenomenon, no states are in between (**Figure 13**). The energy gap (ΔE) between the two energy states is in direct proportion with the external magnetic field and the transition from state α to state β and *vice versa* is allowed. In NMR spectroscopy the transition of α to β can occur by photon

absorption of electromagnetic radiation. Due to strong magnetic fields, which are typically applied, the energy of the photon in equation (2.2) corresponds to the radio frequency range and is equal to the mentioned Larmor frequency ν_0 multiplied by a universal constant h (Planck's constant) quoted in $J \cdot s$ [107], [108].

$$\Delta E_{\alpha \to \beta} = E_{\beta} - E_{\alpha} = \frac{h\gamma B_0}{2\pi} = h\nu_0 \tag{2.2}$$

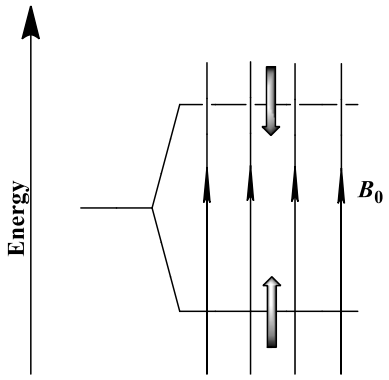

Figure 13: The split on two energy states in the presence of an external magnetic field.

As mentioned above, the information obtained from NMR experiment enables a structure elucidation. This is possible due to characteristic resonant frequencies of different types of nuclei (e.g., ^{1}H, ^{13}C). Nevertheless, because of the different electron distribution of the same kind of atom, for instance ^{1}H, the emergence of subtle alterations in a local magnetic field resulting in the narrow bandwidth of resonant frequencies, can also exist. Thus, resonance frequencies of the same isotope occurring within a molecule can be affected in the presence of, for example double bonds or electronegative atoms. The order of this variation amounts to one part per million (ppm), is defined as

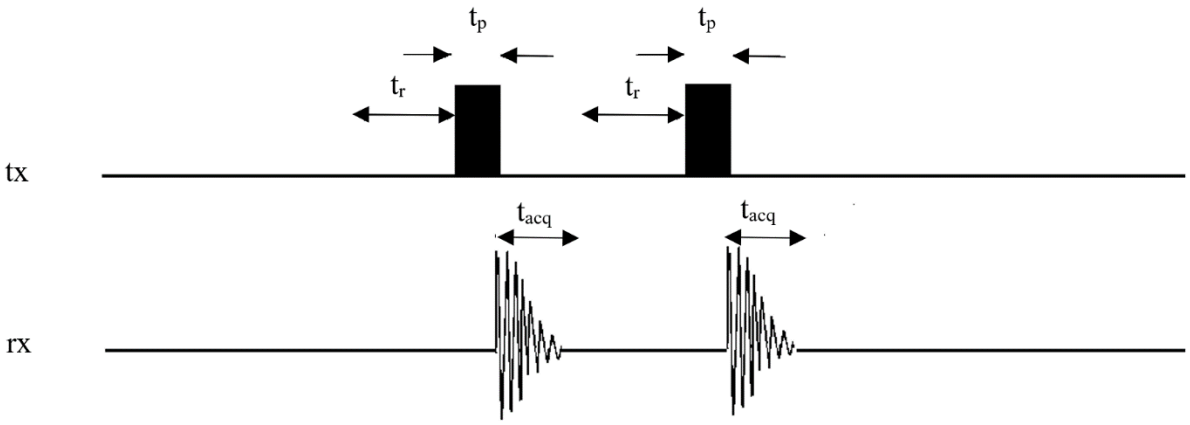

Figure 14: An overview of the typical pulsing NMR experiment approach.

a chemical shift δ and can be visualized in a spectrum, in which each nucleus resonates at its specific frequency giving a peak corresponding to the characteristic chemical environment of hydrogen (^{1}H-NMR spectroscopy) or carbon (^{13}C-NMR spectroscopy) nucleus [107].

A typical NMR experiment consists of repetitive time sequences (**Figure 14**). In order to increase a signal-to-noise ratio, a relaxation delay (t_r) to obtain the spin nuclei equilibrium, and an onset of a strong and short ($t_p = 10$ µs) radio frequency pulse to gain a transient signal (free induction decay, FID), are performed several times. For the FID recording, an acquisition time (t_{acq}) is needed. To obtain the ordinary NMR spectrum with a sufficient signal, several times recorded FID are added together and finally Fourier transformed. Simultaneously, a random noise increases by the adding more slowly than the signal revealing an improvement in signal-to-noise ratio [108].

The mentioned one-dimensional Fourier transfer NMR (FT-NMR) experiment was first published in the mid-1960's by Ernst and Anderson following by the implementation of this idea in two-dimensional FT-NMR a few years later [109], [110]. Nowadays, various 2D-NMR experiments simplify a structure verification significantly. A commonly used set of 2D-NMR approach contains Heteronuclear Single Quantum Coherence (HSQC), Correlation Spectroscopy (COSY), Heteronuclear Multiple-Bond Coherence (HMBC), Total Correlation Spectroscopy (TOCSY) and Nuclear Overhauser Enhancement Spectroscopy (NOESY) experiments.

The HSQC spectrum involves correlations between two different nuclei, for instance ^{13}C nuclei and protons, resulting from $^{1}J_{CH}$ couplings. Therefore, HSQC experiment enables an assignment of protons to their corresponding ^{13}C atoms in CH, CH_2 and CH_3 groups.

A spectrum acquired by HMBC method reveals the same heteronuclear correlations. However, in contrast to HSQC method, HMBC covers correlations of protons and carbon atoms such as $^{2}J_{CH}$, $^{3}J_{CH}$ or $^{4}J_{CH}$ which are separated by two, three or even four bonds, respectively.

In contrast, because of magnetization transfer, a standard COSY spectrum shows diagonal peaks as well as cross peaks generated by spin couplings between two atoms of the same isotope. Correlations are expressed by the coupling constant $^{3}J_{HH}$. While cross peaks in a COSY spectrum correspond to the correlation of two vicinal hydrogen atoms, diagonal peaks represent all peaks occurring in a one-dimensional NMR experiment [108].

An "extended version" of COSY experiment represents TOCSY experiment. Indeed, a spectrum recorded by a TOCSY experiment contains cross peaks between nuclei of the single isotope, which are separated from each other by three bonds, as well as cross peaks derived from an uninterrupted chain of spin couplings. Thus, an isolated spin system such as a monosaccharide owns an extended network of coupling resulting in cross peak-multiplets being observed in a TOCSY spectrum.

In order to determine through-space correlations between nuclei, which are reasonably close to each other, so the distance between those is not greater than 5 Å, a NOESY experiment can be applied. In contrast to COSY experiment, in which a coherence transfer occurs, a NOESY experiment is based on a cross relaxation (dipol-dipol interaction). Accordingly, NOESY spectrum containing cross peaks

between in space-neighboring atoms provides complementary data, which normally cannot be clarified with COSY or HMBC method [106], [108].

2.2.2. Mass spectrometry

The first mass spectrometer called a parabola spectrograph was developed in 1912 by J. J. Thomson. From this time until now, many techniques have been discovered. Following the development of the electron ionization source in 1918 by A. J. Dempster, other discoveries such as the construction of double focusing instrument, quadrupole analyzer, ion source electrospray or reflectron time-of-flight mass spectrometer have revolutionized the analysis of countless volatile and non-volatile compounds. Additionally, permanent improvements in sensitivity, accuracy or resolution have been observed to date. While detection limits of a mass spectrometer reach nowadays attomole levels, the deviation of the measured mass from the theoretical mass called the mass accuracy is better than 1 ppm. Moreover, over the last hundred years, there has been a notable increase of mass resolution. The progress in the instrumentation has improved the resolution from 13, which was reported by Thomson, to a value achieved by Marshall and co-workers, namely 8 million [111]. Noteworthy, high-resolution mass spectrometry (HRMS) provides, as the name suggests, a high mass accuracy, as well as a high resolution. To achieve this, many sophisticated, state-of-the-art instruments are constantly being developed [112]. There are a few important, fundamental principles of mass separation by mass spectrometry. The first principle is based on generation of ions from the compounds investigated. Due to the wide diversity of samples containing either instance gaseous molecules or non-volatile compounds, the great variety of ionization methods have already been developed.

Electron Ionization (EI) represents an example of hard gas phase ionization technique (**Figure 15**). An electron ionization (EI), also referred to as an electron impact ionization, uses an electron beam from so-called thermionic emission sent by rhenium or tungsten filament in the center of ionization chamber. If a beam of ions crosses the electron beam, ions with an odd number of electrons called molecular ions $M^{+\cdot}$ are generated and then accelerated toward a mass analyzer [113]. Since the acceleration of electrons in the beam is 70 eV and this is more than a molecule needs to form a molecule ion, fragment ions are also formed [114]. The resulting fragmentation patterns of organic ions enable structural elucidation beyond spectral comparison using computational methods, more precisely, molecular structural data bases. This explains why this is the experimental method for small molecule such as metabolite, which are previously separated through gas chromatography, gladly employed [115].

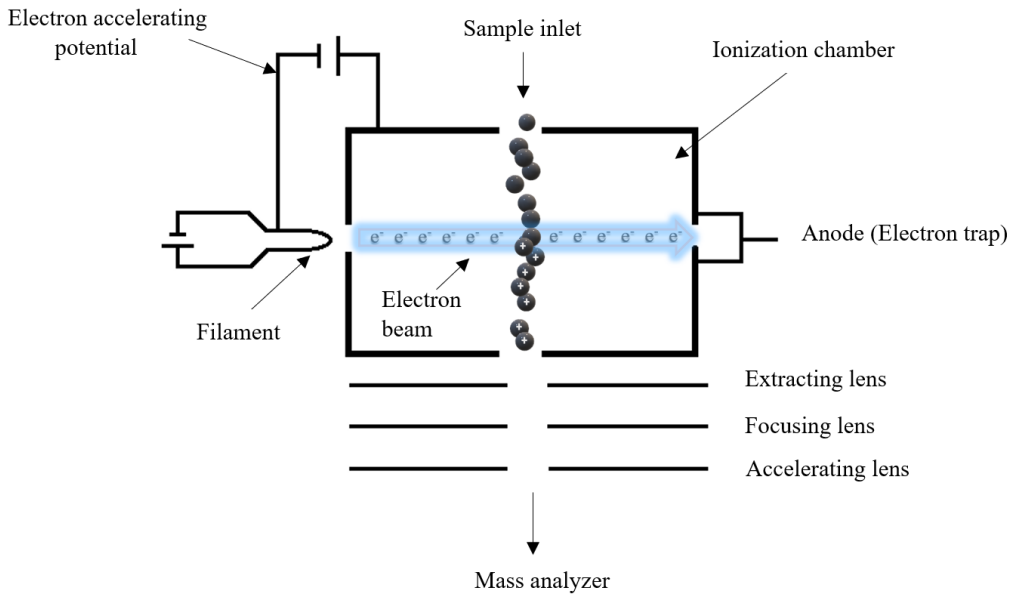

Figure 15: Principal construction of an EI ion.

Due to the loss of information about precursor molecules beyond the electron ionization experiment, softer ionization techniques such as chemical ionization (CI) have been developed as well. The principle of this operation relies on reagent ions formation resulting from bombardment of excess reaction gas molecules with electrons under vacuum, following by reactions of neutral analyte molecules with the formed reagent ions, e.g., CH_5^+, H_3^+, NH_4^+, $Xe^{+\bullet}$, $N_2^{+\bullet}$ or $O_2^{-\bullet}$. The ionization processes occur in ionization chamber, thus a CI ion source is very similar to the EI instrumentation. On one hand, neutral analyt molecules undergo proton transfer, electrophilic addition or anion abstraction reactions by positive-ion chemical ionization (PICI). On the other hand, if analyte molecules are able to form stable negative ions, a negative-ion ionization (NICI) caused by deprotonation or nucleophilic addition may be applied. Therefore, a large number of different ions results from this ionization technique, e.g., $M^{+\bullet}$, $M^{-\bullet}$, $[M + H]^+$, $[M - H]^-$, $[2M + H]^+$ or $[2M - H]^-$. However, the abundance of a certain type of ions depends on polarity, volatility, proton or electron affinity of the compounds to be examined [113].

The next commonly used soft ionization method in mass spectrometry is electrospray ionization (ESI) (**Figure 16**). It is noteworthy that this ionization technique was used for the analysis of all the compounds synthesized in the scope of this work. Normally, the ionization of analytes in ESI occurs after separation by liquid chromatography (LC) and is performed under atmospheric pressure. The solvent with the molecules of interest migrating in the electrospray capillary toward the tip contains ions formed under application of high voltage. Furthermore, the emerging liquid in an electric field applied between the capillary and a counter electrode undergoes deformation and the Taylor cone emitting a jet of droplets is thus made. Due to the solvent evaporation, the droplet size decreases, leaving an accumulation of ions of one charge sign. Since the electrostatic repulsion is larger than

surface tension of the droplet, a Coulomb explosion causing degradation of liquid drops occurs, leading to microdroplets and finally isolated ions. ESI is suitable for the analysis of both polar and mid-polar compounds with a wide range of molecular mass such as peptides, proteins or nucleotides. Because of mass range limitations within standard MS instrumentation, ESI is a very attractive method for the structure elucidation of macromolecules. ESI is able to produce multiple charged ions of large molecules such as $[M + nH]^{n+}$. Therefore, measurements of a m/z ration allow distribution of peaks originated from these molecules into a standard mass spectrum [113], [116].

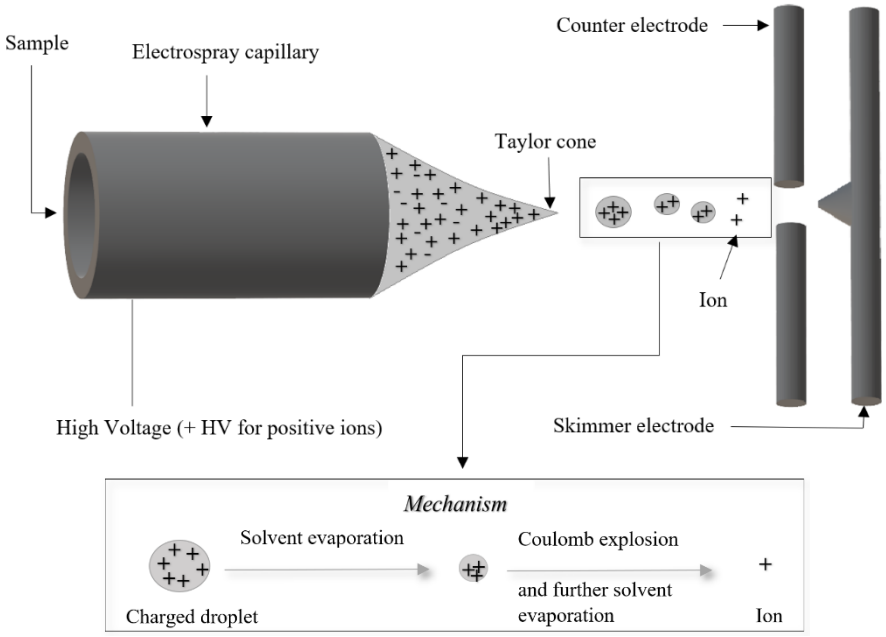

Figure 16: Schematic of ion formation in ESI.

A second fundamental principle of mass spectrometry is based on the measurement of ions generated by the corresponding ionization technique. This is associated with some requirements for mass-to-charge (m/z) analyzer, which encompasses a high vacuum in the system, an ion optic, and a detector. Typically, an ion beam coming from the ion source is diverged, and thereby, losses of ions between an ion source and an ion detector can occur. To avoid this disadvantage, different ion optics such as ion lenses, ion guides or ion funnels have already been developed. In this manner, a "compact package" of ions can reach a mass analyzes without major losses. As mentioned above, the mass-to-charge measuring system requires a high vacuum, as well. Thus, a pressure holding under 10^{-2} Pa reduces collision possibilities between the ions and facilitates undisturbed transfer of ion along its trajectory [117]. Generally, in the mass spectrometry, the ions to be investigated are always expressed as mass-to-charge ratio (m/z). The separation of ions in a mass analyzer involves an acceleration of these ions by applying of a high voltage at the beginning of the flight in a mass analyzer.

Consequently, a defined velocity (given in $m \cdot s^{-1}$) gained by an ion after the acceleration is given by:

$$\boldsymbol{v} = \sqrt{\frac{\boldsymbol{2 \cdot q \cdot U}}{\boldsymbol{m_i}}} \tag{2.3}$$

where q is the charge of an ion (given in C), U is the accelerating potential (given in V), and m_i is the mass of an ion (given in kg). The equation (2.3) is acceptable for any mass analyzer. According to this, a particle with the mass m_i flying any distance s in a vacuum field requires the time t (given in s):

$$\boldsymbol{t} = \frac{\boldsymbol{s}}{\sqrt{\frac{\boldsymbol{2 \cdot q \cdot U}}{\boldsymbol{m_i}}}} \tag{2.4}$$

In other words, the time needed to reach a detector, termed time-of-flight, depends on the mass of an ion as shown in equation (2.4) above. This relationship is thereby used at time-of-flight (TOF) mass analyzer to separate the ions indicated different m/z. Thus, the higher the molecular mass of an ion, the more time is needed to reach a detector. However, in some cases, ions with the same mass do not reach a detector at the same time, due to the kinetic energy distribution derived from the different locations during the acceleration process or various initial time-of-flight of these ions. To avoid this problem, a linear TOF analyzer has been rebuilt giving a reflectron TOF instrument [118]. To minimize the kinetic energy spread of the ions with the same mass, the reflectron redirects the path of these ions. The ions with a higher kinetic energy value fall deeper into the mirror as the less energy ions penetrating less deep into the reflectron. As the slower ions now take shorter paths and the faster ions have to move over longer distances, the time to reach the detector will be the same for both of them (**Figure 17**). Simultaneously, such a reflectron TOF instrument provides a higher mass resolution than the resolution achieved with a simple linear TOF device [113].

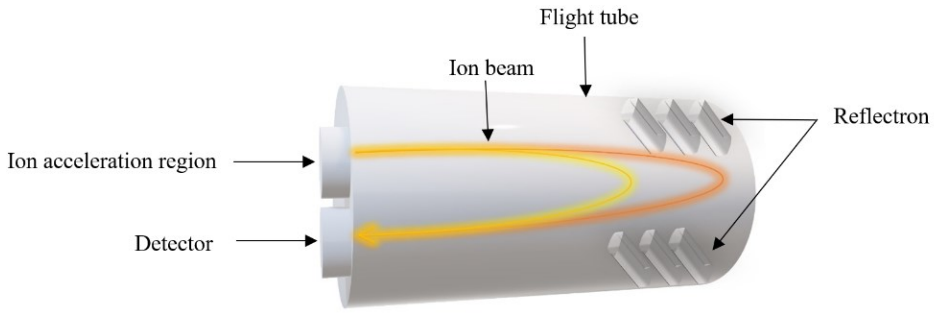

Figure 17: Schematic representation of reflectron TOF analyzer.

As stated above, reflectron TOF analyzer is able to separate isomass ions indicating a kinetic energy spread. The same advantage possesses a double focusing sector-field device (**Figure 18**). In order to separate ions with the same nominal mass, the double focusing sector-field instrument comprises both magnetic and electric fields. While the first field called magnetic sector (momentum analyzer) enables separation and direction focus of the ions with the individual m/z ratio, the second electric field (electrostatic analyzer) affects the ion beam by focusing of individual ions with similar kinetic energy and filtering out ions that have too large deviations in this energy. However, the selection of the ions with specific kinetic energy values causes decrease in sensitivity, and therefore affects the peak height reduction in a mass spectrum. Additionally, the above-described arrangement of both sectors at which magnetic sector takes the position before the electric sector, is called reverse geometry. Unlike this geometry, in forward geometry the magnet is placed after the electric sector [113], [117].

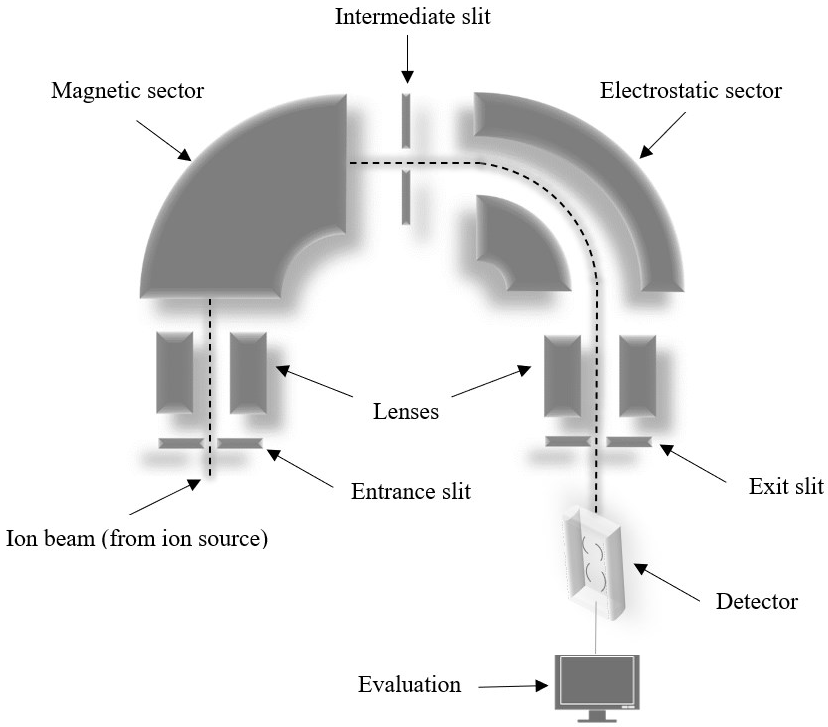

Figure 18: Schematic diagram of double focusing sector-field mass analyzer with reverse geometry.

Unlike reflectron TOF and double focusing sector-field mass analyzers at which ions are resolved *via* time-of-flight and distributed in the space according to their momentum and kinetic energy, respectively, an analytical principle of quadrupole (Q) mass analyzer is based on a stable and an unstable motion of ions between two pairs of mutually arranged electrodes to which voltages are applied (**Figure 19**). A single ion travelling through the space between four rods can pass the

quadrupole mass filter only if it remains on the stable trajectory for the adjusted parameter such as angular frequency ω, time-independent potential (DC) value U and time-dependent potential (AC) or radio frequency (RF) magnitude V. That is, ions that do not meet these requirements are accelerated at these potentials against an electrode and collide with it giving a discharged species, which are not able to be detected [113], [119]. It is worth mentioning that quadrupole is used not only as a mass analyzer, but also as a collision cell in a triple quadrupole tandem mass spectrometer (TQMS). Typically, in a MS/MS experiment the first and third sequentially arranged quadrupole are mass filter working in the same way as stated above, whereas the middle quadrupole is a dissociation cell, in which collisions with an inert gas, e.g., helium, argon, nitrogen, are performed to generate the fragment ion spectra with daughter ions originating from the parent ions detected by the first quadrupole. In brief, the daughter spectra containing typical fragmentation patterns of the compound to be investigated significantly facilitate structure elucidation, due to the availability of different data bases [113], [120], [121].

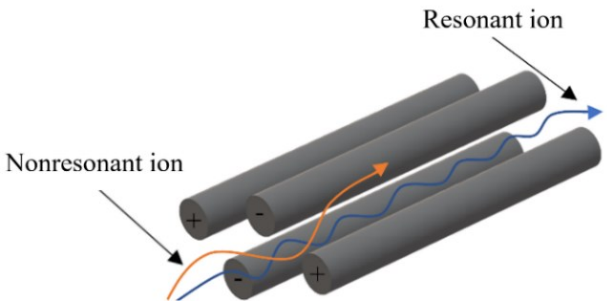

Figure 19: Schematic illustration of the behavior of different ions in the quadrupole.

An ion flown through a mass analyzer subsequently hits a detector, normally a photomultiplier. Since the ion has a certain kinetic energy, this will trigger a cascade of electrons traveling between dynodes. In this way, the kinetic energy of an ion is converted into an electric current, which is measured as follows [121]. The signals obtained at the detector are converted into a mass spectrum, which represents the dependence of the relative abundance on the physical property mass-to-charge ratio referred to as dimensionless m/z. The frequency of an ion occurrence in mass spectrum is set relative to the base peak with the highest abundance of 100% [111]. Assuming that the base peak is a molecular peak, other peaks appearing in the mass spectrum are present since a molecular peak lost a certain fragment during the ionization process. A certain m/z value belongs to each molecular peak and fragment ion peak, which has been detected as an integer nominal or exact m/z value. The benefit of an exact mass over nominal mass is that it can be used to molecular structure determination. Since structure elucidation based on the exact mass requires a resolving power of at least 1 000, the current state of the art equipment with a resolution up to 1 000 000 can solve this problem without much effort [122].

2.2.3. High-pressure liquid-solid chromatography (HPLC)

Less than 70 years after the first research on the separation of substances from biological samples by Mikhail Tswett, researcher Csaba Horváth developed the first packed columns that worked under high pressure called high-performance liquid chromatography (HPLC). This technique was a breakthrough in the history of liquid chromatography, as the method was not only faster, but also well suited for a very wide range of compounds, which could not be separated at the time using even well-developed gas chromatography [123].

Generally, the simplest HPLC system performing a chromatographic separation under high pressure must meet certain requirements. The first important module of a HPLC tower is a high-pressure solvent pump. The high-pressure means a pressure up to 420 bar at which pump works. Thus, the main task of this hardware component is the delivery of solvent mixture to a chromatographic system. Normally, from 0.1 mL to 10 mL of solvent is pressurized into the system within one minute and without fluctuations of the flow [124]. If the mobile phase has the same composition all the time during separation, simple isocratic pumps can be used. However, if a method is developed or an isocratic separation of a substance in a complex sample is not sufficient to obtain this substance, more complicated gradient compositions of a mobile phase have to be used. For this purpose, gradient systems with dual pumps have been developed, where a solvent mixture is generated under high pressure (**Figure 20**). In contrast, HPLC with a mixing valve only has one quaternary pump. Here, the previously mixed solvents with a certain composition are under low pressure and in such a state they are transferred to the pump (**Figure 21**). The advantage of such a pumping system working under low pressure is the possibility to produce complex mobile phases with even four different solvents. Nevertheless, the mixing design with a quaternary pump is not as reproducible as the dual systems and requires additional degassing due to the formation of air bubbles when mixing so many solvents [124], [125].

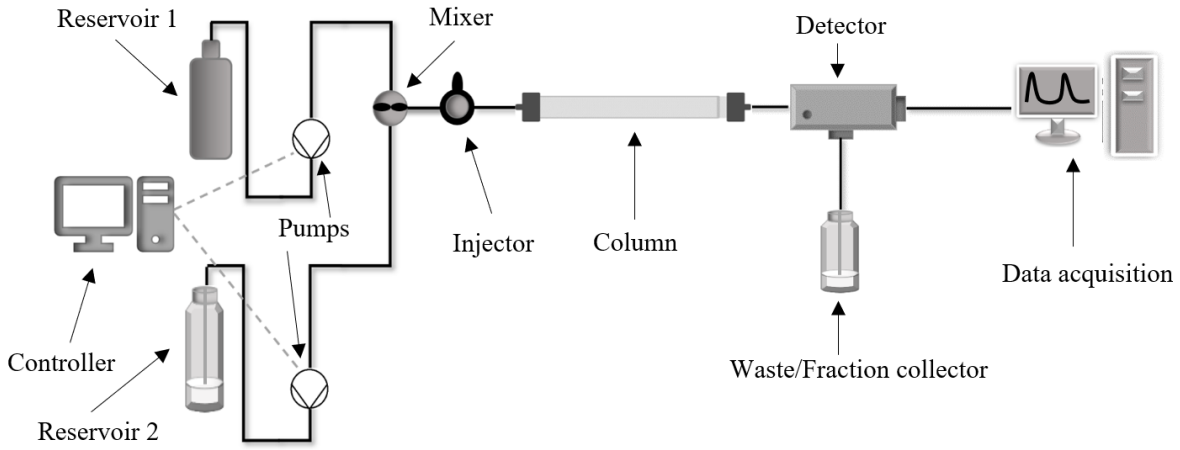

Figure 20: Dual-pump gradient HPLC system with mixing under high-pressure.

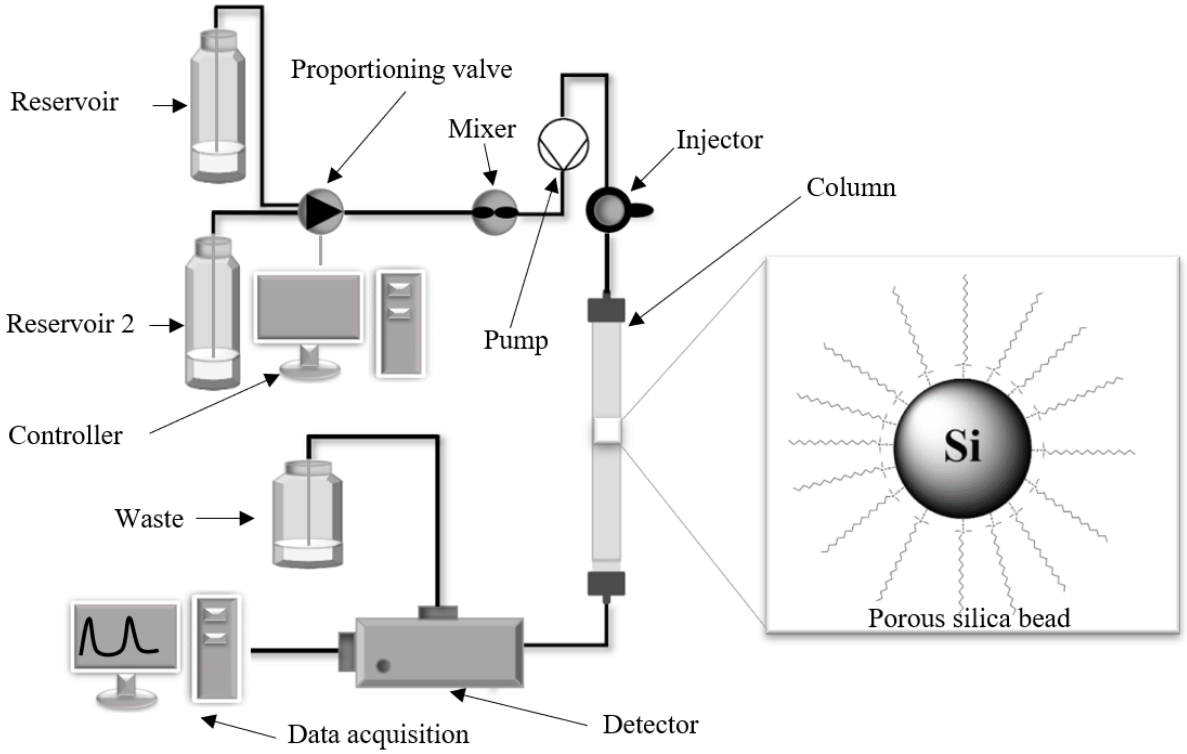

Figure 21: Gradient HPLC with pumping system working under low pressure including a closer look at C_{18} binding material at the stationary phase.

To introduce the sample to the stream of mobile phase, an injection system is necessary. In addition to the injection system, autosamplers are integrated to ensure precise sample collection from a 96-well plate as well as application of the sample to the next module of the HPLC, the column. The column is the most important module in HPLC, as it allows the separation of the different components according to their retention times and is thus useful for analytical, semi-preparative or preparative purposes. A column tube, normally constructed of stainless steel, polyetheretherketone (PEEK) or titanium material, can be packed variously depending on the desired result [124]. Common column packing materials such as silica or alumina are porous to allow interaction between the substances to be separated and the stationary phase. In order to avoid peak broadening due to the slow mass transfer of compounds into and out of the porous particles, smaller particles with a diameter of about 3.5 µm have already been developed. Another reason why the columns are packed with smaller particles is that the smaller particles result in a higher efficiency of the separation, i.e., at a high flow rate of the mobile phase height equivalent to a theoretical plate (HETP) still remains low [126]. HETP or H is perfectly explained by a fundamental chromatographic van Deemter equation (2.5), which is defined as follows:

$$\boldsymbol{H = HETP = A + \frac{B}{u} + C \cdot u} \tag{2.5}$$

where A is eddy dispersion, B is longitudinal diffusion and C is solid-liquid mass transfer resistance. Eddy dispersion correlates with different diffusion paths that two molecules can take if the column is poorly packed or particles migrate along different paths. The second independent coefficient longitudinal diffusion is described by sample self-diffusion mechanism, where the diffusion in the pores of the particle is not considered. The solid-liquid mass transfer resistance depends on the distribution of the concentrations of the same substance in the stationary and mobile phases as well as on the different diffusion paths into a porous particle. The curve represents the dependence of the ground height H on the velocity of the mobile phase u and all three independent parameters A, B and C are included in this curve (**Figure 22**). At a certain flow velocity $u_{optimum}$ the curve shows a minimum and at this point the highest efficiency of a chromatographic separation is observed, because at exactly this velocity, the height equivalent to a theoretical plate ($HEPT$) is the lowest. In addition, the value $HEPT$ or H is directly proportional to the length of the column L and reciprocally in proportion to the number of plates which is labeled as N [124], [127]. It is notable that ultrahigh pressure HPLC (UHPLC) instruments can already achieve the efficiency of 250 000 theoretical plates in less than 60 minutes [126].

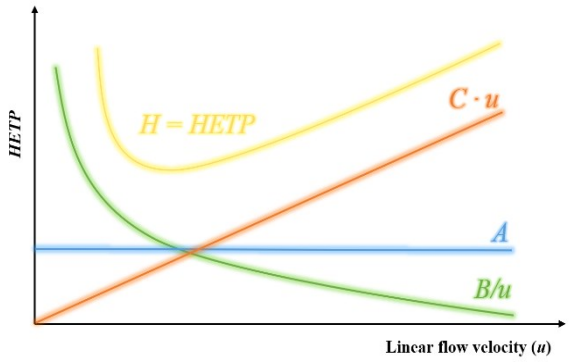

Figure 22: The van Deemter curve including full expression (H), eddy dispersion (A), longitudinal diffusion (B) and mass transfer ($C \cdot u$) curves.

Another important point of a chromatographic separation is the use of diverse column materials. There are different modes for the separation of compounds with different polarities. In particular, the two most common are normal phase liquid chromatography (NPLC) and reversed phase liquid chromatography (RPLC), although RPLC is estimated to be used in more than 70% of cases. While in NPLC the silica packing materials occur unmodified, the RPLC separation mode requires a silylation reaction followed by end-capping to attach the desired alkyl chain length or a certain functional group to -Si-OH groups. The goal of end-capping is to allow the free -Si-OH groups to react with chlorotrimethylsilane to ensure the selectivity of the chromatographic separation. For example, with RPLC not only polar and medium polar but also nonpolar compounds can be separated using a column with lower polarity binding materials such as octadecyl (C_{18})-, phenyl- or octyl (C_8). In this case, since

the solvents with reversed polarity are required for elution, a mobile phase normally contains water, acetonitrile, or methanol [124], [128].

The last module of a HPLC configuration to be discussed is the detector. The commonly used detectors in HPLC are UV/Vis absorbance (UV/Vis), photo diode array (PDA), fluorescence (FI) and mass spectrometry (MS) detector. These detecting modules do not only differ in their selectivity but also in their sensitivity. A fluorescence detector is one of the most sensitive and selective detectors. Here, only substances with specific fluorescent properties can be detected. It is remarkable that the sensitive detector is able to analyze the substances in even femtogram (fg) to picogram (pg) range. The fluorescence detection is done with the help of a xenon flash lamp that sends the beam onto a monochromator and passes it through a cell. Consequently, from the cell where the sample is located, an emission beam is sent, which passes through an emission monochromator and ends up in a photomultiplier. Detection with a mass spectrometer is also characterized, like fluorescence detection, by high specificity and sensitivity (fg-ng). Nowadays, the connection of the LC system from which a condensing liquid comes out with the vacuum of an MS device is no challenge at all. The most common ionization methods and mass analyzers of mass spectrometry have already been described in the chapter 2.2.2. In order to detect a substance with a UV/Vis detector, the substance needs to have absorbing properties in the UV and visual range of the light. The light is generated in a deuterium lamp and strikes a movable monochromator. A beam with a specific wavelength is sent through an exit slit onto the sample, which is placed in a measuring cuvette. The analyte concentration c (given in $mol \cdot m^{-3}$) is then determined using Lambert-Beer's law as shown in equation (2.6) below:

$$\boldsymbol{A = \varepsilon \cdot c \cdot d} \tag{2.6}$$

where A is absorbance, ε is molar absorption coefficient (given in $m^2 \cdot mol^{-1}$) and d is the layer thickness of the cuvette (given in m). Unlike the UV/Vis detector, in a photodiode array (PDA) detector, the light beam generated by the deuterium lamp first passes through the cuvette and then hits the monochromator. The monochromator splits the entire spectrum into individual wavelengths which are detected by the diode array and produce a spectrum with a resolution of 1 nm. Since a spectral range is acquired during a single measurement process, the PDA can be used to detect impurities within a chromatographic peak [124], [129].

3. Results and discussion

3.1. Synthesis

To gain the eight fatty acids-amino acid conjugates (FACs) **1d**, **3b**, **5c**, **6c**, **7c**, **8c**/**8d**, **9b** and **11e**/**11f**/**11g**, a method according to Itoh *et al.* was considered. In this case, an amide-forming reaction was involved, in which **1b**, **3a**, **5b**, **6b**, **7b**, **8a**/**8b**, **9a** and **11b**/**11c**/**11d** were condensed with L-glutamine (**1c**) *via* the corresponding anhydrides (generated from fatty acids and pivaloyl chloride) [56]. On the other hand, Fox *et al.* approach led to the formation of the three FACs **2b**, **4b** and **10b**. Herein, a fatty acid chloride reacted with L-glutamine in the presence of a base to form a L-glutamine derivative [130]. At the end of this chapter is **Figure 25** providing an overview of all the synthesized compounds.

End products purified by chromatography column or by recrystallization were injected to ESI ionization in either positive or negative ion mode. In all synthesized compounds analyzed using TOF as mass analyzer $[M + Na]^+$ ions were formed. Nearly all FACs except **3b** could also be analyzed in ESI-MS as $[M + H]^+$ ion adduct in positive mode. Other ions determined using this spectrometric method included $[M + K]^+$, $[2M + Na]^+$, $[2M + H]^+$, $[M + 2Na – H]^+$ and $[M + H + K]^{2+}$ as well. MS analysis in negative ionization mode enabled detection of $[M – H]^-$ and $[2M – H]^-$ ion adducts for compound **1d**. Moreover, it could be seen that the Na^+ adducts are the most common ions detected. In the case of **1d**, **2b**, **3b**, **4b**, **6c**, **7c**, **8c**/**8d**, **9b**, **10b** and **11c** they were even the most abundant ions in mass spectrum. The formation of sodium adducts in ESI is based on electrostatic interactions of positively charged sodium atoms with negative partial charges on oxygen atoms of the mentioned molecules [74], [131]. These species are formed when the solvents such as water or acetonitrile have impurities or glass vessels are used [132]. Since the samples were dissolved in a mixture of acetonitrile, methanol and 1% water before ESI-MS measurement and were also stored in glass vials after the synthesis, it can be determined that the two components could have an effect on the formation of above stated $[M + Na]^+$, $[2M + Na]^+$and $[M + 2Na – H]^+$ ions in the ESI processes.

Using negative ion mode in ESI, the detection of compounds such as flavonoids, iridoids or coumarins have already been reported [133]. By applying a high negative voltage (- 4.5 kV) in the soft ionization technique, which is ESI, two negatively charged ions were formed at compound **1d**, which are $[M – H]^-$ (at m/z 329.2089) and $[2M – H]^-$ (at m/z 659.4247). This confirms that hydroxylated FACs can also be ionized at the negative voltage.

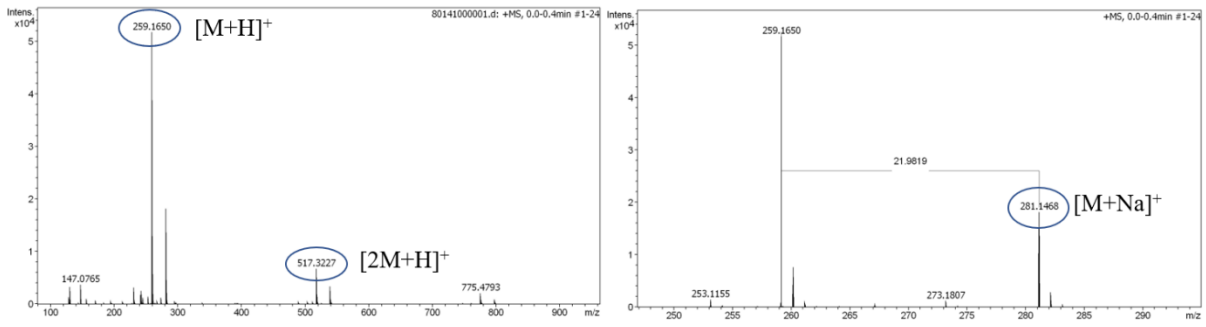

Figure 23: ESI-HRMS spectrum of compound **5c**.

Further analysis of the synthetized FACs was conducted *via* ^{1}H-NMR and ^{13}C-NMR spectroscopy. In order to verify that the compounds produced are the desired ones, the values of the shifts in ^{1}H-NMR spectrum from the literature were considered (**Table 1**). Itoh *et al.* have reported the shift of two hydrogen atoms in the 2′ position, located at 4.38 ppm [56]. In this ppm range, the values for the ^{1}H-atoms from the same position in the structure could also be found for all synthetized compounds except compound **4b**, which revealed a shift at 4.12 ppm (chapter 6). Nonetheless, almost the same chemical shift viz. 4.11 ppm appeared in *Fox et al.* [130]. To verify whether the reaction of amide formation between the L-glutamine and a given fatty acid worked well, exactly these ^{1}H-atoms (H-2′), which are in the α-position of the amino acid, were taken into consideration. Thus, it has been reported that the chemical shift of α-^{1}H atom in L-glutamine equals 3.78 ppm [134]. Here, H-2′ showed an increasing of a chemical shift due to the coupling of L-glutamine with a fatty acid, which could be confirmed by the shifts appearing in the range from 4.12 ppm to 4.63 ppm in ^{1}H-NMR spectra (chapter 6). The presence of oxygen atoms in the carboxyl group of the fatty acid moiety reduces the electron density in adjacent nuclei causing the previously mentioned trend.

The two non-equivalent ^{1}H-atoms in position 3′ resulted in two multiplets, doublet of doublet of triplets or doublet of triplet of doublets with the shifts in the literature-like ppm-ranges, 1.91 – 1.98 ppm as well as 2.14 – 2.30 for 3′a and 3′b protons, respectively [56]. The exception was in turn compound **4b** with the shifts at slightly lower ppm ranges, as can be taken from chapter 0. However, when the two chemical shifts are compared with the literature values found in *Fox et al.*, no clear differences can be observed (**Table 1**) [130]. Additionally, the two 3′-protons were associated with the same carbon atom, which was confirmed by a 2D-NMR spectroscopy. Indeed, HSQC-spectra of FACs revealed correlations between 3′-carbons and its attached protons, which verifies that the 3′a and 3′b belong to the same ^{13}C-atom.

When comparing the chemical shifts of H-4′ atoms of each synthesized compound (chapter 6), it can be seen that they are close to the literature values (**Table 1**) [56]. Only compound FAC **11** stands out with the slightly higher shifts, which are in the range of 2.57 to 2.59 ppm.

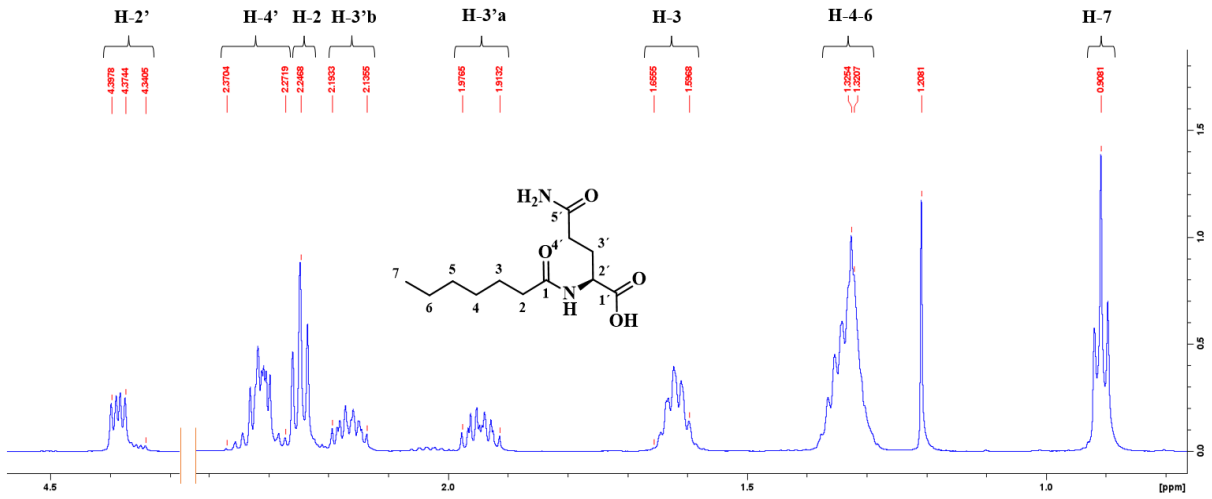

Figure 24: [1]H-NMR spectrum of compound **5c**.

Table 1: Literature data of chemical shifts of L-glutamine moiety of volicitin and (S)-*N*-α-undec-10-enoylglutamine in [1]H-NMR spectra. TMS as an internal standard was used for both spectra. Volicitin was dissolved in CD_3OD for the recording of [1]H-NMR spectrum. [1]H-NMR of (S)-*N*-α-undec-10-enoylglutamine was recorded in deuterated DMSO as solvent [56], [130].

position of H-atom in L-glutamine moiety	**δ according to Itoh *et al.* [56] (ppm)**	**δ according to Fox *et al.* [130] (ppm)**
H-2′	4.38 (1H, dd, *J* = 5.0, 9.0 Hz)	4.11 (1H, ddd, *J* = 5.0, 8.0, 9.0 Hz)
H-3′a	1.90 – 1.99 (1H, m)	1.71 (1H, dtd, *J* = 6.5, 9.0, 14.0 Hz)
H-3′b	2.12 – 2.20 (1H, m)	1.90 (1H, dtd, *J* = 5.0, 8.0, 14.0 Hz)
H-4′	2.27 – 2.35 (2H, m)	2.05 – 2.12 (2H, m)

Due to the high specificity of the oxymercuration-demercuration reaction, a similar compound to volicitin denoted as **1d** could be synthesized (chapter 6.1). The similarity includes a hydroxy group located in the penultimate position of the carbon atom in the fatty acid moiety. To investigate the effectiveness of this reaction, both 1D- and 2D-NMR methods were used. The desired introduction of the hydroxyl group into undec-10-enoic acid moiety was confirmed with the presence of a triplet of quartet (tq) at 3.70 ppm in [1]H-NMR spectrum as well as shift of the C-10 atom at 68.7 ppm in [13]C-NMR spectrum. In addition, a cross peak in COSY spectrum showing the neighborhood to the three

H-11 protons shifted at 1.14 ppm as doublet was observed (**Figure 26**). The residues from the unreacted starting material, which was the undec-10-enoic acid moiety, were also seen in ^{1}H-NMR spectrum, confirmed by the peaks at 4.91 ppm, 4.98 ppm, and 5.81 ppm, they were, however, negligible [130].

The results of the acylation with acyl chlorides could also be monitored by NMR spectroscopy. Friedel-Crafts acylation of two alkenes such as octadec-9-enoic acid (**3a**) and undec-10-enoic acid (**1a**) gave a mixture of α,β- as well as β,γ-unsaturated linear and branched products **8c**/**8d** and **9b** possessing keto groups, as can be seen in chapter 0 and 6.9. Therefore, the distinctive points of the desired acylation of unsaturated fatty acids with acyl chlorides would be signals in ^{13}C-NMR showing the high shifts above 200 ppm occurring after the insertion of a keto group, as could be seen in the successful results of Biermann and Metzger [99]. Unfortunately, no signals above 200 ppm were detectable, which does not necessarily mean that the reaction did not work. To prove that it was indeed the desired product, shifts originating from the carbon atoms, which were adjacent to the keto groups of the compounds **9b** and **8c/8d**, could also be used. The shifts of the corresponding carbon and hydrogen atoms taken from the literature and the ^{1}H-NMR and ^{13}C-NMR measurements are given in the **Table 2**. It is apparent that the shifts of the **9b** compound resulting from the ^{13}C-NMR measurements did not show any significant differences. Meanwhile, in the ^{1}H-NMR spectrum of **9b**, slightly higher shifts of the hydrogen atoms were detected, when compared with the literature values of (*E*)-12-oxoheptacos-9-enoic acid [99]. Further examination of the NMR spectra of compounds **8c/8d** allows conclusions to be drawn that the shifts of both hydrogen and carbon atoms from positions 9/10 and 2′′ are almost indistinguishable from the published values for rac-(*E*)-9-(1-oxoheptyl)-octadec-10-enoic acid and rac-(*E*)-9-(1-oxoheptyl)-octadec-8-enoic acid (**Table 2**) [99].

Table 2: Literature ^{13}C- and ^{1}H-NMR data of chemical shifts of (*E*)-12-oxoheptacos-9-enoic acid as well as (*E*)-9-(1-oxoheptyl)-octadec-10-enoic acid and (*E*)-9-(1-oxoheptyl)-octadec-8-enoic acid compared to the values from the compounds **8c/8d** and **9b**.

position in 8c/8d or 9b	**δ according to Metzger *et al.*** [99]		**δ measured for 8c/8d**		**δ measured for 9b**	
	^{1}H-NMR (ppm)	**^{13}C-NMR (ppm)**	**^{1}H-NMR (ppm)**	**^{13}C-NMR (ppm)**	**^{1}H-NMR (ppm)**	**^{13}C-NMR (ppm)**
9/10	3.00 (1H, m)	56.7	2.98 – 3.00 (2×1H, m)	56.8	-	-
2′′	2.45 (2×2H, m)	41.3	2.29 – 2.55 (2×2H, m)	41.5	-	-
11	2.84 (2H, d, *J* = 6.9 Hz)	46.8	-	-	3.07 – 3.10 (2H, m)	46.9
13	2.09 (2H, t, *J* = 7.2 Hz)	42.2	-	-	2.38 – 2.42 (2H, m)	42.5

However, for the compounds **8c**/**8d** no shifts above 200 ppm could be found, it is reasonable to assume that the FACs **8c**/**8d** dissolved in deuterated chloroform are responsible for the formation of the micelles, since the substance possesses lipophilic properties and the presence of traces of impurities such as sodium or other cations could not be excluded. For this reason, many significant signals were suppressed and both ^{1}H- and ^{13}C-NMR spectra gave relatively poor information regarding shifts of ^{1}H and ^{13}C nuclei, respectively. Nevertheless, with the aid of ^{1}H-NMR spectrum, an H-9 signal with a shift of 2.99 ppm was detected, thereby indicating the successful synthesis of the desired products **8c**/**8d**.

The last compounds to be mentioned are FACs **11e**/**11f**/**11g** synthesized by the procedure of Biermann and Metzger [99]. Following the successful acylation of undec-10-enoic acid (**1a**) with octanoyl chloride (**10a**), a further method of Grahame *et al*. was applied to obtain a mixture of hydroxylated fatty acids **11c**/**11d**, which could be then coupled to the amino acid L-glutamine (**1c**) by Itoh *et al.* experimental procedure giving the desired FACs **11e**/**11g** [56], [135]. Compound **11f** could also be found in the mixture of FACs signaling that the sodium borohydride reduction of ketone **11b** was incomplete and this intermediate product as ketone as well as hydroxylated compounds **11c** and **11d** were implemented in the next step giving the mixture of the end products **11e**/**11f**/**11g**. In common with all synthesis products, this one was also purified by column chromatography. However, the results were unsatisfactory, since neither the mixture could be separated into individual compounds nor unwanted **11f** was removed as ketone. To yield a pure product, further optimization of the reaction steps and column chromatographic separation would be recommended for future research.

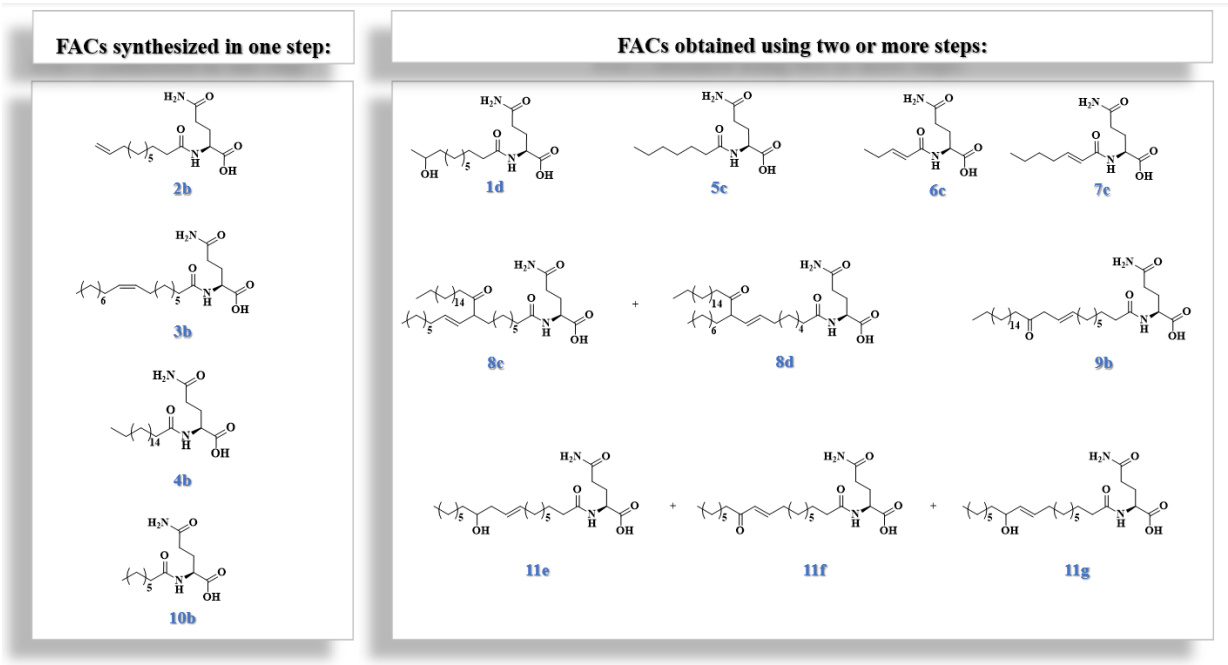

Figure 25: Overview of the synthesized FACs.

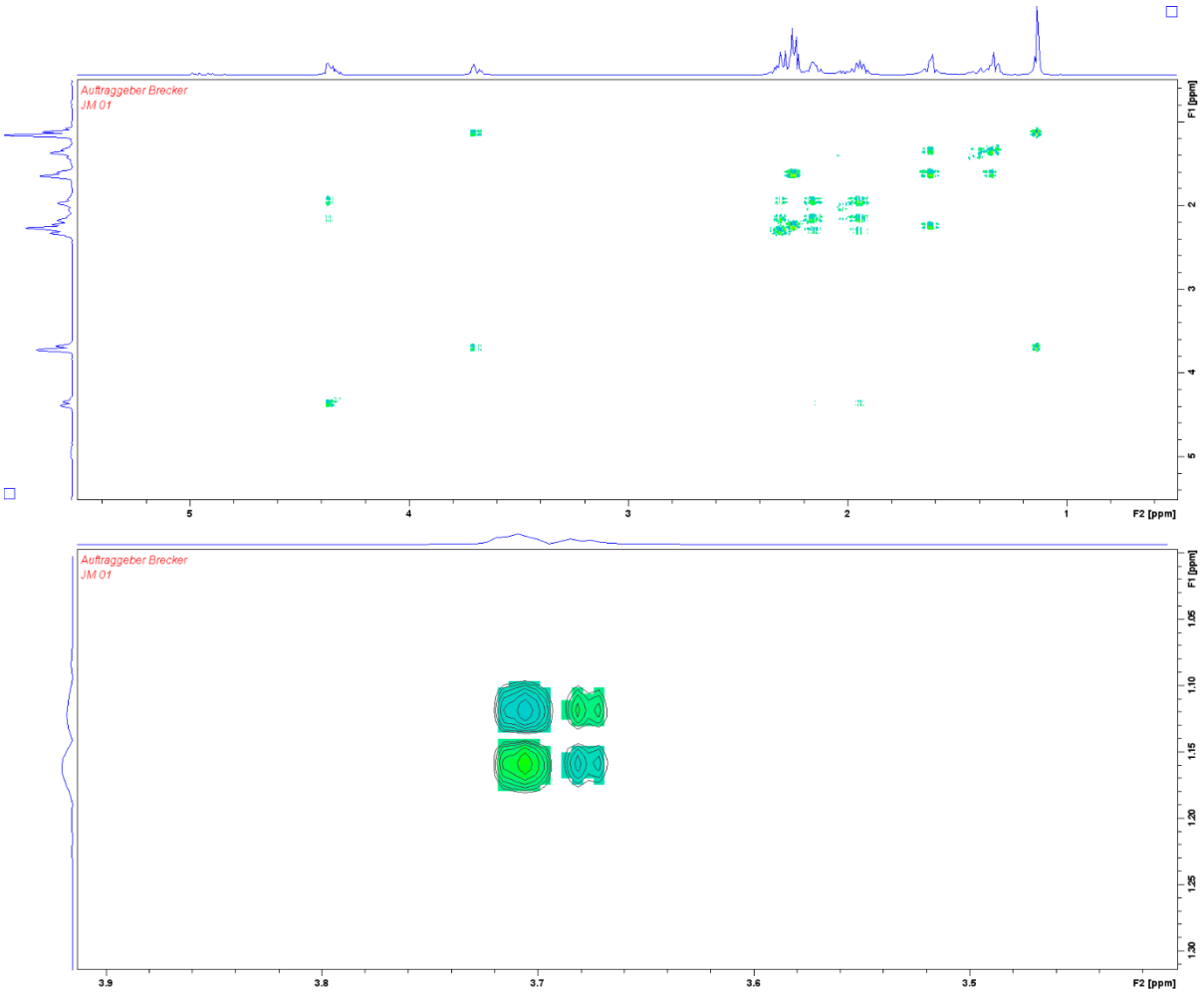

Figure 26: COSY spectrum of compound **1d**.

3.2. *Vinca minor* experiments

Vinca minor as a source of a wide monoterpenoid indole alkaloid (MIA) spectrum offers an excellent opportunity for various research purposes [68]. In this work, one of the vinca alkaloids vincamine isolated from the leaves of periwinkle after the treatment with the previously synthesized fatty acid-amino acid conjugates (FACs) was a goal of the investigation. As outlined in chapter 1.3, the environment factors such as light or mechanical wounding provoke the plant to produce higher amounts of MIAs [72]. Accordingly, the important representative of MIAs such as vincamine seems to be more concentrated during stressful situations for the plants. However, season, growth phase or climate are as well common contributors to these changes, so it is not easy to specify exactly which of the aforementioned factors is responsible for the change in vincamine levels in *V. minor* [136]. Therefore, the experimental values, more precisely, the calculated concentrations of vincamine were referred relatively to the control values originating from the plants, which were neither artificially wounded nor treated with any synthesized substance or solvent. The HPLC method is well suited for this purpose, since not only the retention times for the identification of the vincamine but also the peak area for the quantification could be accomplished by this method. The HPLC-chromatogram in **Figure 27** reveals two main peaks corresponding to the vincamine with a retention time t_R = 14.4 min and an unknown compound (here: vincaminic acid) with a retention time t_R = 7.9 min, which was further elucidated *via* tandem mass spectrum (MS/MS spectrum).

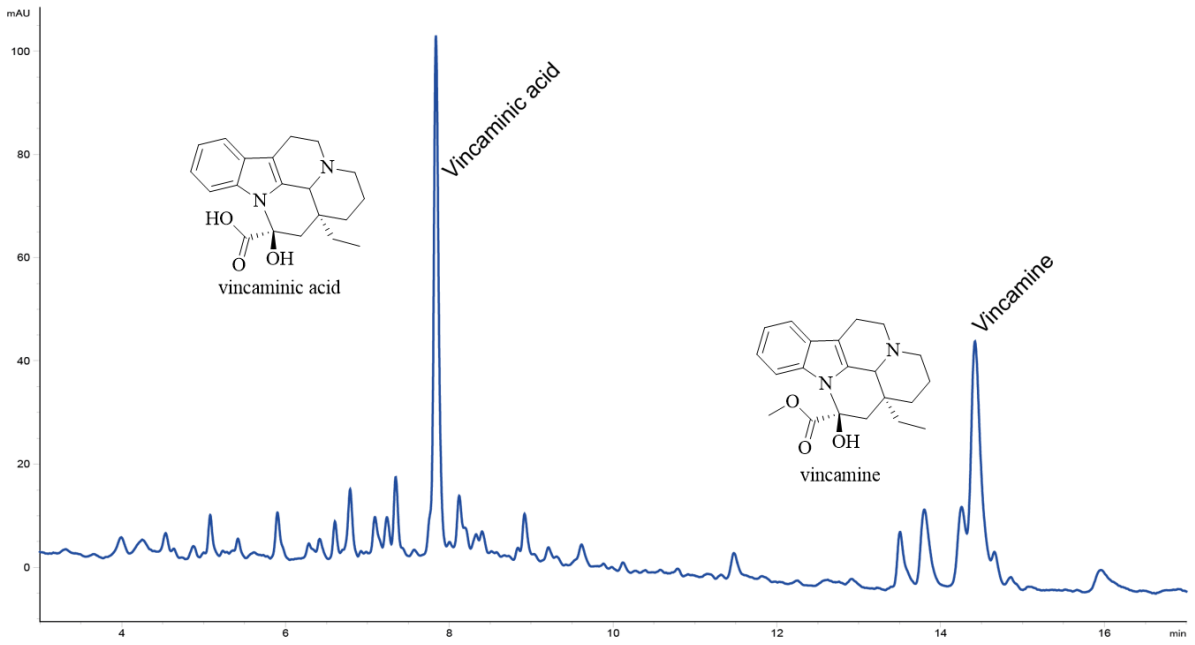

Figure 27: HPLC separation of natural products in *V. minor*.

When checking HR-ESI-MS spectrum displayed in **Figure 28** (the spectrum above), a protonated molecular ion $[M + H]^+$ at *m/z* 341.1856 in positive ion mode could be detected. Moreover, the MS^2 fragmentations of this compound produced a few peaks in positive ion mode (**Table 3**). Occurrence of the fragment ion at *m/z* 323.1747 indicated the loss of water. The cleavage of H_2O and formation of an ion $[M + H - H_2O]^+$ was already reported for vincamine [137]. A further examination of the product ions obtained after the MS/MS experiment leads to the conclusion that the unknown compound under investigation is a bioactive monoterpenoid indole alkaloid (MIA). This could be confirmed by the presence of characteristic fragment ion at m/z 144.0802, which was also detected at ajmaline, yohimbine and ajmalicine due to retro Diels-Alder (RDA) reaction [138]. In addition, a fragment ion at *m/z* 144.0802 indicated an indole moiety resulting from the detachment of a terpene unit from the parent ion $[M + H]^+$, in which the bond between the carbon atom at position 14 and the nitrogen atom at position 1 was cleaved [139]. Since a reversed phase C_{18} column was used for the HPLC separation and the unknown compound eluted earlier than vincamine, this may indicate that the compound possesses more polar properties than vincamine. For the increase in polarity of the compound being explored, the $-CH_3$ group of C-22 could be exchanged for an -OH group indicating that the compound being sought is the vincaminic acid. The corresponding fragmentation of vincaminic acid according to MS/MS data is displayed in **Figure 29**. As can be seen from the previous studies, a further product ion found at *m/z* 297.1956 was also present after UHPLC-MS analysis of yohimbine-like compound. However, the fragment was designated as an "extra ion" that caused for the distortion of the MS spectrum there [137].

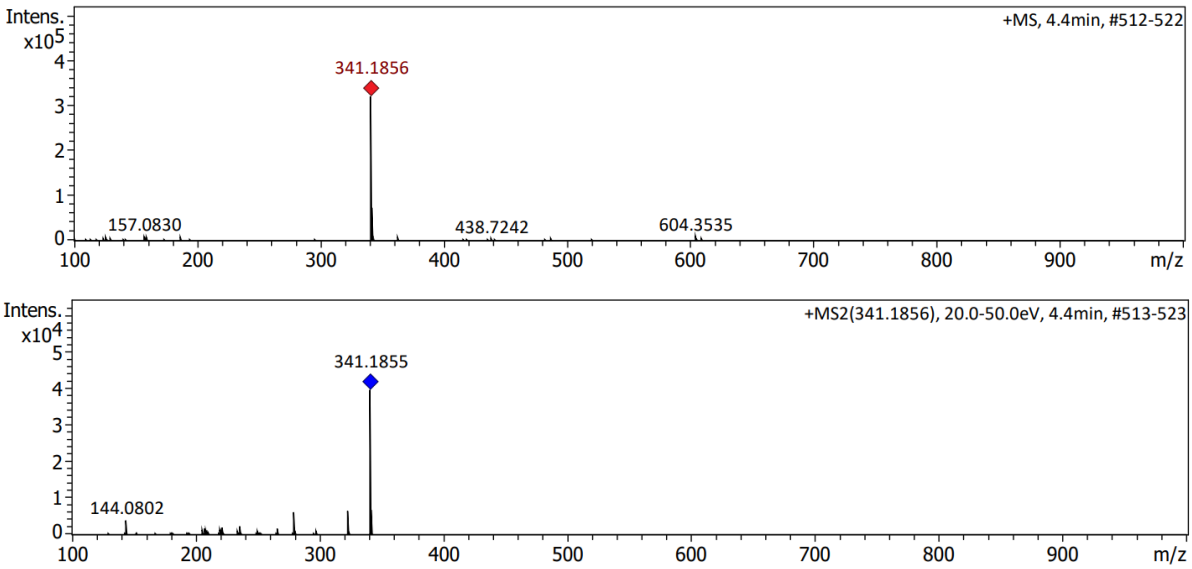

Figure 28: HRMS-ESI-MS spectrum with molecular ion (above) as well as MS/MS spectrum (below) of putative vincaminic acid.

Table 3: MS/MS data after fragmentation of putative vincaminic acid in positive ion mode.

measured *m/z* of fragments	ion formula	calculated *m/z*
144.0802	$C_{10}H_{10}N$	144.0808
206.0959	$C_{15}H_{12}N$	206.0964
220.1114	$C_{16}H_{14}N$	220.1121
236.1430	$C_{17}H_{18}N$	236.1434
266.1165	$C_{17}H_{16}NO_2$	266.1176
279.1850	$C_{19}H_{23}N_2$	279.1856
297.1956	$C_{19}H_{25}N_2O$	297.1961
323.1747	$C_{20}H_{23}N_2O_2$	323.1754

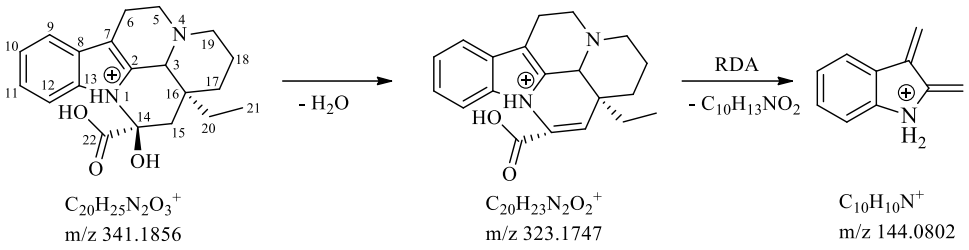

Figure 29: Fragmentation of vincaminic acid according to MS/MS data.

In order to determine the concentration of vincamine, a calibration curve displayed in **Figure 30** was required. The calibration was carried out after HPLC analysis involving absorption measurement of vincamine standards (standards concentrations: 29.6 µg/mL, 74 µg/mL, 148 µg/mL and 296 µg/mL) at λ = 230 nm. The absorption values were additionally referred to an internal standard with a concentration of 300 µg/mL. A high coefficient of determination (R^2 = 0.9995) of the trend line allows the conclusion that the regression line fits the data well and is therefore an appropriate tool for the evaluation of vincamine concentrations.

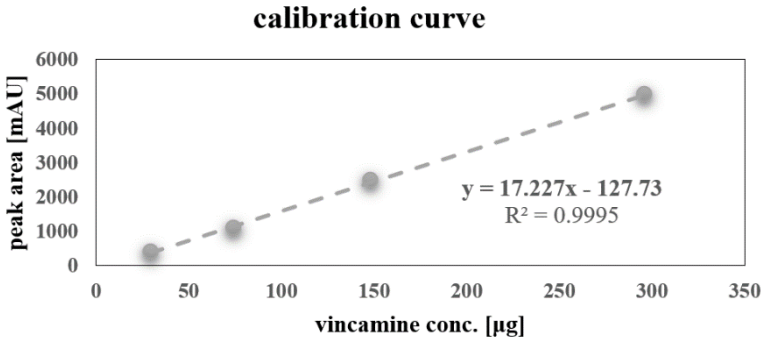

Figure 30: Calibration curve presenting the vincamine concentration in x axis and peak area in y axis.

.

Based on the calculated concentrations of vincamine in untreated *V. minor* leaves used as a control as well as after a caterpillar *Spodoptera littoralis* attack (**C**), an artificial wounding (**A**), a treatment with the solvent (**B**) or synthesized FACs termed **1d**, **2b**, **3b**, **4b**, **5c**, **6c**, **7c**, **8c**/**8d**, **9b** and **10b**, relative changes of vincamine levels were determined. For this purpose, the identified concentrations of vincamine in treated plants were divided by the values of the untreated ones. Consequently, relative vincamine concentrations stated in % were plotted in boxplot diagrams (**Figure 31**). Since the included outliers make it difficult to illustrate the differences between individual boxplots, a range of the y axis between 0 and 270 % was selected in the software program RStudio, and then a new zoomed-in diagram with the outliers hidden but included was created as presented in **Figure 32**.

Surprisingly, the relative vincamine concentration pattern of plants treated with the FACs **3b**, **6c** and **8c**/**8d** was different from the periwinkle leaves treated with **1d**, **2b**, **4b**, **5c**, **7c**, **9b**, **10b**, **A**, **B** and **C**. Especially the effects of the treatment with **6c** stood out clearly as shown in **Figure 32**. Thus, it was decided to repeat the experiments with exactly these substances in order to obtain more data points. Following this, a new zoomed-in diagram with corresponding boxplots was compiled (**Figure 33**). However, in this case the relative vincamine concentrations were determined after treatment with FACs **1d**, **2b**, **4b**, **5c**, **7c**, **9b** and **10b**, as well as **A**, **B**, **C** in the triplicate and the additional experiments with **3b**, **6c** and **8c**/**8d** added more data points, more specifically the re-experiment yielded 13 relative concentration values per treating substance.

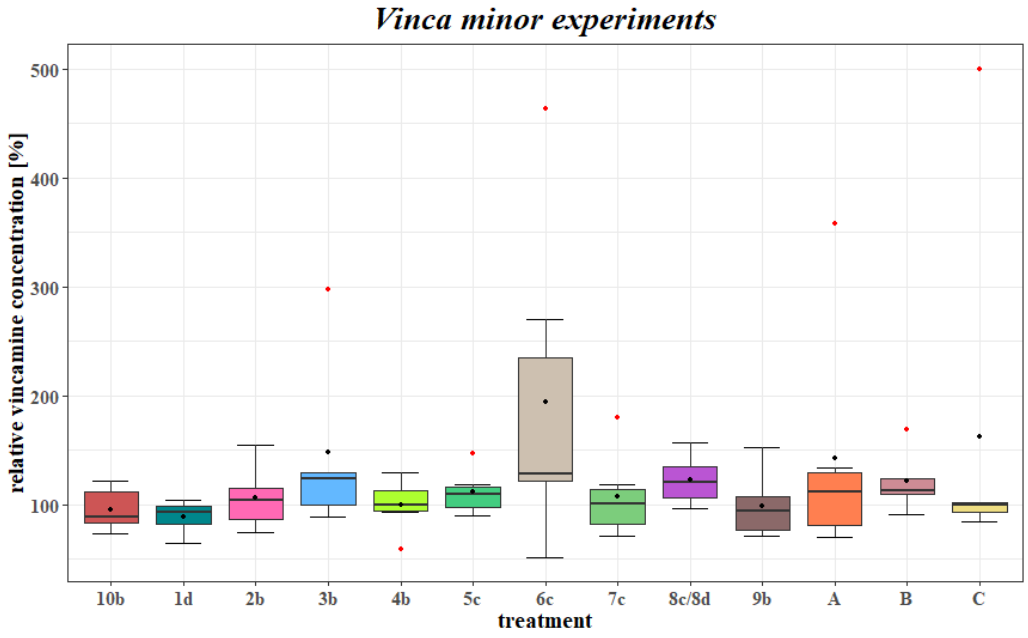

Figure 31: Relative vincamine concentrations after the treatment of *V. minor* in the triplicate. The black dots denote the calculated mean values of the relative vincamine concentrations, and the red dots indicate outliers.

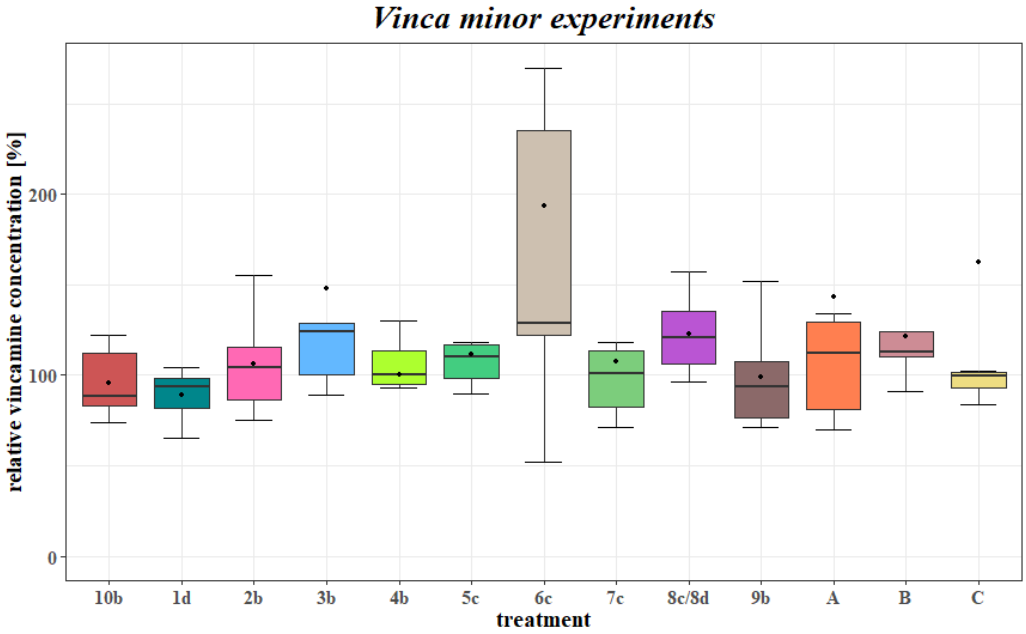

Figure 32: Zoomed-in diagram of the relative vincamine concentrations after the treatment of *V. minor* in triplicate.

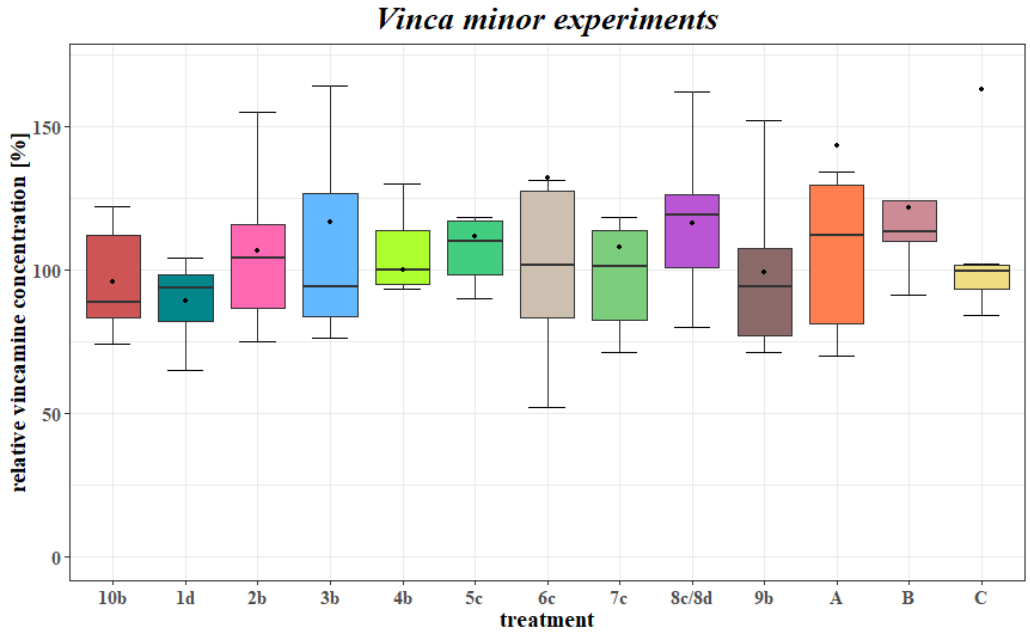

Figure 33: Zoomed-in diagram of relative vincamine concentrations including triplicate experiments with **1d**, **2b**, **4b**, **5c**, **7c**, **9b**, **10b**, **A**, **B** and **C**. In the case of **3b**, **6c** and **8c/8d** more data points for the generation of the boxplots were used.

In order to investigate whether biosynthetic pathways towards the synthesis of vincamine after 24 h, 48 h, 72 h or 6 d were induced, additional experiments were required. According to this, *V. minor* plants were treated with the substance **6c** and the leaves (three replicates for each treatment) were harvested at first, second, third and sixth day from the beginning of the treatment. In order to better illustrate the decrease in relative vincamine concentrations, the medians of the respective boxplots were connected by a dashed line (**Figure 34**).

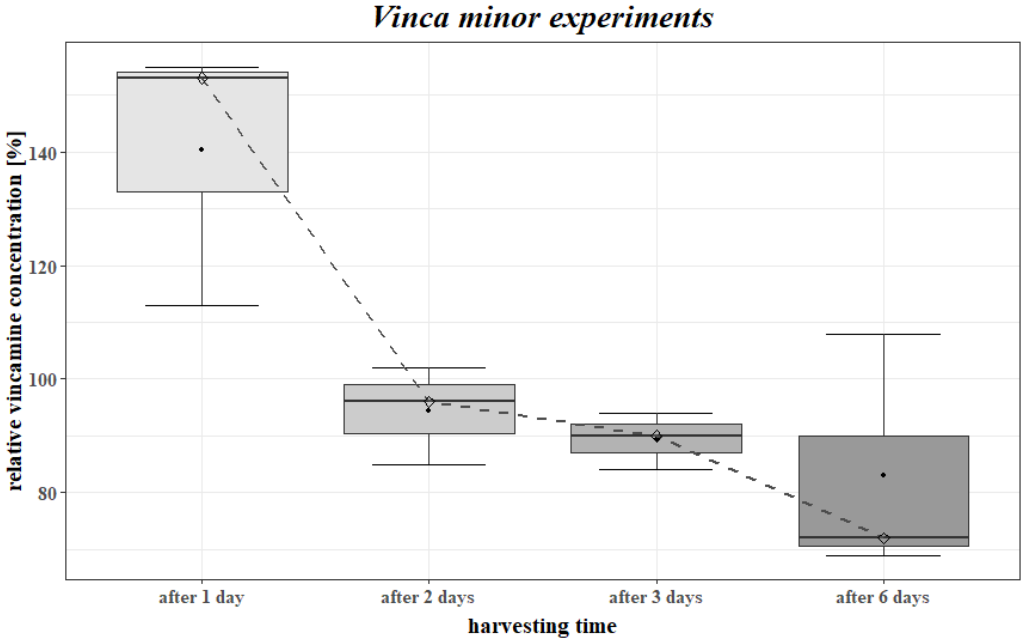

Figure 34: Relative concentration of vincamine in *V. minor* after a certain harvesting time.

In general, metabolism of MIAs is strongly dependent of various biotic and abiotic situations to which a plant is exposed. As discussed in detail in the previous chapter 1.3, there are a variety of factors that stimulate plant defense mechanisms to protect themselves. Especially light, UV, mechanical wounding, herbivore, salt concentration, high temperatures as well as nutrient such as sulfur deficiency could affect the accumulation of these specialized metabolites [68], [72]–[75]. According to this, the content of alkaloids in periwinkle seems to be higher when the plant grows in the sun [140]. Whereas the described biotic and abiotic stress factors are a prominent trigger of the increase of the vincamine concentration, it is worth mentioning that the time season, flowering time, or growth conditions also could contribute to the gene expression of the enzymes involving in MIAs pathway (**Figure 36**) [136], [141].

Indeed, to distinguish which of the above factors had an influence on the *V. minor* at the given time and climate conditions was nearly impossible within the scope of this work. In addition, the experiments were carried out in the vegetation period of periwinkle and the outdoor temperatures mostly showed above 30 °C. Therefore, the consideration of abiotic stresses such as treatment with the previously mentioned synthesized FACs that force plants to produce an array of different defense

substances was only feasible by studying the values set relative to the control plants. Only in this way could conclusions be drawn about the effects of the substances on plant defense strategies.

The results presented in this work indicate an enhancement of production of bioactive compound such as eburnamine-type MIA vincamine. Surprisingly, the quantitative analysis of the content of this alkaloid after the treatment with synthesized FACs demonstrates alterations of biochemical fluxes of treated plants harvested at the appointed times. For instance, the relative concentration of vincamine 8 d after the application of the substance **6c** increased significantly as showed in the **Figure 32**. While the relative amount of vinca alkaloid after the treatment with **3b** or **8c**/**8d** might indicate increased production of vincamine in stressed leaves of *V. minor*, the plant defense strategy after the application of the FAC **6c** containing short-chain fatty acid moiety (five carbon atoms) seems to be massively induced. Subsequently, a twofold higher vincamine concentration was observed in the treated leaves when compare to the blank leaves. In contrast, plants treated with caterpillars *Spodoptera littoralis* and FAC **1d** showed no significant changes in relative vincamine concentrations. Therefore, these results were not in agreement with the publication of Alborn *et al.*, which have demonstrated that the FAC called volicitin isolated from oral secretion of beet armyworm (BAW; *Spodoptera exigua* Hübner) caterpillars contributed to the indirect defense strategies of plants. Volicitin possessing a hydroxyl group in position 17 of the fatty acid chain triggers an elicitor activity [49]. In order to investigate whether a similar functionalized fatty acid is characterized by the same properties, in the scope of this thesis a fatty acid moiety with the hydroxyl group in the next to last position of the carbon chain was synthesized and applied in the form of a FAC **1d** to *V. minor* in triplicate. Since regurgitate investigation of larvae of the Egyptian cotton leafworm (*Spodoptera littoralis*) also revealed volicitin, these caterpillars were applied to the plants but only for 2 to 3 h [96]. Subsequently, the plant extracts were analyzed for the amounts of vincamine and compared with other treatments. As mentioned above, no significant changes in vincamine level in periwinkle leaves were declared after treatment with volicitin-like substance **1d** and volicitin from caterpillar saliva. Instead, it can be suggested that compound **6c** has a stronger triggering potential than volicitin, as it caused much more potent effects on *V. minor* metabolism toward the biosynthesis of MIAs. Furthermore, with regard to the results shown in **Figure 32**, it can be said that the treatment of the plants under study with **2b**, **4b**, **5c**, **7c**, **9b**, **A** and **B** did not provide significant differences with respect to the control plants, as the relative vincamine concentrations totaled approximately 100 %.

Recent study of evergreen herbaceous shrub *V. minor* towards the MIA pathway elucidation has contributed greatly to the scientific research of this plant. With the aid of transcriptomics and gene co-expressions analysis further lacking steps of the biosynthesis of MIAs in *V. minor* could be discovered (**Figure 5**) [68]. Nevertheless, the understanding of MIAs pathway up- or down-regulation in response to environmental factors in Apocynaceae is still insufficient. Although a large number of gene-encoding enzymes, transporters as well as regulators involved in this biosynthetic pathway have been elucidated in recent years, the combination of stress factors and their effect on MIA accumulation is

nowadays not fully understood [142]. It is worth mentioned that many sophisticated studies are still needed in the near future to elucidate the complete vincamine biosynthetic pathway and the combined influences from the environment affecting this pathway. Liu *et al.* suggested that the results of the impact of individual stress factors on plants have been better studied to date than the combined ones [142]. However, if taking a well-known plant hormone methyl jasmonate (MeJa) as a single stress factor into account, various contradictory effects of the modulation of MIA pathway could be compiled, as it will be demonstrated in the following [139].

MeJA as a trigger of increased production of secondary metabolites influences common enzymes involving in MIAs pathway such as previously mentioned D4H, DHT, TDC and STR (section 1.3). These were observed to be activated, which led to increased production of certain indole alkaloids. In addition, analyses of *Catharanthus* seedlings treated with MeJa showed alterations in the amount of tabersonine, which is one of the prominent compounds involved in MIA pathway [77], [78]. It is noteworthy that coupling of jasmonate with the amino acid isoleucine allows this compound to exhibit a particularly active gene expression property [143]–[145]. Moreover, jasmonate signaling to boost the biosynthesis of certain defense proteins or enzymes and subsequently induced gene expression as a result of an herbivore attack was also observed in many cases [146]–[148].

MeJa effects on MIA are also associated with contradictions as has been shown in *C. roseus* as well as *V. minor*. Thus, studies of the *C. roseus* hairy root cultures and leaves revealed increased indole alkaloid biosynthesis in the first one, whereas in the second one no changes of the contents of this type of alkaloids were evident [149]–[151]. Furthermore, the concentrations of the major alkaloids in *V. minor* seem to be variable at 8 and 14 d after the treatment with MeJa. Less vincamine and vincadifformine at 8 d after treatment with MeJa reflected in higher amounts of minovincine, minovincinine and 9-methoxyvincamine. After 14 d, however, the opposite effect was observed, as the increased conversion of strictosidine to vincamine and vincadifformine resulted in increased concentrations of both vinca alkaloids [139], [152]. Subsequently, conclusion could be drawn that the concentration of vincamine and other vinca alkaloids such as vincadifformine may vary over time. In addition, it can be assumed that treatment with MeJa may alter the concentration levels of the indole alkaloids.

In current work a substance **6c** whose structural formula was similar to that of MeJa was applied to the *V. minor* plants and caused a tremendous induction of vincamine production. This structural similarity involves a short carbon chain with a double bond, which is present in both compounds, **6c** and MeJa (**Figure 35**). Moreover, as mentioned

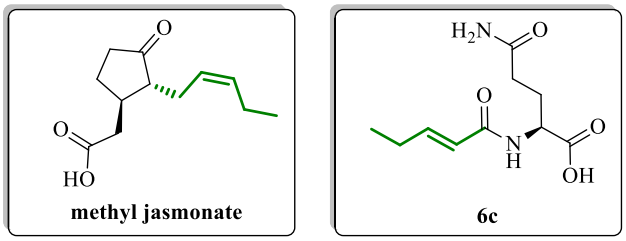

Figure 35: Comparison of structural formulas of methyl jasmonate (MeJA) and synthesized **6c**.

above, jasmonates conjugated with an amino acid isoleucine have been reported to have particularly high bioactivity [143]–[145]. Since **6c** is a fatty acid conjugated to an amino acid L-glutamine, it could also be hypothesized that this structural property also contributed to the changes in biosynthetic fluxes toward the production of vinca alkaloids.

Based on insights mentioned above and the results presented in the **Figure 32**, as well as **Figure 34**, a few statements could be made about the experiments on *V. minor*. First of all, it could be assumed that the production of the vincamine continued immediately after the substance was applied. Consequently, in the course of time, less vincamine was produced or/and the available MIA was presumably converted into other alkaloids such as minovincine, minovincinine and 9-methoxyvincamine, as already described in a previously study on periwinkle (**Figure 34**) [139], [152]. Unfortunately, this could not be confirmed by means of an HPLC experiment, since no evidence of the presence of the three conversion products of vincamine was found in the chromatograms evaluated. Instead, another compound called vincaminic acid was detected, as described in more detail in the same section below. Therefore, further consideration of the phenomenon of decreasing vincamine concentration including more replicates would be recommended.

In contrast, the diagram in **Figure 32** showed a significantly increased level of relative vincamine concentration at 8 d after treatment with FAC **6c**, which may indicate a contradiction. This could be explained by the fact that the vincamine concentration 24 h after application of **6c** was probably still significantly higher and was converted more slowly than in the previously mentioned experiment displayed in **Figure 34**. It could also be the case that similar processes to those described in the above studies have taken place in the *V. minor* treated in this work. Thus, as a result of the treatment with MeJa, first the decrease in vincamine concentration was seen, followed by the increase of the same alkaloid as a result of the conversion from the precursor molecule strictosidine. However, the report discussed 14 d after which the production of vincamine is ramped up [139], [152]. In the present case, these changes were observed after only 8 d, suggesting that vincamine biosynthesis occurred much more rapidly.

Another influence on these inconsistent results could be the small number of measurements included. In fact, the other diagram (**Figure 34**) consisting of more data points resulting of more replicates does not show as pronounced a change in relative vincamine concentrations as shown in **Figure 32**, which leads to the conclusion that more experiments would be necessary to achieve more reproducible results.

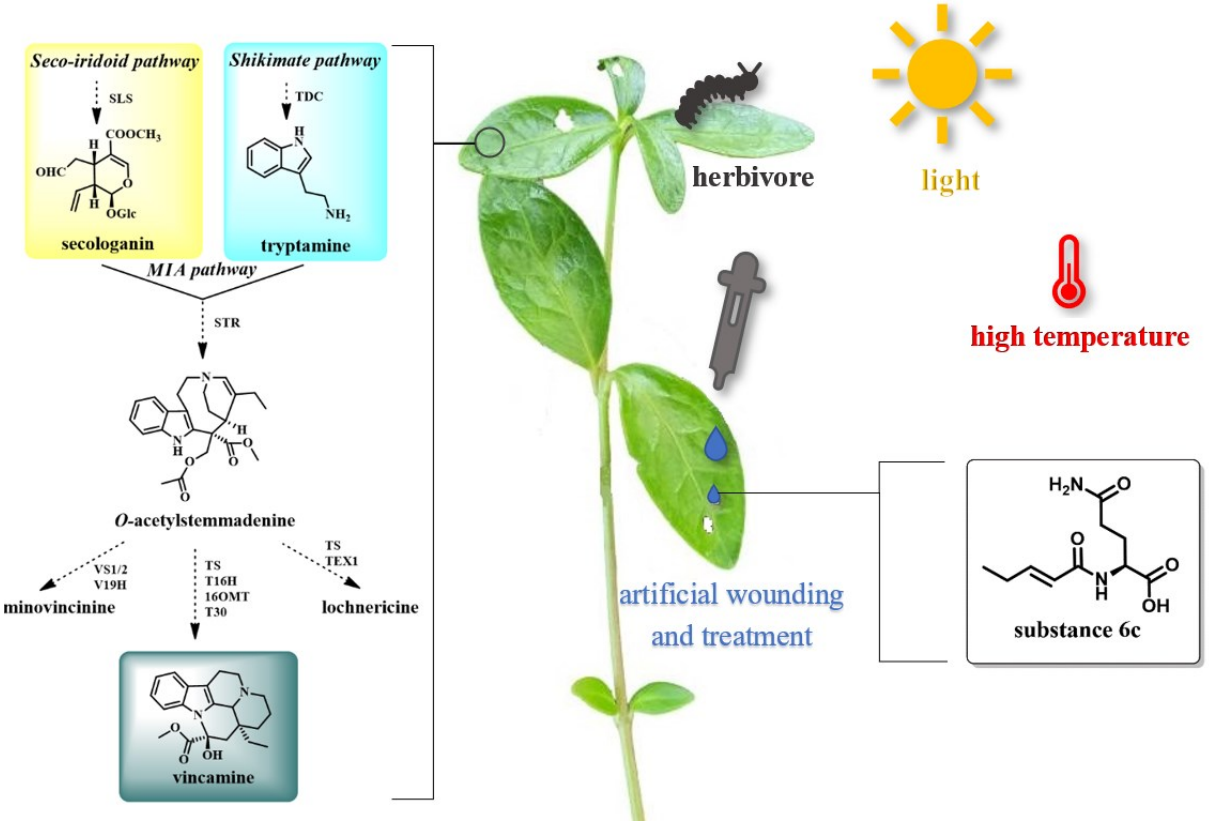

Figure 36: Putative MIA pathway operated in *V. minor* as a consequence of biotic and abiotic stress factors. The following enzymes are involved: secologanin synthase (SLS), tryptophan decarboxylase (TDC), strictosidine synthase (STR), vincadifformine synthase 1/2 (VS1/2), vincadifformine 19-hydroxylase (V19H), tabersonine synthase (TS), tabersonine 16-hydroxylase (T16H), 16-hydroxytabersonine-*O*-methyltransferase (16OMT), tabersonine 3-oxidase (T3O), tabersonine 6,7-epoxidase 1 (TEX1).

3.3. *Populus* experiments

Like other plant species, *Populus* trees also known as poplars have developed defensive strategies against herbivores, too. Among these strategies salicylate-like phenolic glycosides (PGs) also referred to as salicinoids play a key role [81]–[83]. The three significant salicinoids present in poplars include tremulacin, tremuloidin and the most widespread PG salicortin [83], [84]. Since the specialized metabolites are always present in *Populus* species regardless of the attack from the herbivore, they belong to the constitutive plant defensive strategies [83].

In general, the amount of salicinoids biosynthesized in different poplar species is genetically determined [153]. However, the comprehensive variations of PG levels depending on foliar development as well as season were also reported [84], [154]. The analyses of the contents of salicinoids in Salicaceae bark have shown that the lowest concentration is generally envisaged in August [155], [156]. Moreover, among one tree mature twigs often exhibited lower PGs abundance than the younger ones, probably due to *de novo* biosynthesis or PGs transport within a species [84], [157]. As expected for the constitutive defense strategies, the stress influence is less pronounced. This was confirmed in a recent study by Fellenberg *et al.* that did not provide positive results in attempts to induce gene expression by stress [83]. Nonetheless, there are a few studies that prove the contrary. Thus, Clausen *et al.* have shown that phenyl glycoside production in *Populus tremuloides* can occur as early as 24 h after attack by herbivores [85]. However, the same effect was observed after 4, 9 – 12 d as well as even 8 weeks in the quaking aspen [93], [158], [159].

Briefly, based on the fact described above that young trees contain more phenyl glycosides than older ones and thus an induced strategy towards PGs production would not lead to any further improvement of the situation of juvenile trees attacked by herbivores, it could be assumed that the induced mechanism might be more expressed in mature poplars [84].

Numerous reports have demonstrated that PG contents are strongly dependent on intrinsic traits such as genotype and ontogeny [84]. In this work, the abundance of two salicinoids such as tremulacin and tremuloidin were determined and plotted against q to provide an overview of the potentially correlation of phenotypic variation of *Populus* hybrids to their genomic ancestry (q). The relationship between varying q in hybrid individuals and phenotypic variance reflecting the concentrations of these salicinoids is thus discussed in more detail [160]. In this case, however, what is involved is not the constitutive but the induced defense strategies of poplar hybrids. Thus, the results of the experiments of treatment with stress factors under question such as caterpillars, **1d**, **5c**, **8c**/**8d** and **10b** are set relative to the calculated concentration values of the two PGs after treatment with solvent and thus the salicinoids already present are neglected.

The salicinoids containing extracts were analyzed using HPLC system with UV detection. The absorption measurement was carried out at 230 nm, since PGs are the chromophore compounds possessing π electrons in their chemical structure [84]. Peaks were assigned using retention times and UV spectra of tremulacin and tremuloidin. The assignment of tremulacin and tremuloidin to the

respective peaks in chromatograms was performed using specific UV spectra exhibited by these compounds as well as retention times. According to the chromatogram obtained after the measurement of compound **2b** (**Figure 37**), tremuloidin eluted earlier than tremulacin, due to its more hydrophilic properties. The retention times were 10.4 min and 12.0 min for tremuloidin and tremulacin, respectively.

For determination of concentrations of tremuloidin and tremulacin, calibration curves using standard solutions with concentrations of tremuloidin and tremulacin from 0.125 mg/mL to 1 mg/mL were established. Whereas the linear equation for tremuloidin was y = 14928x + 172.3 at the coefficient of determination R^2 = 0.9533, the linear equation of tremulacin was attributed another equation, viz., y= 14654x - 598.87 with a higher coefficient of determination R^2 = 0.9799. Therefore, the evaluation of tremuloidin and tremulacin concentrations in *Populus* species with different genotypes as well as the subsequent display of results in dependence upon genomic ancestry (*q*) were enabled. The colored dots associated with the lines correspond to the mean values of the relative salicinoid concentrations. The error bars represent the standard deviations, as depicted in **Figure 38** and **Figure 39**.

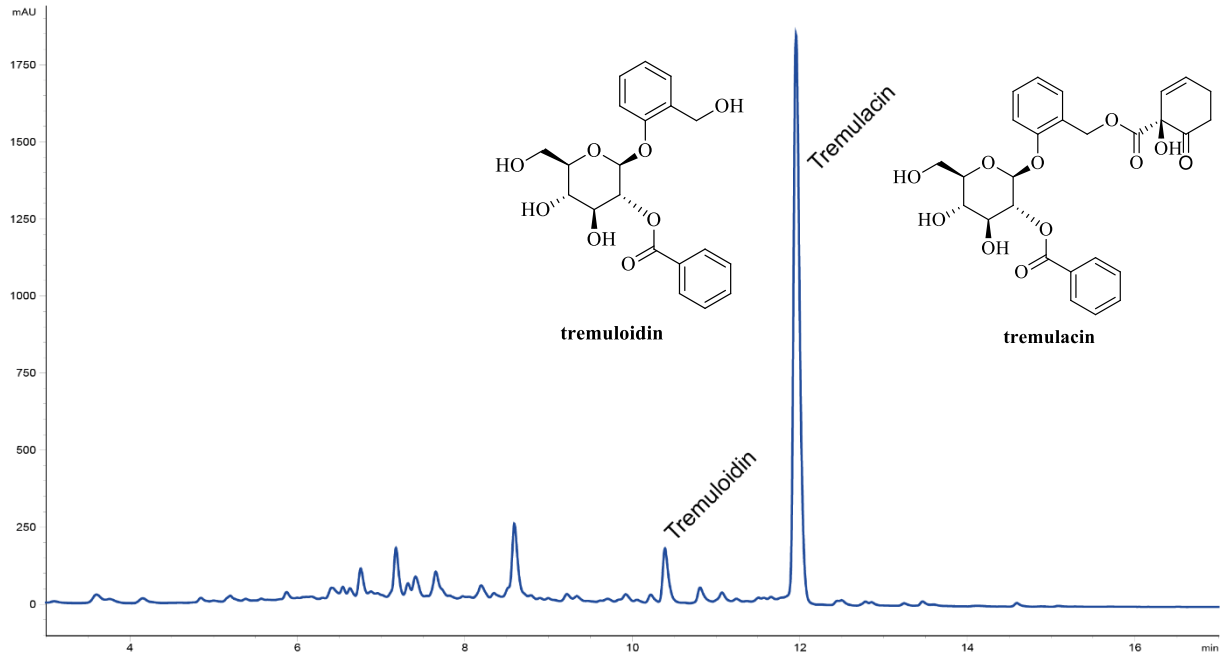

Figure 37: HPLC speratаion of natural products in *Populus* hybrids.

Considering the relationships between genomic ancestry (*q*) and relative tremulacin and tremuloidin concentration in % in **Figure 38** as well as **Figure 39**, it can be said that there is a downward trend towards *Populus alba*-like individuals that are on the right side of the respective diagrams. *Populus tremula*-like individuals positioned on the left side of the respective diagrams exhibit higher values of relative tremulacin and tremuloidin concentrations in %. The slight discrepancies between the two *Populus* species are a sufficient argument to suggest that there are

phenotypic traits of genomic architecture, which is very similar to previous study of Bresadola *et al.* that addressed phenotypic variation within ecologically distinct forest trees *Populus alba* and *Populus tremula* and their hybrids. However, in this report it was mentioned that no correlations could be seen between heritability and these phytochemical defensive traits. The explanation for this, according to the report, would be a lack of so-called admixture mapping potency, so it is not related to heritability [160].

Further examination of the diagrams in **Figure 38** and **Figure 39** leads to the conclusion that the plant response 8 d after treatment with the above-mentioned substances and caterpillars shows no significant deviations from the control, which was a solvent, more precisely a mixture of ethanol, a nonionic detergent Tween® 20, and water (EtOH : Tween® 20 : H_2O – 1 : 0.2 : 8.8 v/v/v). The exception was compound **10b** with a relative tremulacin concentration of about 120 %, which could mean that the *Populus tremula*-like individuals developed some kind of induced defensive strategy after treatment with this compound. Since the values of relative tremulacin and tremuloidin concentrations are sometimes less than 100 %, especially in *Populus alba*-like individuals, it would be said that the solvent triggered a stronger defensive response to some poplars than the synthesized substances or caterpillars. This can probably be explained by the fact that the solvent was applied as a control in July. As mentioned above, the lowest concentrations of salicinoids in poplars were observed in August [155], [156]. Since the substances were applied in August and the control in July, one could speculate that the statements extracted from the diagrams might not be significant. In order to obtain valid results, several treatment experiments would have to be conducted in which control solutions would be applied simultaneously. The higher number of replicates for the study of the induction of tremulacin and tremuloidin biosynthesis as a result of treatment with different substances or caterpillars is also necessary with respect to the fact that there were studies exhibiting investigations of PGs contents after different harvesting time as stated above in the same section [85], [93], [158], [159]. In fact, more measurements for the evaluation of the results would be beneficial as it would not only allow more comparisons with the previous studies but also ensure the reproducibility of the results.

Another explanation of the relatively low salicinoid concentrations compared to control could be the fact of the use of differently aged leaves to the experiments. As explained above, young leaves have enough PGs to protect themselves against environmental stressors. Especially because plant resources are precious, the juvenile leaves produce fewer defensive substances such as salicinoids than the mature poplar leaves possessing smaller quantities of these compounds [84]. One could thereby speculate that for the lower values of tremulacin and tremuloidin produced, the treatment of the younger leaves was responsible.

It is noticeable that tremuloidin concentration in **Figure 39** was not determined after treatment with **8c**/**8d** and **10b**. The reason for this were low tremuloidin signals detected after HPLC measurement, being close to the noise signal, as the amount of this salicinoid was very low in *Populus* hybrids

extracts to be investigated. In contrast, more signals of the HPLC measurement of the extracts containing tremulacin could be recorded, permitting the generation of a complete diagram as displayed in **Figure 38**. Regarding this fact, the distribution of the relative concentrations of tremulacin and tremuloidin was presented as boxplots in two diagrams, where the first is represented by *Populus tremula*-like individuals (**Figure 40**) and the second possesses the measured values belonging to poplars with a genomic ancestry of 0.58 (**Figure 41**). To some extent, significant differences in tremulacin and tremuloidin concentrations can be seen at first look in the two diagrams, whereas the larger part of the boxplots pairs shows a higher tremulacin concentration. The almost four times higher tremulacin concentrations as opposed to tremuloidin amounts in *Populus tremula* were also confirmed by UHPLC-ESI/TOFMS measurement, as demonstrated in the report by Abreu *et al.* [82]. The higher tremulacin *versus* tremuloidin concentrations are also in agreement with the study of European aspen, using the same experimental method for the determination of their concentrations [153]. The reason why tremulacin occurs in higher concentrations than tremuloidin in the strenuous environment could be the high toxicity of the HCH moiety it possesses [84], [85]. Thus, herbivores following tremulacin consumption exhibited lower survival and performance, as demonstrated by Lindroth *et al.* [161].

In some cases, a lower concentration of tremulacin might not necessarily indicate a lack of defense mechanism in poplars. Due to the fact that salicortin acts not only as a potential substrate for the synthesis of tremulacin, but also for other substances carrying the toxic HCH moiety, such as 2′-cinnamoylsalicortin, one could assume that this is a matter of rivalry between the two compounds in the biosynthetic pathway [153]. It would be interesting to add 2′-cinnamoylsalicortin to the future studies as well, in order to exclude the competition, or rather to explore it.

Furthermore, treatment of poplar hybrids with the potential stressors such as synthesized compounds **5c**, **8c**/**8d** and caterpillars probably stimulated the biosynthesis of tremulacin as well as tremuloidin, which can be confirmed by boxplots indicating relative concentration values of over 100 % (**Figure 40**). Since a specific enzyme is involved in the biosynthesis of this salicinoid, it suggests that the genes encoding the activity of this enzyme referred to as salicyl benzoate UDP-glycosyltransferase UGT71L1 were expressed by the application of the triggers so that the biosynthesis of tremulacin could occur. In order to verify this more precisely, the concentrations of salicortin could also be employed in future studies, since the biosynthesis of the compound is also dependent on the above-mentioned enzyme [83].

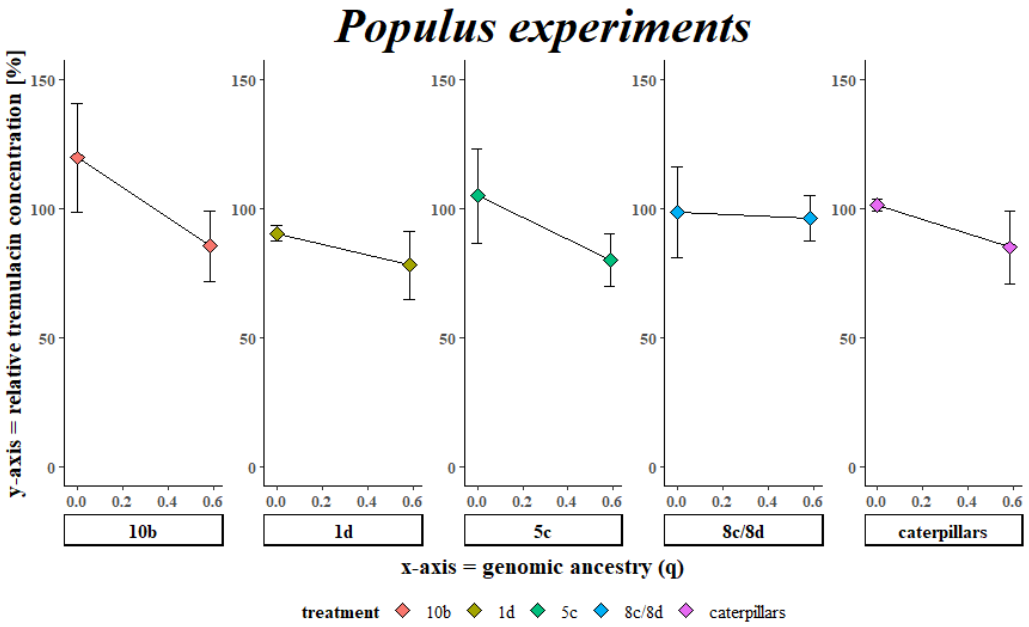

Figure 38: Relations between genomic ancestry (q) and relative tremulacin concentration (%) in *Populus alba* × *Populus tremula* hybrids.

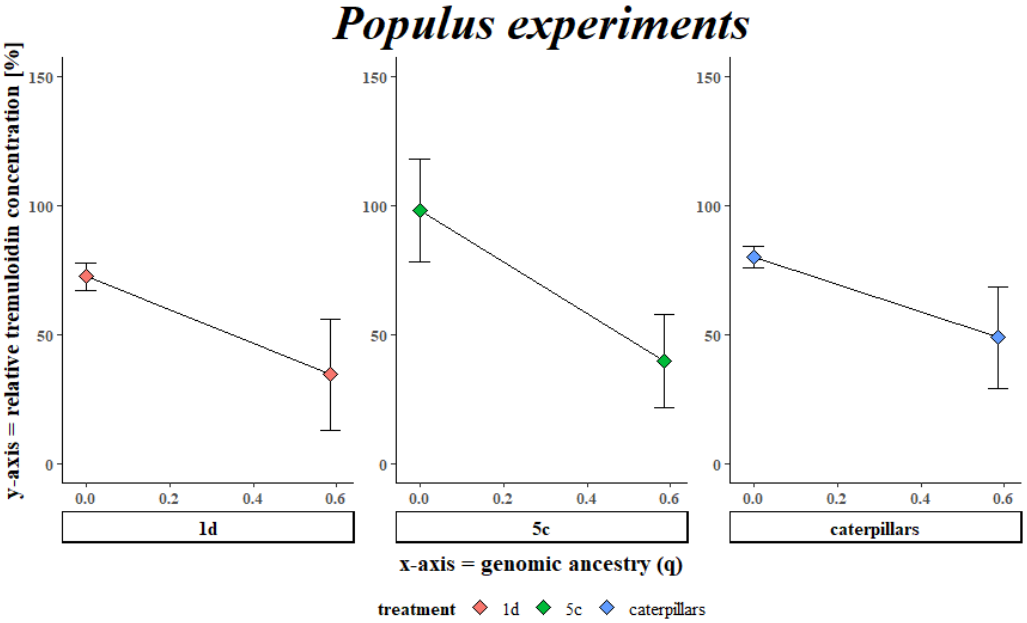

Figure 39: Relationship between genomic ancestry (q) and relative tremuloidin concentration (%) in *Populus alba* × *Populus tremula* hybrids.

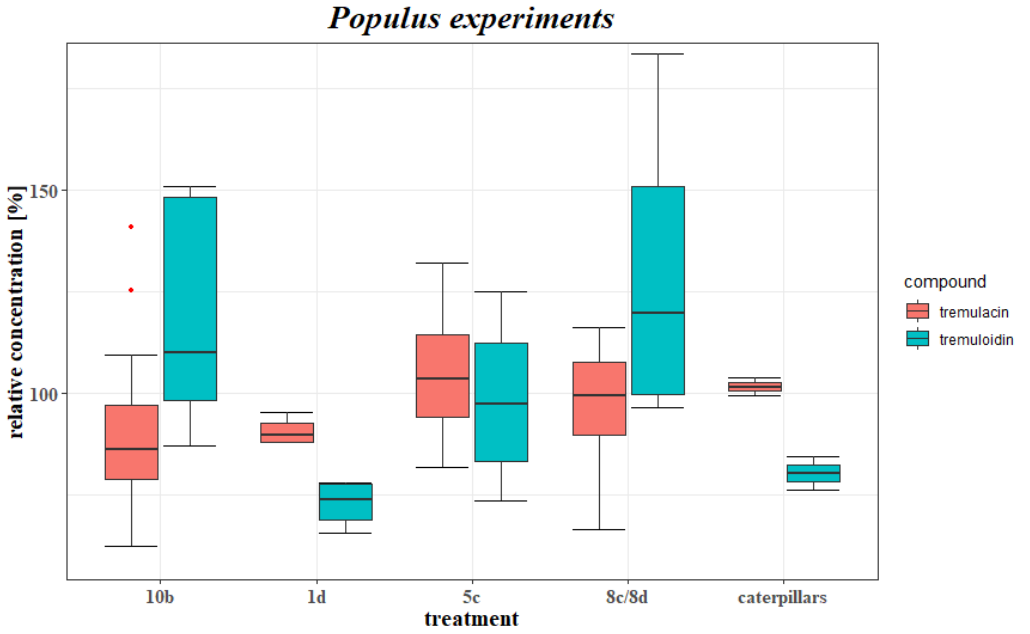

Figure 40: Distribution of relative tremulacin and tremuloidin concentration in *Populus tremula*-like individuals depending on the treatment.

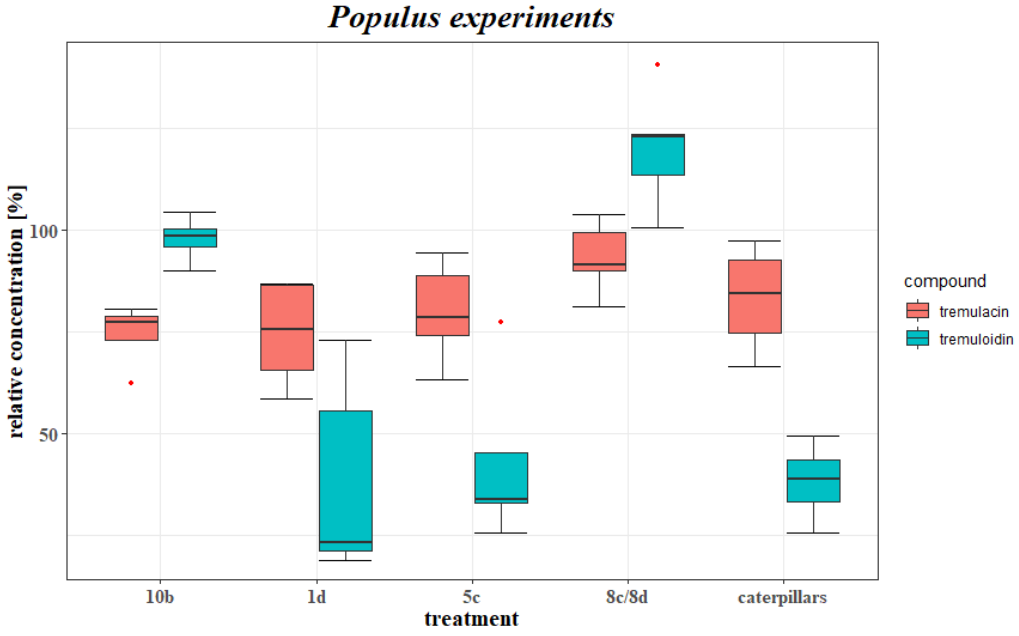

Figure 41: Distribution of relative tremulacin and tremuloidin concentration in *Populus alba*-like individuals depending on the treatment.

4. Conclusion and future prospects

The main objective of this thesis was to draw the conclusions about the plant defense strategies after the application of potential elicitors on *Vinca minor* and *Populus alba* × *Populus tremula* hybrids leaves. The substances and caterpillars to be applied encompassed fatty acid-amino acid conjugates (FACs) and *Spodoptera littoralis* larvae, respectively. To study the effectiveness of the impact of the FACs synthesized in the first part of this work, the syntheses would have to work properly, and the subsequent purification steps would have to yield pure products. Concerning the fact that the synthesis of most of the compounds worked well, which could be confirmed by NMR and MS measurements, it can be generally concluded that the synthesis strategies used in this thesis can be further recommended. Unfortunately, the biggest challenge of this work has been the purification steps with column chromatography as well as recrystallization. In order to reduce the product losses mirrored in lower yields and the presence of undesirable by-products such as ketone **11f** in the hydroxylated products **11e** and **11g**, further optimization of the chromatographic separation including trials with other solvents as well as utilization of other mobile phase gradients would be advisable. Moreover, it can also be said that the application of thin layer chromatography (TLC) to provide an overview of the purity of the synthesized compounds provides many advantages, not only in terms of solvent savings but also significant labor time reduction.

In the second section of this thesis, the impacts of the previously prepared analogs of volicitin on monoterpenoid indole alkaloid (MIA) vincamine and phenyl glycosides (PG) tremulacin as well as tremuloidin biosynthesis in plants were investigated. For this purpose, the previously synthesized FACs termed **1d**, **2b**, **3b**, **4b**, **5c**, **6c**, **7c**, **8c**/**8d**, **9b** and **10b** were applied to the leaves of *V. minor* from the family Apocynaceae. Simultaneously, effects of the application of caterpillar *Spodoptera littoralis* (**C**), solvent (**B**) and of an artificial wounding were also monitored. The results presented in this thesis clearly show that the volicitin analog **6c** carries potential plant response-triggering property. Quantitative analyses of vincamine levels at 8 d after treatment with **6c** have demonstrated a twofold increase in vincamine levels in contrast to other FACs or even caterpillars. The significant difference in vincamine concentration after the **6c** treatment could mean that the biosynthesis of monoterpenoid indole alkaloid (MIA) such as vincamine was stimulated starting from tryptamine and secologanin. This stimulation involves the activation of a number of different enzymes that participate in the MIA biosynthesis pathway, among which are mainly strictosidine and tabersonine synthase [68]. Accordingly, the study of the biosynthetic pathways of MIAs is intriguing due to the fact that the nitrogen present in their structures seems to be a limiting factor for the plant. In addition, it could be concluded that the shikimate pathway makes an important contribution to MIAs biosynthetic flux, as it is responsible for the production of nitrogen-carrying tryptamine, which is a key intermediate for the vincamine biosynthesis. Since not all enzymes responsible in the biosynthesis of vincamine have been found to date, further elucidation of this MIAs pathway towards vincamine hereby defined as “definitely non waste alkaloid” would be an interesting topic for future research [67], [162].

Due to the over-responsiveness of the plant after the application of FACs **6c**, the latter was used for further experiments on *V. minor*. According to the results of the additional plant trials, a finding could be made that the production of the "non waste alkaloid" to be investigated takes place immediately after the application of the stress-inducing substances and not after 8 d as expected. In conclusion, this result has opened the door for further research towards vincamine biosynthesis.

In the current work observations could also be made concerning the biosynthesis of two significant salicinoids tremulacin and tremuloidin after application of caterpillars *Spodoptera littoralis*, **1d**, **5c**, **8c**/**8d** and **10b** to the *Populus* hybrids (*Populus alba* × *Populus tremula*) belonging to the Salicaceous family. Despite the fact that the results were not as distinct as those of *V. minor* plants, it was still possible to draw some conclusions about the defensive strategies induced by these trees. Apart from the low number of data measured for the two salicinoids, which resulted from very low concentrations near the noise signals, causal relationship between the genomic ancestry of the poplars and concentrations of tremulacin and tremuloidin could be observed. In this context, *Populus tremula*-like individuals indicated higher values of relative tremulacin and tremuloidin concentrations than *Populus alba*-like species. Nevertheless, the concentrations of the two salicylate-like phenolic glycosides (PGs) tended to be at a rather low level when compared to the concentrations occurring after treatment with solvent. As the amount of salicinoids biosynthesized in *Populus* species is not only genetically determined but also foliar development as well as season seem to have a great influence on the level of these substances, more measurements for the evaluation of the results would be recommendable for future research [84], [153], [154]. Conducting the experiments over the entire vegetation period and observing salicinoid levels at different times after application of various elicitors would provide more results for comparison with previous studies, which would become more reproducible. In addition, another more common salicinoid called salicortin could also be included in future studies, as it is found in higher concentrations in poplars, likewise tremulacin [163]–[165]. Moreover, the biosynthesis of the salicortin depends on the same enzyme responsible for the production of tremulacin and tremuloidin, so with the help of the parallel studies of the three mentioned PGs, one could also get more statements about the enzyme and the enigmatic biosynthetic pathway in which this enzyme is involved [83].

5. Experimental

5.1. General

In general, all reactions were performed under argon atmosphere. All solvents and reagents obtained from Merck KGaA, Thermo Fischer Scientific, Alpha Aesar, Tokyo Chemical Industry Co., Ltd. or Carl Roth GmbH + Co. KG were used directly, i.e., the chemicals were not purified.

Both intermediates and end products were observed by means of thin layer chromatography (TLC). For this purpose, aluminum sheets with unmodified silica gel (SiOH), more specifically TLC plates ALUGRAM Xtra Nano-SILGUR, 10x10cm, were used.

The synthesized end products and optionally also intermediates were purified by column chromatography using silica gel 60 (230-400 mesh).

Electrospray ionization (ESI) mass spectrometric analyzes in the mass range 50-1900 m/z and positive or negative ion mode were obtained on ESI-Qq-TOF mass spectrometer - maXis UHR-TOF (Bruker Daltonik GmbH, Bremen, Germany). Based on the mass accuracy of $\Delta m/z \leq 5$ ppm and with the use of Software (Bruker Compass 1.5 for OTOF series - otofControl Version 3.2, DataAnalysis Version 4.1) as well as isotopic pattern matching (SmartFormula algorithm) sum formulas of the detected ions were established. The capillary voltage was set to -/+ 4500 V and the flow of dry gas (nitrogen) was 4.0 L/min. Sample introduction was carried out *via* direct infusion in ACN/MeOH +1% H_2O (flow rate: 3 µL/min). Tandem mass spectrum (MS/MS) was acquired in positive ion mode using a timsTOF fleX (Bruker Daltonik GmbH, Bremen, Germany) instrument with ESI in positive ion mode as an ion source (capillary voltage: 4500 V, m/z range: 100 – 1550 m/z, set collision cell RF: 700.0 Vpp, set nebulizer: 2.2 bar, set dry gas: 10.0 L/min). The data was processed using Bruker Compass DataAnalysis Version 5.3.

^{1}H-NMR (spectrometer frequency: 600 MHz) and ^{13}C-NMR (spectrometer frequency: 150 MHz) spectra were recorded on Bruker AV III 600 device (AVANCE, Bruker BioSpin, Rheinstetten, Germany) at 300 K with CD_3OD (δ = 3.31 ppm for ^{1}H-NMR and δ = 49.15 ppm for ^{13}C-NMR), $CDCl_3$ (δ = 7.24 ppm for ^{1}H-NMR and δ = 77.23 ppm for ^{13}C-NMR) as well as DMSO (δ = 2.50 ppm for ^{1}H-NMR and δ = 39.51 ppm for ^{13}C-NMR) as internal standards. The chemical shifts (δ) and the coupling constants (*J*) were given in parts per million (ppm) and hertz (Hz), respectively. The common splitting patterns included singlet (s), doublet (d), triplet (t), quintet (quin), sextet (sext), doublet of doublets (dd), doublet of triplets (dt), doublet of triplet of doublets (dtd), doublet of doublet of triplets (ddt), triplet of quartets (tq) and multiplets (m).

The plant material to be studied was obtained from the Department of Botany and Biodiversity Research of the University of Vienna. Both *V. minor* and *Populus* hybrids were grown in plant pots and were poured with water regularly, as the average outdoor temperature during the experiments was approximately 30 °C. To enable better extraction results, the dried plant material was placed in an QIAGEN Tissue Lyser II for the purpose of grinding. Other equipment used for the extraction included a VWR Ultrasonic Cleaner and an Eppendorf Centrifuge 5417R.

HPLC analyses were performed on an Agilent 1100 equipment using Agilent Hypersil BDS-C_{18} reversed-phase column (3µm, 100 × 4 mm). The mobile phase contained eluent A (10 mM NH_4OAc) and eluent B (ACN). To obtain 1 L of eluent A, 1 L pure water and 0.8 g NH_4OAc were mixed and filtered to remove possible impurities. Elution was started with 5% of eluent B and 95% of eluent A. The composition of the mobile phase was temporally changed, thus, the percentage of eluent B after 12 min increased to 60%. The HPLC-measurement was taken for 17 min. Additionally, the injection volume was 2.5 µL and the mobile phase flow rate was set to 0.5 mL/min.

For plotting boxplots and linear regression curves including error bars, the software R (© 2009 – 2021 RStudio, PBC) with following packages was used: ggplot2, readxl and extrafont.

5.1.1. Fatty acid-amino acid conjugates (FACs) synthesis

*5.1.1.1. Synthesis of N-(10-hydroxyundecanoyl)-L-glutamine (**1d**)*

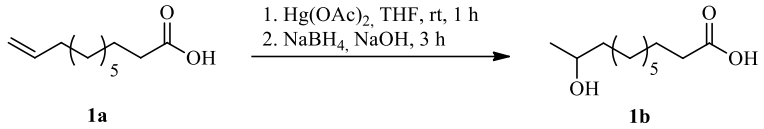

Figure 42: Synthesis of hydroxylated fatty acid **1b** starting from allyl fatty acid **1a**.

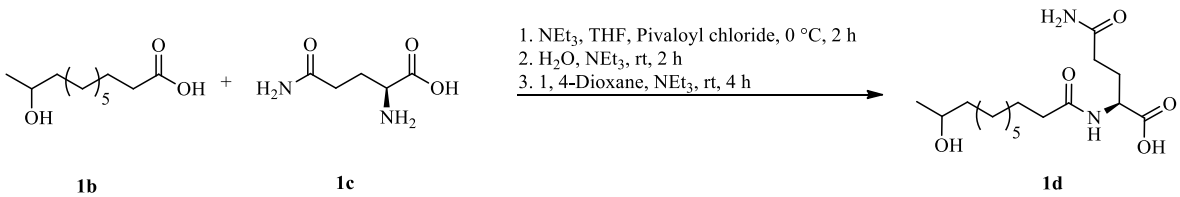

Figure 43: Synthesis of FAC **1d** starting from hydroxylated fatty acid **1b** and L-glutamine (**1c**).

A reaction mixture of mercury (II) oxide (4.13 g, 19.0 mmol), water (12.5 mL) and glacial acetic acid (4.2 mL, 73.4 mmol) was warmed up to 50 °C and stirred to give a colorless solution of mercury (II) acetate. The reaction mixture was charged followed by water (17.5 mL) and tetrahydrofuran (THF) (30 mL) producing a yellow solution. Thereafter, an appropriate amount of 10-undecenoic acid (3.32 g, 18.0 mmol, **1a**) was added and the reaction mixture was stirred at room temperature for 1 h. Then aqueous NaOH solution (3 M, 30 mL) was added, and the mixture was carefully reduced with sodium borohydride ($NaBH_4$) solution (0.40 g, 10.6 mmol $NaBH_4$ in 30 mL of 3 M NaOH). This reaction mixture was stirred further for 3 h at room temperature. The elemental mercury formed during the reaction was separate in a dropping funnel. Afterwards the solution was adjusted to pH 1 with aqueous HCl solution (4 M) and extracted with dichloromethane (DCM) (30 mL × 2). The combined organic layers were washed with water (50 mL) and dried (Na_2SO_4). Excess DCM was removed under

reduced pressure to yield 0.98 g (27%) of **1b** as a white powder. Due to sufficient purity, which was reviewed by NMR, the desired hydroxylated fatty acid (**1b**) was employed for the next step without any purification.

Fatty acid-amino acid conjugate (FACs) was prepared by stirring an appropriate amount of **1b** (976 mg, 4.83 mmol) with triethylamine (807 µL, 5.79 mmol) in THF (34 mL). The mixture was cooled to 0 °C and pivaloyl chloride (641 µL, 5.24 mmol) was added. The reaction mixture was stirred at the same temperature for 2 h and then quickly filtered and the filter cake was rinsed with THF (35.4 mL). The filtrate and washings were combined, then diluted with 1,4-dioxane (31 mL) and stored until the next step. Meanwhile, for the preparation of FAC, L-glutamine (1.41 g, 9.62 mmol, **1c**) was dissolved in water (11.3 mL). Triethylamine (1.34 mL, 9.65 mmol) was added to the solution and the mixture was stirred at room temperature for 2 h. Thereafter, the L-glutamine solution and the acylating agent from the previous step were combined and stirred for 20 min. Triethylamine (679 µL, 4.87 mmol) was added and the reaction mixture was stirred further at room temperature for 4 h. Afterwards aqueous HCl solution (4 M) was added and the mixture with pH 3 was transferred into water (30 mL). Extraction was carried out with DCM (30 mL × 3) and the organic layer was washed with brine (25 mL), dried over $MgSO_4$ and the solvent was removed *in vacuo*. Because of insufficient purity of this crude, further purification *via* column chromatography over silica gel (54 g, gradient from DCM : CH_3OH – 100 : 0 v/v% to DCM : CH_3OH – 60 : 40 v/v%) was needed to obtain 157 mg (19% in 2 steps) of pure **1d** as a white powder.

*5.1.1.2. Synthesis of (S)-N-α-undec-10-enoyl-L-glutamine (**2b**)*

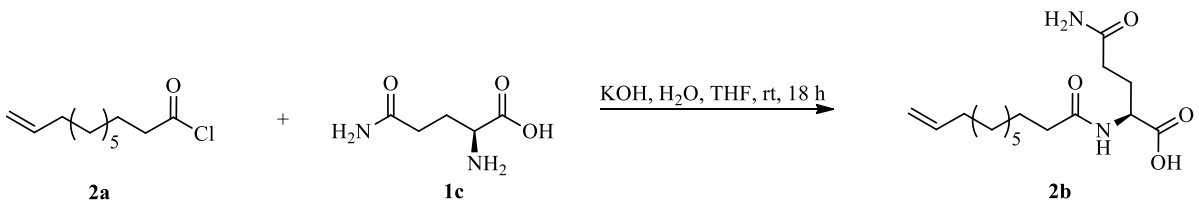

2a **1c** **2b**

Figure 44: Synthesis of FAC **2b** starting from 10-undecenoyl chloride (**2a**) and L-glutamine (**1c**).

10-Undecenoyl chloride (2.03 g, 10.0 mmol, **2a**) was dissolved in THF (20 mL) and added dropwise to a solution of L-glutamine (1.47 g, 10.1 mmol, **1c**) and KOH (1.14 g, 20.3 mmol) in water (20 mL) over 15 min at room temperature. The reaction mixture was stirred at the same temperature for 18 h and finally the solvent was evaporated under reduced pressure. The resulting volume of the solution of approximately 25 mL was adjusted to pH 1 with aqueous HCl solution (4 M) and the precipitated crude was filtered and washed with water (25 mL) and ether (25 mL). The precipitate was further

purified by recrystallization from ethylacetate to give (S)-*N*-α-undec-10-enoyl-L-glutamine (**2b**) as a white powder (yield 0.980 g, 31%).

*5.1.1.3. Synthesis of N-((9Z)-octadec-9-enoyl)-L-glutamine (**3b**)*

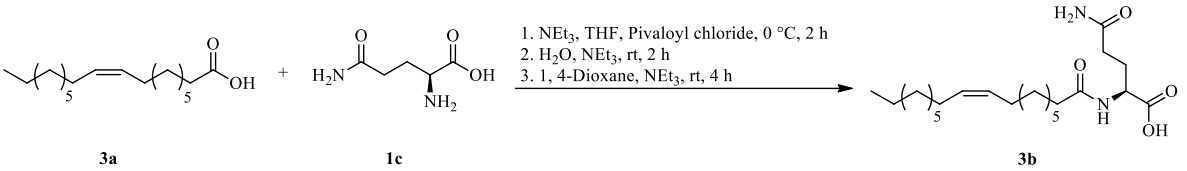

3a **1c** **3b**

Figure 45: Synthesis of FAC **3b** starting from (9*Z*)-octadec-9-enoic acid (**3a**) and L-glutamine (**1c**).

N-((9*Z*)-Octadec-9-enoyl)-L-glutamine (**3b**) was prepared by mixing (9*Z*)-octadec-9-enoic acid (1.39 g, 4.92 mmol, **3a**) with triethylamine (570 µL, 4.08 mmol) in THF (24 mL). The mixture was cooled to 0 °C and pivaloyl chloride (456 µL, 3.70 mmol) was added. The reaction mixture was stirred at 0 °C for 2 h and then quickly filtered. The filter cake was rinsed with THF (25 mL). The filtrate and washings were collected and combined, then diluted with 1,4-dioxane (22 mL) and stored until the next step. For the preparation of *N*-((9*Z*)-octadec-9-enoyl)-L-glutamine (**3b**), L-glutamine (0.996 g, 6.82 mmol, **1c**) was dissolved in water (8 mL). Triethylamine (950 µL, 6.82 mmol) was added to the solution and the mixture was stirred at room temperature for 2 h. Thereafter, the L-glutamine solution and the acylating agent from the previous step were combined and stirred for 20 min. Triethylamine (480 µL, 3.44 mmol) was added and the reaction mixture was stirred further at room temperature for 4 h. Afterwards aqueous solution of HCl (4 M) was added and the mixture was adjusted to pH 3. The solution containing desired FAC was transferred into water (25 mL) and extracted with DCM (25 mL × 3). The organic layer was washed with brine, dried ($MgSO_4$) and the mixture was concentrated *in vacuo*. The crude was chromatographed twice over silica gel (12.1 g and 17.7 g, gradient from DCM : CH_3OH – 100 : 0 v/v% to DCM : CH_3OH – 60 : 40 v/v%) to give **3b** as an off-white crystal like product (yield 157 mg, 8%) . Additionally, the column chromatography purification process was performed twice, due to impurities still present after the first column chromatography process.

*5.1.1.4. Synthesis of (S)-N-α-octadecanoyl-L-glutamine (**4b**)*

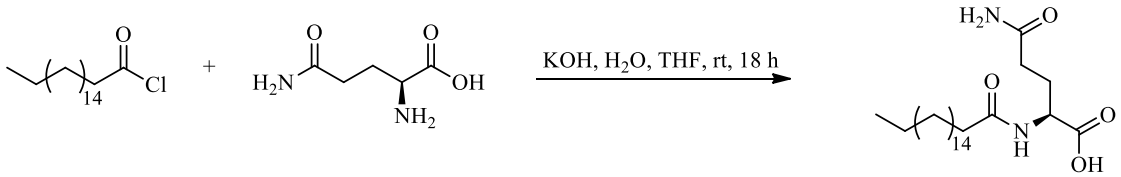

4a **1c** **4b**

Figure 46: Synthesis of FAC **4b** starting from octadecanoyl chloride (**4a**) and L-glutamine (**1c**).

Octadecanoyl chloride (3.01 g, 9.95 mmol, **4a**) was dissolved in THF (20 mL) and added dropwise to a solution of L-glutamine (1.46 g, 10.0 mmol, **1c**) and KOH (1.14 g, 20.3 mmol) in water (20 mL) over 15 min at room temperature. The reaction mixture was stirred at the same temperature for 18 h and concentrated *in vacuo*. The reduced volume of the solution (approximately 25 mL) was adjusted to pH 1 with aqueous HCl solution (4 M) and the crude was filtered and washed with water (10 mL) and diethyl ether (Et_2O) (10 mL). The precipitate was further purified by recrystallization from ethanol to yield a white powder **4b** (yield 1.64 g, 40%).

*5.1.1.5. Synthesis of N-(heptanoyl)-L-glutamine (**5c**)*

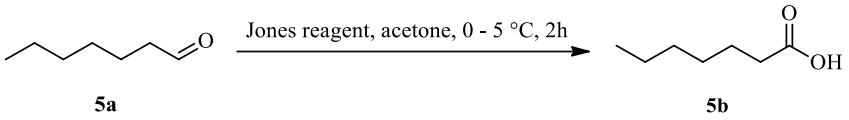

Figure 47: Synthesis of heptanoic acid (**5b**) starting from heptanal (**5a**).

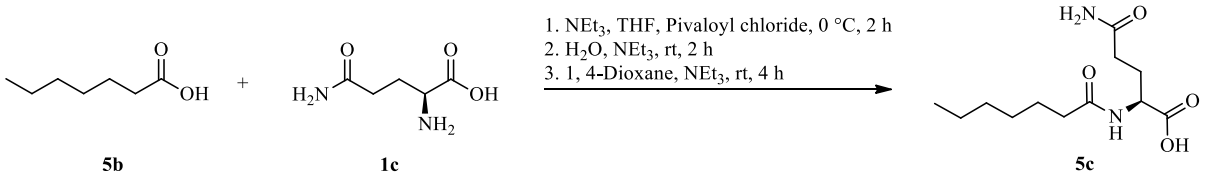

Figure 48: Synthesis of FAC **5c** starting from heptanoic acid (**5b**) and L-glutamine (**1c**).

Heptanal (1.51 g, 13.1 mmol, **5a**) was dissolved in acetone (15 mL). The solution was then cooled to 0 - 5 °C and Jones reagent (4.05 mL, 2.67 g CrO_3 in 2.3 mL concentrated H_2SO_4 and 7.7 mL H_2O) was added dropwise (approximately 100 µL/portion) over 5 min. The reaction mixture was stirred for 2 h at the same temperature and the solvent was removed under reduced pressure. The residue was diluted with water (25 mL) and the mixture was extracted with ethyl acetate (25 mL × 3). The organic layer was successively washed with 10% aqueous K_2CO_3 (30 mL × 2). The aqueous phase was adjusted to pH 1 with HCl solution (4 M), extracted with ethyl acetate (25 mL × 3) and the organic layer was washed with water (15 mL), dried over Na_2SO_4 and concentrated *in vacuo*. Due to sufficient purity, the intermediate product **5b** (yield 1.49 g, 87%) was employed without any purification for the next reaction.

N-(Heptanoyl)-L-glutamine (**5c**) was prepared by stirring **5b** (1.49 g, 11.4 mmol) with triethylamine (1.91 mL, 13.7 mmol) in THF (80.4 mL). The mixture was cooled to 0 °C, pivaloyl chloride (1.52 mL, 12.4 mmol) was added and the reaction mixture was stirred at the same temperature

for 2 h. Afterwards the suspension was quickly filtered, and the filter cake was rinsed with THF (84 mL). The filtrate and washings were combined, diluted with 1,4-dioxane (74 mL) and stored until the next step. Simultaneously, L-glutamine (3.33 g, 22.8 mmol) was dissolved in water (26.8 mL). Triethylamine (3.18 mL, 22.8 mmol) was added to the solution and the mixture was stirred at room temperature for 2 h. Thereafter the L-glutamine solution and the acylating agent from the previous reaction were combined and stirred for 20 min. Then triethylamine (1.61 mL, 11.6 mmol) was added, and the reaction mixture was stirred further at room temperature for 4 h. Then the aqueous HCl solution (4 M) was added portionwise until the solution was pH 3. The reaction mixture was poured into water (30 mL), extracted with DCM (40 mL × 3) and the combined organic phases were washed with brine (25 mL) and dried ($MgSO_4$). Excess DCM was removed under reduced pressure and the crude was further chromatographed over silica gel (108 g, gradient from DCM : CH_3OH – 100 : 0 v/v% to DCM : CH_3OH – 60 : 40 v/v%) to yield **5c** as an off-white powder (yield in 2 steps 947 mg, 28%).

*5.1.1.6. Synthesis of N-((2E)-pent-2-enoyl)-L-glutamine (**6c**)*

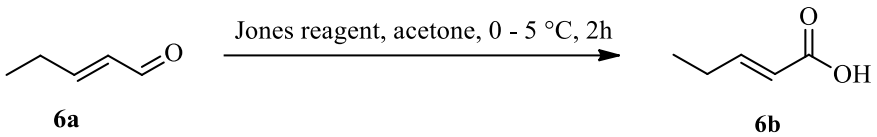

Figure 49: Synthesis of (2*E*)-pent-2-enoic acid (**6b**) starting from (2*E*)-pent-2-enal (**6a**).

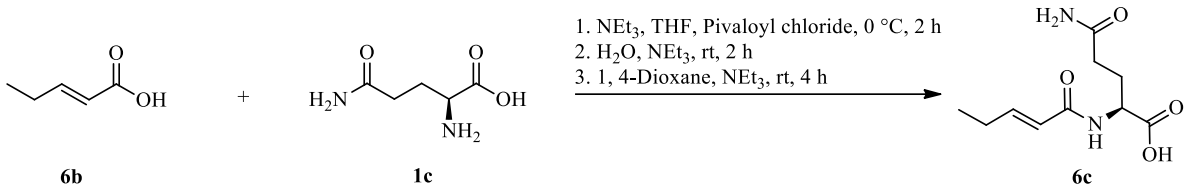

Figure 50: Synthesis of FAC **6c** starting from (2*E*)-pent-2-enoic acid (**6b**) and L-glutamine (**1c**).

(2*E*)-Pent-2-enal (1.20 g, 14.3 mmol, **6a**) was dissolved in acetone (12 mL) and the solution was cooled to 0 - 5 °C. Jones reagent (4.42 mL, 2.67 g CrO_3 in 2.3 mL concentrated H_2SO_4 and 7.7 mL H_2O) was charged dropwise (approximately 100 µL/portion) over 5 min and the reaction mixture was stirred for 2 h at the same temperature. The solvent was evaporated under reduced pressure, the residue was diluted with water (20 mL) and the mixture was extracted with ethyl acetate (20 mL × 3). The combined organic phases were washed with 10% aqueous K_2CO_3 (30 mL × 2). The aqueous phase was adjusted to pH 1 with HCl solution (4 M) and extracted with ethyl acetate (20 mL × 3).

Afterwards the organic layer was washed with water (10 mL), dried over Na_2SO_4 and concentrated *in vacuo*. Due to sufficient purity, the intermediate product **6b** (yield g, %) was employed without any purification for the next step.

N-((2*E*)-Pent-2-enoyl)-L-glutamine (**6c**) was prepared using an amount of 0.48 g pent-2-enoic acid (4.77 mmol, **6b**) with 802 µL triethylamine (5.76 mmol) in 33.8 mL THF. The mixture was cooled to 0 °C followed by addition of pivaloyl chloride (0.638 mL, 5.21 mmol) and the reaction mixture was stirred at the same temperature for 2 h. Then the suspension was quickly filtered, and the filter cake was washed with THF (35.2 mL). The filtrate and washings were collected, diluted with 1,4-dioxane (31 mL) and stored until the next reaction. In addition, for the preparation of **6c**, L-glutamine (1.45 g, 9.92 mmol) was dissolved in water (11.3 mL). Triethylamine (1.34 mL, 9.61 mmol) was added to the solution and the mixture was stirred at room temperature for 2 h. Finally, the L-glutamine solution and the acylating agent from the previous step were combined under stirring for 20 min. Triethylamine (0.675 mL, 4.84 mmol) was added and the reaction mixture was stirred further at room temperature for 4 h. Afterwards aqueous HCl solution (4 M) was added and the mixture with pH 3 was transfer into water (20 mL). Extraction was carried out with DCM (25 mL × 3) and the organic layer was washed with brine (20 mL), dried over $MgSO_4$ and the solvent was removed *in vacuo*. Because of insufficient purity of this crude, further purification *via* column chromatography over silica gel (57.5 g, gradient from DCM : CH_3OH – 100 : 0 v/v% to DCM : CH_3OH – 40 : 60 v/v%) was needed to give **6c** as a pale orange sticky/viscous product (yield in 2 steps 282 mg, 31%).

5.1.1.7. Synthesis of N-((2E)-hept-2-enoyl)-L-glutamine (7c)

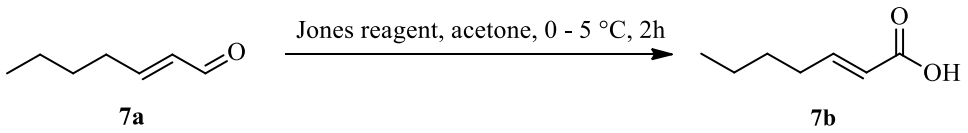

Figure 51: Synthesis of (2*E*)-hept-2-enoic acid (**7b**) starting from (2*E*)-hept-2-enal (**7a**).

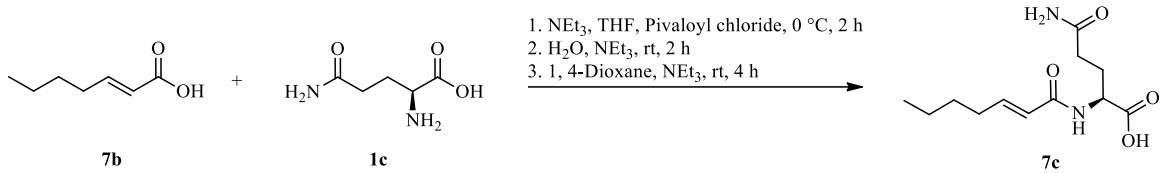

Figure 52: Synthesis of FAC **7c** starting from (2*E*)-hept-2-enoic acid (**7b**) and L-glutamine (**1c**).

To a solution of (2*E*)-hept-2-enal (457 mg, 4.08 mmol, **7a**) in acetone (10 mL) at 0 - 5 °C Jones reagent (1.25 mL, 2.66 g CrO_3 in 2.3 mL concentrated H_2SO_4 and 7.7 mL H_2O) was added dropwise (approximately 100 µL/portion) over 5 min. The reaction mixture was stirred for 2 h at the same temperature. After this time, the solvent was removed under reduced pressure and the resulting emulsion was diluted with water (15 mL) and extracted with ethyl acetate (15 mL × 3). The organic layer was then washed with 10% aqueous K_2CO_3 (20 mL × 2) and the biphasic system was separated. The pH of aqueous phase was adjusted to 1 with 4 M HCl and the solution was extracted with ethyl acetate (15 mL × 3). The organic layer was washed with water (10 mL), dried (Na_2SO_4) and the solvent was removed under reduced pressure. The intermediate product **7b** (yield 0.295 g, 56%) with sufficient purity was directly employed for the next reaction.

Fatty acid-amino acid conjugate (FACs) **7c** was prepared by mixing (2*E*)-hept-2-enoic acid (0.253 g, 1.97 mmol, **7b**) with triethylamine (329 µL, 2.36 mmol) in THF (13.9 mL). The mixture was cooled down to 0 °C and pivaloyl chloride (262 µL, 2.14 mmol) was added dropwise. The reaction mixture was stirred at the same temperature for 2 h. After filtration, the filter cake was rinsed with THF (14.4 mL) and the filtrate and washings were combined. 1,4-dioxane (12.72 mL) was added and the mixture was stored until the next step. Meanwhile, L-glutamine (0.574 g, 3.93 mmol, **1c**) was dissolved in distilled water (4.62 mL). Triethylamine (549 µL, 3.94 mmol) was added to the clear solution and the stirring was continued at room temperature for the next 2 h. Then, the L-glutamine solution and the acylating agent from the previous step were combined and stirred for 20 min. Triethylamine (277 µL, 1.99 mmol) was added and the reaction mixture was stirred further at room temperature for 4 h. Afterwards aqueous HCl solution (4 M) was added and the mixture with pH 3 was transferred into water (25 mL). The mixture was extracted with DCM (30 mL × 3) and the organic phase was washed with brine (15 mL), dried over $MgSO_4$ and the solvent was removed *in vacuo*. The raw product was purified *via* column chromatography (gradient from DCM : CH_3OH – 100 : 0 v/v% to DCM : CH_3OH – 40 : 60 v/v%) to afford the a pale yellow sticky/viscous product (yield in 2 steps 197 mg, 19%).

*5.1.1.8. Synthesis of N-(9-(1´´-oxooctadecanoyl)-octadec-10-enoyl)- L-glutamine (**8c**) and N-(10-(1´´-oxooctadecanoyl)-octadec-8-enoyl)- L-glutamine (**8d**)*

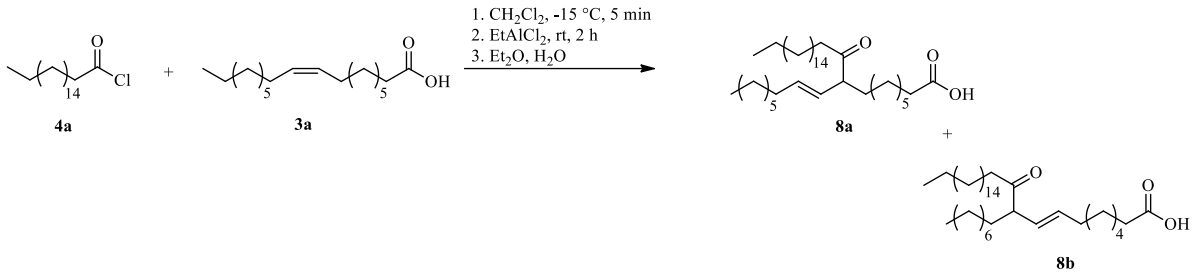

Figure 53: Synthesis of branched fatty acids **8a** and **8b** starting from octadecanoyl chloride (**4a**) and (9*Z*)-octadec-9-enoic acid (**3a**).

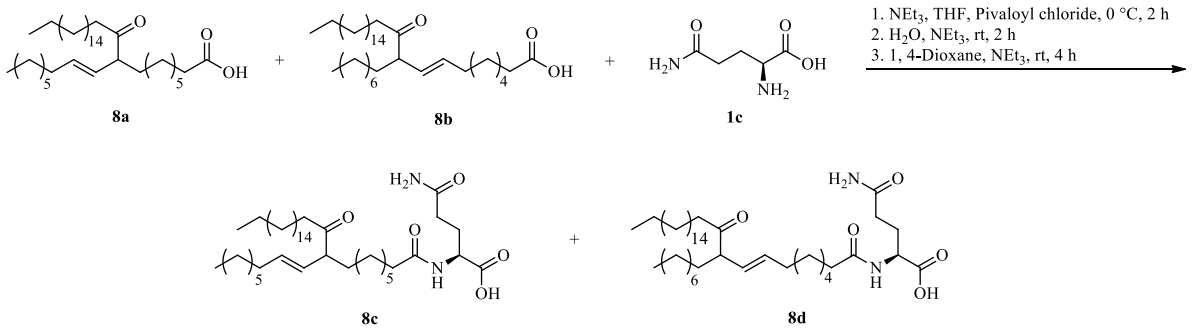

Figure 54: Synthesis of branched FACs **8c** and **8d** starting from branched fatty acids **8a** and **8b**.

A solution of (9*Z*)-octadec-9-enoic acid (1.22 g, 4.34 mmol, **3a**) and acylating agent octadecanoyl chloride (1.51 g, 4.98 mmol, **4a**) in DCM (10 mL) was stirred under N_2 (1 atm) at -15 °C for 5 min. The acylation of **3a** was induced by carefully, dropwise addition of ethylaluminium dichloride (1 M in hexane) in equivalent amount of 10 mL (10 mmol). The reaction mixture was further stirred at room temperature for 2h. Afterwards the reaction was quenched with Et_2O (100 mL) and water (40 mL) and 10% HCl was dropwise added to dissolve remaining aluminum salts. The clear solution was transferred into a dropping funnel and the organic layer was separated, washed with water (30 mL × 3), dried over Na_2SO_4 and the solvent was removed under reduced pressure. The crude was chromatographed (gradient from heptane : EtOAc – 90 : 10 v/v% to heptane : EtOAc – 80 : 20 v/v%) afforded branched β,γ-unsaturated ketones with carboxy functions **8a**/**8b** as a white powder (yield 1.40 g, 61%).

Branched fatty acid-amino acid conjugate (FAC) **8c/8d** was prepared using an appropriate amount of branched fatty acid **8a/8b** (1.40 g, 2.56 mmol) with triethylamine (426 µL, 3.06 mmol) in THF (18 mL). The mixture was cooled to 0 °C and 2,2-dimethylpropanoyl chloride (339 µL, 2.77 mmol) was added. The reaction mixture was stirred at the same temperature for 2 h and then quickly filtered. The filter cake was rinsed with THF (19 mL). The filtrate and washings were collected, 1,4-dioxane (16.5 mL) was employed and the mixture was stored until the next step. Meanwhile, for the preparation of **8c/8d**, L-glutamine (0.749 g, 5.12 mmol, **1c**) was dissolved in water (5.98 mL). Triethylamine (711 µL, 5.10 mmol) was added to the solution and the mixture was stirred at room temperature for 2 h. Then, the L-glutamine solution and the acylating agent from the previous step were combined and stirred for further 20 min. Triethylamine (359 µL, 2.57 mmol) was added and the reaction mixture was stirred further at room temperature for 4 h. Afterwards 10% HCl was added until pH shown 3 and the mixture was poured into water (25 mL). Extraction was carried out with DCM (15 mL × 3) and the organic layer was washed with brine (15 mL), dried ($MgSO_4$) and the solvent was removed *in vacuo*. The raw product **8c/8d** was purified *via* column chromatography over silica gel (35 g, gradient from DCM : CH_3OH – 100 : 0 v/v% to DCM : CH_3OH – 60 : 40 v/v%) to give a **8c/8d** as an off-white solid (yield in 2 steps 1.19 g, 41%).

*5.1.1.9. Synthesis of N-(12-oxononacosa-9-enoyl)-L-glutamine (**9b**)*

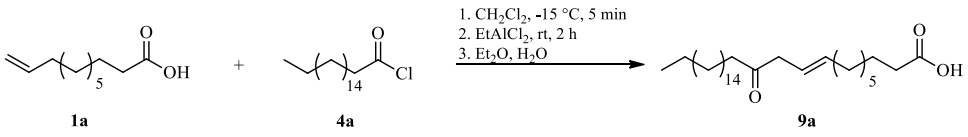

Figure 55: Synthesis of unsaturated ketone with carboxy function **9a** starting from 10-undecenoic acid (**1a**) and octandecanoyl chloride (**4a**).

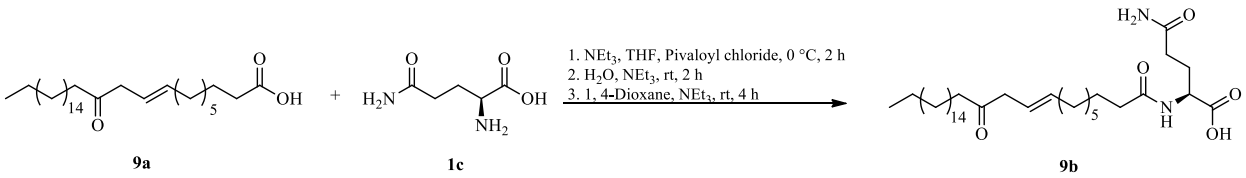

Figure 56: Synthesis of FAC **9b** starting from unsaturated ketone with carboxy function **9a** and L-glutamine (**1c**).

A solution of 10-undecenoic acid (0.918 g, 4.98 mmol, **1a**) and octadecanoyl chloride (1.52 g, 5.01 mmol, **4a**) in DCM (10 mL) was stirred under N_2 (1 atm) at -15 °C for 5 min. Ethylaluminium dichloride (1 M in hexane) in equivalent amount of 10 mL (10 mmol) was added dropwise and the reaction mixture was stirred at room temperature for 2h. The reaction was quenched with Et_2O (100 mL) and water (40 mL). Afterwards 10% HCl was dropwise added to dissolve remaining aluminium salts. The organic phase was separated, washed with water (30 mL × 3), dried over Na_2SO_4 and the solvent was removed under reduced pressure. The raw product was purified by recrystallization from acetone to yield β,γ-unsaturated ketone with carboxy functions **9b** as a white powder (yield 0.208 mg, 9%).

Further reaction was carried out by stirring long carbon chain fatty acid **9a** (0.208 g, 0.462 mmol) with triethylamine (76.9 µL, 0.552 mmol) in THF (3.24 mL). The mixture was cooled to 0 °C, 2,2-dimethylpropanoyl chloride (61.1 µL, 0.498 mmol) was added and the stirring was continued at the same temperature for 2 h. After filtration the filter cake was washed with THF (3.24 mL). The collected filtrate and washings were diluted with 1,4-dioxane (2.97 mL) and stored until the next step. Simultaneously, for the preparation of **9b**, L-glutamine (0.134 g, 0.917 mmol, **1c**) was dissolved in water (1.08 mL) and triethylamine (128 µL, 0.920 mmol) was added to the solution and the mixture was stirred at room temperature for 2 h. Thereafter the same solution and the **9b** from the previous step were combined and stirred for 20 min. Triethylamine (64.7 µL, 0.464 mmol) was added and the reaction mixture was stirred further at room temperature for 4 h. Afterwards 10% HCl was added and therefore pH was set to 3. The mixture was transferred into water (25 mL) and extraction was carried out with DCM (15 mL × 3) and the organic layer was washed with brine (15 mL), dried over $MgSO_4$ and the solvent was removed *in vacuo*. Because of insufficient purity of this crude, further purification *via* column chromatography over silica gel (12 g, gradient from DCM : CH_3OH – 100 : 0 v/v% to DCM : CH_3OH – 60 : 40 v/v%) was needed to obtain **9b** as a white solid (yield in 2 steps 16.2 mg, 1%).

*5.1.1.10. Synthesis of of (S)-N-α-octanoyl-L-glutamine (**10b**)*

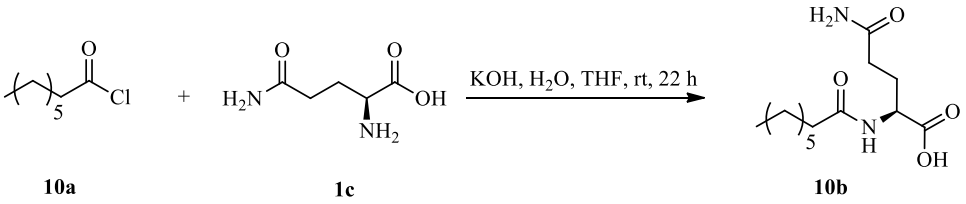

Figure 57: Synthesis of FAC **10b** starting from octanoyl chloride (**10a**) and L-glutamine (**1c**).

Octanoyl chloride (863 µL, 5 mmol, **10a**) was dissolved in THF (10 mL) and added dropwise to a solution of L-glutamine (0.741 g, 5.07 mmol, **1c**) and KOH (0.596 g, 10.6 mmol) in distilled water (10 mL) over 10 min at room temperature. The reaction mixture was stirred at the same temperature for 22 h and finally the solvent was evaporated under reduced pressure. The resulting volume of the solution of approximately 12.5 mL was adjusted to pH 1 with aqueous HCl solution and the precipitated raw product was filtered, washed with water (5 mL) and Et_2O (5 mL). The precipitate was further purified by recrystallization from ethyl acetate to give a pure product **10 b** as a white powder (yield 347 mg, 26%).

*5.1.1.11. Synthesis of N-(12-hydroxynonadec-9-enoyl)-L-glutamine (**11e**)*

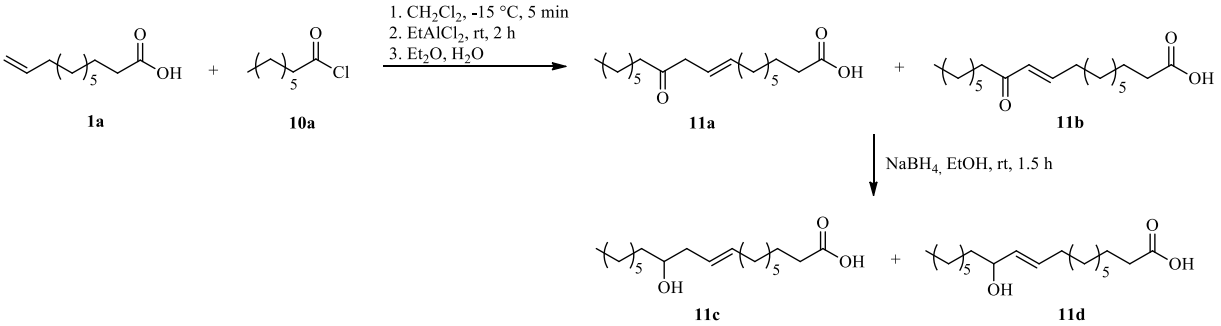

Figure 58: Synthesis of unsaturated ketone with carboxy function **11a/11b** starting from 10-undecenoic acid (**1a**) and octanoyl chloride (**10a**). Reduction of unsaturated ketone with carboxy function **11a/11b** to hydroxylated fatty acids **11c/11d**.

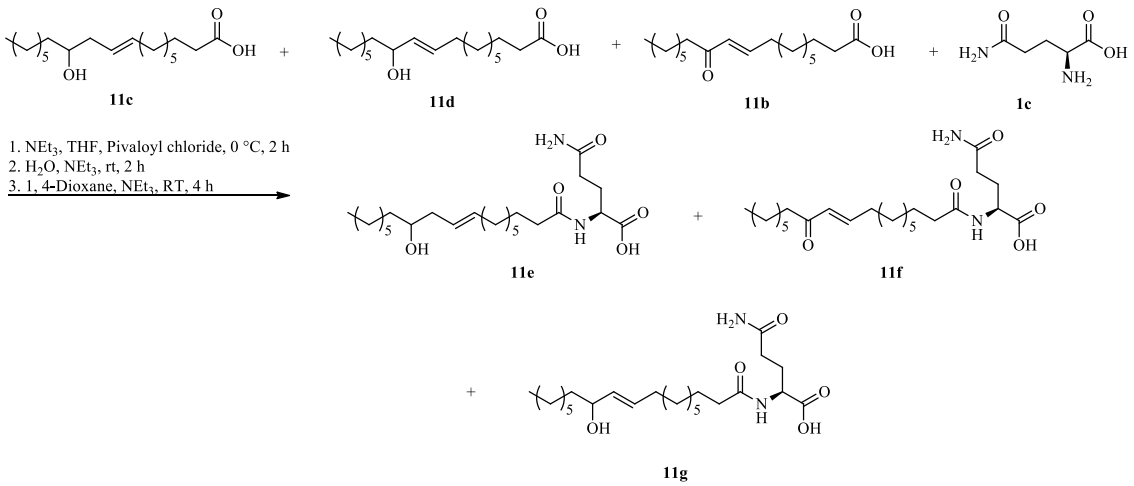

Figure 59: Synthesis of hydroxylated FACs **11e/11f/11g** starting from hydroxylated fatty acid **11b/11c/11d** and L-glutamine (**1c**).

A mixture of 10-undecenoic acid (1.86 g, 10.1 mmol, **1a**) and acylating agent octanoyl chloride (1.69 g, 10.4 mmol, **10a**) in DCM (15 mL) was first prepared. The stirring was performed under N_2 (1 atm) at -15 °C. After 5 min ethylaluminium dichloride (1 M in hexane) in equivalent amount of 20 mL (20 mmol) was carefully, slowly added to the solution. The reaction mixture was stirred at room temperature for 2h and the reaction was quenched with Et_2O (200 mL) and water (80 mL). Then 10% HCl was dropwise added to dissolve remaining aluminium salts. The clear solution was transferred into dropping funnel and the organic layer was separated, washed with water (90 mL × 3), dried over Na_2SO_4 and the solvent was removed under reduced pressure. The crude was chromatographed over silica gel (63.1 g, gradient from heptane : EtOAc – 90 : 10 v/v% to heptane : EtOAc – 40 : 60 v/v%) afforded β,γ-unsaturated ketone with carboxy function **11a**/**11b** as a white solid (yield 1.46 g, 47%).

In the next step ketone **11a/11b** (1.46 g, 4.71 mmol) was reduced using $NaBH_4$ (0.189 g, 5.01 mmol) in ethanol (40 mL). The reaction mixture was stirred at room temperature for 1.5 h and glacial acetic acid was added to destroy an excess $NaBH_4$. The neutralized solution was washed with water (40 mL) and the solvent was removed under reduced pressure to give **11c/11d** (yield in 2 steps 1.91 g, 61%).

Compounds **11e/11f/11g** was prepared by stirring **11b/11c/11d** (1.91 g, 6.12 mmol) with triethylamine (1.02 mL, 7.34 mmol) in THF (43.1 mL). Pivaloyl chloride (0.813 mL, 6.64 mmol) was added at 0 °C and the reaction mixture was stirred at the same temperature for 2 h. After filtration, filter cake was rinsed with THF (45 mL). The filtrate and washings were combined and diluted with 1,4-dioxane (40 mL). Meanwhile, L-glutamine (1.78 g, 12.2 mmol, **1c**) was dissolved in water (14.36 mL) and triethylamine (1.71 mL, 12.2 mmol) was added to the solution. The mixture was stirred at room temperature for 2 h. Thereafter this solution and the acylating agent from the previous step were combined, stirred for 20 min and triethylamine (0.861 mL, 6.14 mmol) was added. The reaction mixture was stirred further at room temperature for 4 h. Then, 10% HCl was added dropwise until pH was 3 and the mixture was poured into water (15 mL). For the extraction DCM (30 mL × 3) was used and the organic layer was washed with brine (20 mL), dried ($MgSO_4$) and the solvent was removed *in vacuo*. Further purification of crude *via* column chromatography (gradient from DCM : CH_3OH – 100 : 0 v/v% to DCM : CH_3OH – 40 : 60 v/v%) was needed to yield **11e/11f/11g** as an off-white solid (yield in 3 steps 412 mg, 9%).

5.1.2. *Vinca minor* und *Populus* hybrids experiments

To investigate whether the synthesized eleven compounds act on biosynthetic pathways in plants, the substances were dissolved in a mixture of ethanol, a nonionic detergent Tween® 20, and water (EtOH : Tween® 20 : H_2O – 1 : 0.2 : 8.8 v/v/v). The concentration of the prepared solutions of the synthesized substances was 0.4 mM throughout. The experiments were carried out in triplicate, more

precisely four leaves from one plant were each punched twice with a hole punch, taking care to treat the rather young leaves. The exception was the treatment of compounds **3b**, **6c**, and **8c**/**8d**, which included an additional 10 replicates each, as the experiments were repeated again based on the earlier encouraging results. Immediately after punching the leaves, 2.5 µL of each of the previously prepared solutions of the synthesized compounds were applied to the wounds with the aid of a pipette. The *Spodoptera littoralis* caterpillars were also applied to the plants for 3 to 4 h. To prevent the caterpillars from being eaten by a bird or escaping, they were kept in a tea strainer. The time of feeding the caterpillars with the above-mentioned plants was also not exceeded, as they would possibly eat whole leaves and no plant material would be provided for extraction and further investigation. Eight days later, a harvest and drying at 40 °C of the leaves artificially wounded and treated with the substances was carried out. However, to determine after how many days biosynthetic pathways are induced, the damaged and treated leaves of *V. minor* were also harvested after the first, second, third and sixth days following by immediate transfer to the drying chamber. *Populus* hybrids have not been studied in this manner.

For the determination of natural products in *V. minor* and *Populus* hybrids, approximately 20 mg of dried leaves were ground in an QIAGEN Tissue Lyser II (30 s^{-1} for 4 min) giving a green and fine powder. Each Eppendorf tube containing the plant material was supplied with 0.5 mL of methanol. The mixture was vortexed and then transferred to an ultrasonic bath for 10 min at room temperature. Subsequently, to enable the supernatant (extraction solution) to be collected, all Eppendorf tubes were centrifuged (15 min, rt, 14000 × g). The extraction procedure described above was repeated a total of three times. The combined extracts were dried overnight under a fume hood and the next day the remaining solvent was evaporated in a vacuum centrifuge. The remaining residue was weighed and brought to a concentration of 10 mg/mL with DMSO. For the HPLC measurement, 50 µL of each extract was collected and transferred to a 96-well plate.

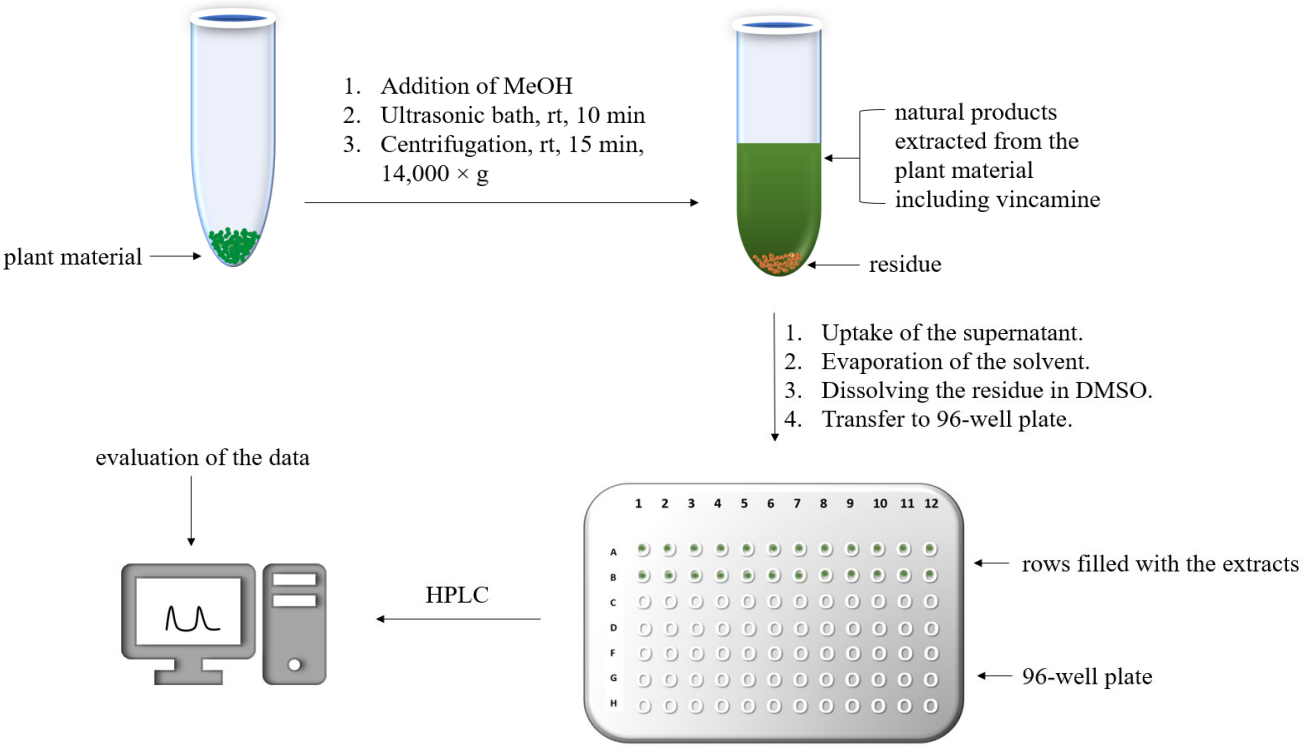

Figure 60: Workflow for the extraction of natural products and subsequent the HPLC - measurement.

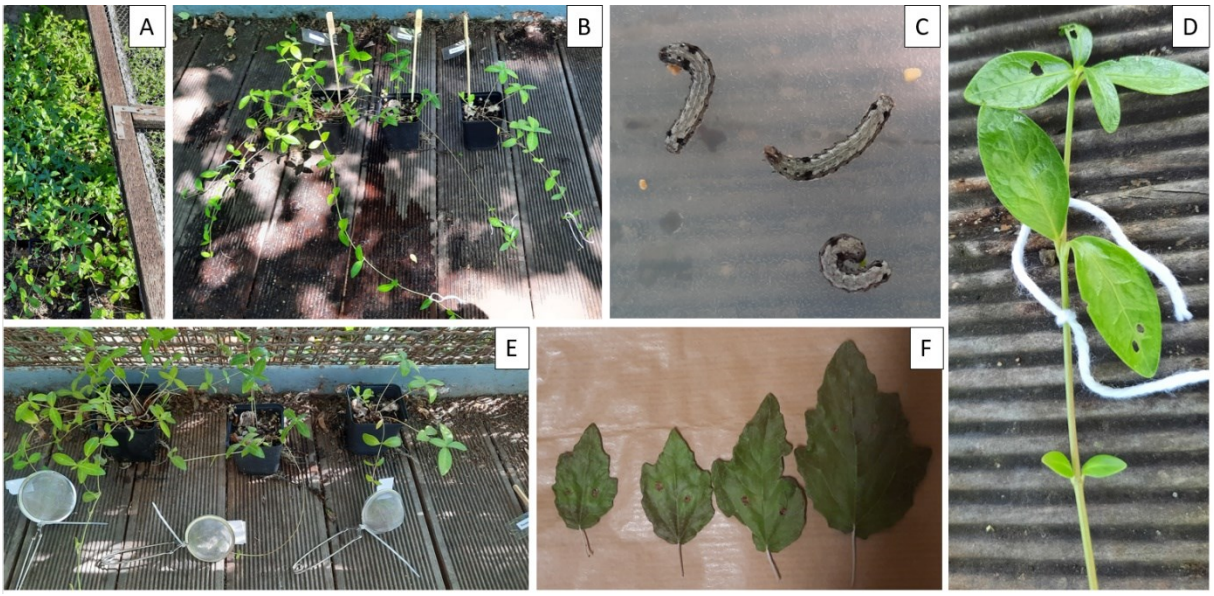

Figure 61: *V. minor* plants used for experiments (A). Performing experiments in the triplicate and marking with the flags (B). *Spodoptera littoralis* caterpillars applied to plants (C). *V. minor* leaves wounded by the caterpillars (D). Caterpillars fixed in a tea strainer when feeding on *V. minor* leaves (E). Punched, **11e**/**11f**/**11g** substance-treated and subsequently dried leaves of *Populus* hybrids before weighing (F).

6. Characterization

6.1. *N*-(10-Hydroxyundecanoyl)-L-glutamine (1d)

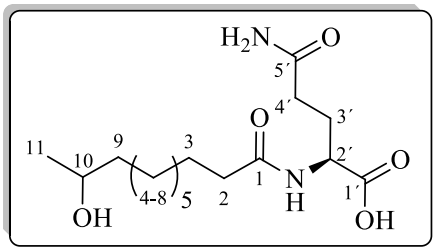

Isolated yield: 157 mg (19% in 2 steps).

Table 4: HRMS (ESI) data of *N*-(10-hydroxyundecanoyl)-L-glutamine (**1d**).

molecular ion	calculated m/z	found m/z
$[M-H]^-$	329.2082	329.2089
$[M+H]^+$	331.2227	331.2226
$[M+Na]^+$	353.2047	353.2048
$[M+K]^+$	369.1786	369.1785
$[2M-H]^-$	659.4237	659.4247
$[2M+Na]^+$	683.4202	683.4199

Table 5: NMR data of *N*-(10-hydroxyundecanoyl)-L-glutamine (**1d**).

position	***N*-(10-Hydroxyundecanoyl)-L-glutamine (1d)**	
	^{1}H-NMR (600 MHz, CD_3OD)	**^{13}C-NMR** (150 MHz, CD_3OD)
	δ ^{1}H (ppm)	δ ^{13}C (ppm)
1	-	176.5 (s)
2	2.25 (2H, t, *J* = 7.5 Hz)	37.1 (t)
3	1.62 (2H, m)	27.0 (t)
4 - 8	1.21 – 1.45 (10H, m)	28.4 (t)/30.4 (t)/30.5 (t)/30.7 (t)/30.9 (t)
9	1.21 – 1.45 (2H, m)	40.4 (t)
10	3.70 (1H, tq, *J* = 6.3, 5.8 Hz)	68.7 (d)
11	1.14 (3H, d, *J* = 6.0 Hz)	23.6 (q)
1′	-	175.7 (s)
2′	4.37 (1H, dd, *J* = 8.7, 5.0 Hz)	53.8 (d)
3′a	1.94 (1H, ddt, *J* = 16.2, 8.1, 5.8 Hz)	28.9 (t)
3′b	2.16 (1H, ddt, *J* = 16.2, 8.1, 5.8 Hz)	
4′	2.31 (2H, dd, *J* = 8.7, 7.3, 5.8 Hz)	33.0 (t)
5′	-	178.0 (s)

6.2. (S)-*N*-α-Undec-10-enoyl-L-glutamine (2b)

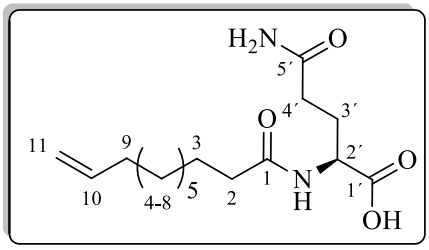

Isolated yield: 0.980 g (31%).

Table 6: HRMS (ESI) of (S)-*N*-α-undec-10-enoyl-L-glutamine (**2b**).

molecular ion	calculated m/z	found m/z
$[M+H]^+$	313.2122	313.2099
$[M+Na]^+$	335.1941	335.1935
$[M+K]^+$	351.1681	351.1597
$[M+2Na-H]^+$	357.1761	357.1755

Table 7: NMR data of (S)-*N*-α-undec-10-enoyl-L-glutamine (**2b**).

position	**(S)-*N*-α-Undec-10-enoyl-L-glutamine (2b)**	
	^{1}H-NMR (600 MHz, CD_3OD)	**^{13}C-NMR** (150 MHz, CD_3OD)
	δ ^{1}H (ppm)	δ ^{13}C (ppm)
1	8.19 (1H, d, *J* = 7.5 Hz, CON – *H*)	175.1 (s)
2	2.25 (2H, t, *J* = 7.6 Hz)	37.0 (t)
3	1.57 – 1.65 (2H, m)	27.0 (t)
4 - 7	1.32 – 1.40 (8H, m)	30.3 – 30.6 (t)
8	1.57 – 1.65 (2H, m)	30.3 – 30.6 (t)
9	2.01 – 2.06 (2H, m)	35.0 (t)
10	5.81 (1H, ddt, *J* = 17.1, 10.2, 6.7 Hz)	140.3 (d)
11´a	4.91 (1H, dd, *J* = 13.6, 1.3 Hz)	114.8 (t)
11´b	4.98 (1H, dd, *J* = 13.6, 1.3 Hz)	
1´	-	177.8 (s)
2´	4.39 (1H, dd, *J* = 5.0, 9.1 Hz)	53.4 (d)
3´a	1.95 (1H, dtd, *J* = 14.0, 8.2, 5.8 Hz)	28.7 (t)
3´b	2.16 (1H, dtd, *J* = 14.0, 8.2, 5.8 Hz)	
4´	2.27 – 2.36 (2H, m)	32.9 (t)
5´	6.78 (1H, s, CON – H_2)	176.6 (s)
	7.56 (1H, s, CON – H_2)	

6.3. *N*-((9Z)-Octadec-9-enoyl)-L-glutamine (3b)

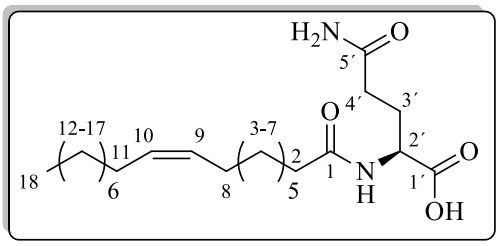

Isolated yield: 157 mg (8%).

Table 8: HRMS (ESI) of *N*-((9*Z*)-octadec-9-enoyl)-L-glutamine (**3b**).

molecular ion	calculated m/z	found m/z
$[M+Na]^+$	433.3037	433.3038
$[2M+Na]^+$	843.6181	843.6175

Table 9: NMR data of *N*-((9*Z*)-octadec-9-enoyl)-L-glutamine (**3b**).

position	***N*-((9Z)-Octadec-9-enoyl)-L-glutamine (3b)**	
	^{1}H-NMR (600 MHz, CD_3OD)	**^{13}C-NMR** (150 MHz, CD_3OD)
	δ ^{1}H (ppm)	δ ^{13}C (ppm)
1	7.94 (1H, d, *J* = 7.64 Hz, CON – *H*)	176.3 (s)
2	2.24 (2H, t, *J* = 7. 6 Hz)	37.2 (t)
3	1.60 – 1.65 (2H, m)	27.1 (t)
4 – 7, 12 - 15	1.21 – 1.33 (16H, m)	30.4 - 31.0 (t)
8, 11	2.03 (4H, dt, *J* = 8.9, 6.8 Hz)	28.3 (t)
9 - 10	5.30 – 5.41 (2H, m)	131.0 (d)
16	1.21 – 1.33 (2H, m)	33.1 (t)
17	1.21 – 1.33 (2H, m)	23.9 (t)
18	0.90 (3H, t, *J* = 7.0 Hz)	14.6 (q)
1′	-	178.2 (s)
2′	4.35 (1H, dd, *J* = 8.4, 5.1 Hz)	54.3 (d)
3′a	1.95 (1H, dtd, *J* = 14.6, 7.9, 5.7 Hz)	29.4 (t)
3′b	2.14 (1H, dtd, *J* = 14.6, 7.9, 5.7 Hz)	
4′	2.29 (2H, dd, *J* = 15.8, 6.8 Hz)	33.2 (t)
5′	6.75 (1H, s, CON – H_2)	176.3 (s)
	7.58 (1H, s, CON – H_2)	

6.4. (S)-*N*-α-Octadecanoyl-L-glutamine (4b)

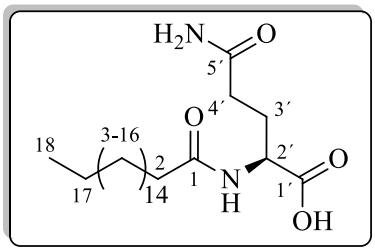

Isolated yield: 1.64 g (40%).

Table 10: HRMS (ESI) of (S)-*N*-α-octadecanoyl-L-glutamine (**4b**).

molecular ion	calculated m/z	found m/z
$[M+H]^+$	413.3374	413.3364
$[M+Na]^+$	435.3193	435.3183
$[M+K]^+$	451.2933	451.2920
$[M+2Na-H]^+$	457.3013	457.3001

Table 11: NMR data of (S)-*N*-α-octadecanoyl-L-glutamine (**4b**).

position	**(S)-*N*-α-Octadecanoyl-L-glutamine (4b)**	
	^{1}H-NMR (600 MHz, DMSO)	**^{13}C-NMR** (150 MHz, DMSO)
	δ ^{1}H (ppm)	δ ^{13}C (ppm)
1	8.00 (1H, d, *J* = 7.6 Hz, CON – *H*)	172.3 (s)
2	2.17 (2H, t, *J* = 7.4 Hz)	35.1 (t)
3	1.43 – 1.51 (2H, m)	28.5-29.0 (t)
4 - 16	1.13 – 1.33 (26H, m)	24.5/28.5-29.0/31.3/33.7 (t)
17	1.13 – 1.33 (2H, m)	22.1 (t)
18	0.85 (3H, t, *J* = 6.9 Hz)	13.9 (q)
1′	12.09 (1H, br s, O - *H*)	173.5 (s)
2′	4.12 (1H, dd, *J* = 14.9, 6.8 Hz)	51.5 (d)
3′a	1.72 (1H, dtd, *J* = 13.9, 8.2, 6.0 Hz)	26.9 (t)
3′b	1.91 (1H, dtd, *J* = 13.9, 8.2, 6.0 Hz)	
4′	2.09 (2H, dd, *J* = 6.9 Hz)	31.4 (t)
5′	6.73 (1H, s, CON – *H*$_2$)	173.5 (s)
	7.27 (1H, s, CON – *H*$_2$)	

6.5. *N*-(Heptanoyl)-L-glutamine (5c)

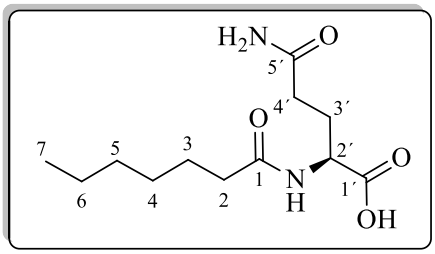

Isolated yield: 947 mg (28% in 2 steps).

Table 12: HRMS (ESI) of *N*-(heptanoyl)-L-glutamine (**5c**).

molecular ion	calculated m/z	found m/z
$[M+H]^+$	259.1652	259.1650
$[M+Na]^+$	281.1472	281.1468
$[2M+H]^+$	517.3232	517.3227

Table 13: NMR data of *N*-(heptanoyl)-L-glutamine (**5c**).

position	***N*-(Heptanoyl)-L-glutamine (5c)**	
	^{1}H-NMR (600 MHz, CD_3OD)	**^{13}C-NMR** (150 MHz, CD_3OD)
	δ ^{1}H (ppm)	δ ^{13}C (ppm)
1	8.19 (1H, d, *J* = 8.7 Hz, CON – *H*)	176.4 (s)
2	2.25 (2H, t, *J* = 7.5 Hz)	36.8 (t)
3	1.60 – 1.64 (2H, m)	26.8 (t)
4	1.30 – 1.38 (6H, m)	30.0 (t)
5	1.30 – 1.38 (6H, m)	32.7 (t)
6	1.30 – 1.38 (6H, m)	23.6 (t)
7	0.91 (3H, t, *J* = 6.7 Hz)	14.4 (q)
1′	-	175.0 (s)
2′	4.34 – 4.40 (1H, m)	53.3 (d)
3′a	1.91 – 1.98 (1H, m)	28.5 (t)
3′b	2.14 – 2.19 (1H, m)	
4′	2.27 – 2.37 (2H, m)	32.8 (t)
5′	6.80 (1H, s, CON – H_2)	177.7 (s)
	7.57 (1H, s, CON – H_2)	

6.6. *N*-(Pent-2-enoyl)-L-glutamine (6c)

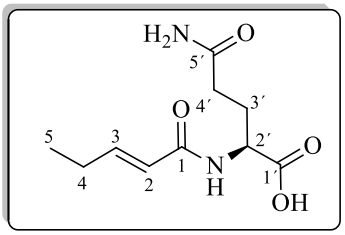

Isolated yield: 282 mg (31% in 2 steps).

Table 14: HRMS (ESI) of *N*-(pent-2-enoyl)-L-glutamine (**6c**).

molecular ion	calculated m/z	found m/z
$[M+Na]^+$	251.1002	251.1001
$[M+H]^+$	229.1183	229.1179

Table 15: NMR data of *N*-(pent-2-enoyl)-L-glutamine (**6c**).

position	***N*-(Pent-2-enoyl)-L-glutamine (6c)**	
	^{1}H-NMR (600 MHz, CD_3OD)	**^{13}C-NMR** (150 MHz, CD_3OD)
	δ ^{1}H (ppm)	δ ^{13}C (ppm)
1	-	168.5 (s)
2	6.01 (1H, d, *J* =24.8 Hz)	123.7 (d)
3	6.84 (1H, dt, *J* = 15.4 Hz, 6.4 Hz)	147.4 (d)
4	2.22 (2H, m)	26.1 (t)
5	1.08 (3H, t, *J* = 7.4 Hz)	12.8 (t)
1′	-	178.1 (s)
2′	4.40 (1H, dd, *J* = 8.3 Hz, 5.0 Hz)	54.5 (d)
3′a	1.94 (1H, m)	29.4 (t)
3′b	2.20 (1H, m)	
4′	2.35 (2H, m)	33.0 (t)
5′	-	181.0 (s)

6.7. *N*-(Hept-2-enoyl)-L-glutamine (7c)

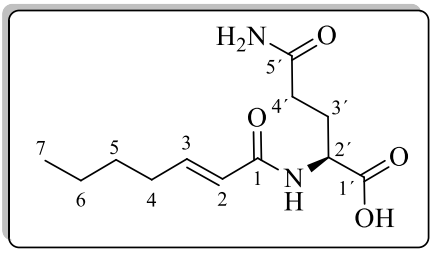

Isolated yield: 197 mg (19% in 2 steps).

Table 16: HRMS (ESI) of *N*-(hept-2-enoyl)-L-glutamine (**7c**).

molecular ion	calculated m/z	found m/z
$[M+H]^+$	257.1496	257.1494
$[M+Na]^+$	279.1315	279.1315
$[M+2Na+H]^+$	301.1135	301.1131
$[2M+Na]^+$	535.2738	535.2734

Table 17: NMR data of *N*-(hept-2-enoyl)-L-glutamine (**7c**).

position	***N*-(Hept-2-enoyl)-L-glutamine (7c)**	
	^{1}H-NMR (600 MHz, CD_3OD)	**^{13}C-NMR** (150 MHz, CD_3OD)
	δ ^{1}H (ppm)	δ ^{13}C (ppm)
1	8.20 (1H, m, CON – *H*)	168.9 (s)
2	6.00 (1H, d, *J* = 15.4 Hz)	124.3 (d)
3	6.81 (1H, dt, *J* = 15.4, 7.0 Hz)	146.3 (d)
4	2.14 – 2.24 (2H, m)	32.7 (t)
5	1.46 (2H, quin, *J* = 7.4 Hz)	31.6 (t)
6	1.37 (2H, sext, *J* = 7.3 Hz)	23.2 (t)
7	0.94 (3H, t, *J* = 7.3 Hz)	14.2 (q)
1′	-	175.1 (s)
2′	4.45 (1H, dd, *J* = 8.7, 4.9 Hz)	53.4 (d)
3′a	1.94 – 2.00 (1H, m)	28.7 (t)
3′b	2.14 – 2.24 (1H, m)	
4′	2.32 (2H, dd, *J* = 14.9, 7.2 Hz)	32.7 (t)
5′	6.96 (1H, m, CON – *H*$_2$)	177.7 (s)
	7.57 (1H, m, CON – *H*$_2$)	

6.8. *N*-(9-(1´´-Oxooctadecanoyl)-octadec-10-enoyl)-L-glutamine (8c) and *N*-(10-(1´´-Oxooctadecanoyl)-octadec-8-enoyl)-L-glutamine (8d)

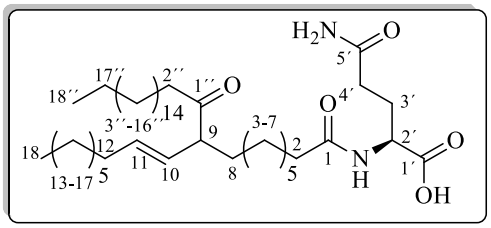

8c

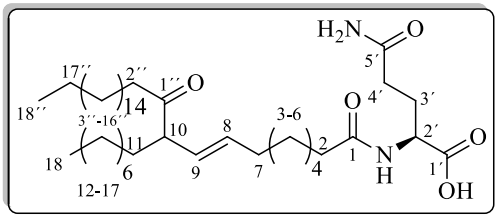

8d

Isolated yield: 1.19 g (41% in 2 steps)

Table 18: HRMS (ESI) of *N*-(9-(1´´-oxooctadecanoyl)-octadec-10-enoyl)-L-glutamine (**8c**) and *N*-(10-(1´´-oxooctadecanoyl)-octadec-8-enoyl)-L-glutamine (**8d**).

molecular ion	calculated m/z	found m/z
$[M+H+K]^{2+}$	358.2729	358.2688
$[M+H]^{+}$	677.5827	677.5828
$[M+Na]^{+}$	699.5646	699.5645
$[M+K]^{+}$	451.2933	451.2920
$[2M+Na]^{+}$	1376.1401	1376.1424

Table 19: NMR data of *N*-(9-(1´´-oxooctadecanoyl)-octadec-10-enoyl)-L-glutamine (**8c**) and *N*-(10-(1´´-oxooctadecanoyl)-octadec-8-enoyl)- L-glutamine (**8d**). Unless otherwise noted, the shifts refer to all two compounds. Abbreviation "n.d." means "not defined".

position	***N*-(9-(1´´-Oxooctadecanoyl)-octadec-10-enoyl)-L-glutamine (8c) and *N*-(10-(1´´-Oxooctadecanoyl)-octadec-8-enoyl)-L-glutamine (8d)**	
	^{1}H-NMR (600 MHz, CD_3OD)	**^{13}C-NMR** (150 MHz, CD_3OD)
	δ ^{1}H (ppm)	δ ^{13}C (ppm)
1	-	n.d.
1´´	-	n.d.
2, 2´´	2.29 – 2.55 (2×4H, m)	36.1/ 41.5 (t)
3, 3´´	1.47 – 1.67 (2×4H, m)	25.6/24.0 (t)
7 (for **8d**), 12 (for **8c**)	1.97 – 2.01 (2×2H, m)	32.6 (t)
6 (for **8d**), 13 (for **8c**)	1.44 (2×2H, m)	28.8 – 29.7 (t)
9 (for **8c**), 10 (for **8d**)	2.98 – 3.00 (2×1H, m)	56.8 (d)
9 (for **8d**), 10 (for **8c**)	5.20 – 5.35 (2×1H, m)	128.0 (d)
8 (for **8d**), 11 (for **8c**)	5.48 – 5.55 (2×1H, m)	134.5 (d)
8 (for **8c**), 11 (for **8d**)	1.47 – 1.67 (2×2H, m)	28.8 – 29.7 (t)
4 – 7 (for **8c**)	1.14 - 1.38 (8H, m)	28.8 – 29.7/26.5 (t)
4 – 5 (for **8d**)	1.14 - 1.38 (4H, m)	28.8 – 29.7 (t)
14 – 17 (for **8c**)	1.14 - 1.38 (8H, m)	28.8 – 29.7/31.9/23.0 (t)
12 – 17 (for **8d**)	1.14 - 1.38 (12H, m)	26.5/28.8 – 29.7/31.9/23.0 (t)
4´´ – 17´´	1.14 - 1.38 (2×28H, m)	28.8 – 29.7/31.9/23.0 (t)
18, 18´´	0.86 (2×6H, t, J = 6.7 Hz)	14.1 (q)
1´	-	n.d.
2´	4.47 - 4.63 (2×1H, m)	52.4 (d)
3´a	1.98 (1H, m)	27.2 (t)
3´b	2.19 – 2.38 (1H, m)	
4´	2.50 – 2.55 (2×2H, m)	31.4 (t)
5´	-	n.d.

6.9. *N*-(12-Oxononacosa-9-enoyl)-L-glutamine (9b)

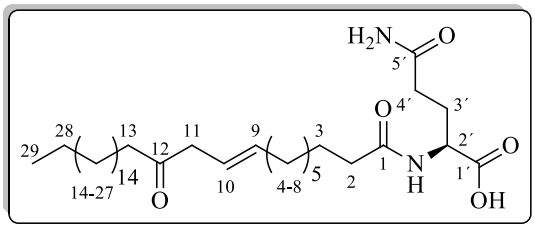

Isolated yield: 16.2 mg (1% in 2 steps).

Table 20: HRMS (ESI) of *N*-(12-oxononacosa-9-enoyl)-L-glutamine (**9b**).

molecular ion	calculated m/z	found m/z
$[M+H]^+$	579.4731	579.4731
$[M+Na]^+$	601.4551	601.4551
$[M+2Na+H]^+$	623.4370	623.4372
$[2M+Na]^+$	1179.9210	1179.9208

Table 21: NMR data of *N*-(12-oxononacosa-9-enoyl)-L-glutamine (**9b**). Abbreviation "n.d." means "not defined".

position	***N*-(12-Oxononacosa-9-enoyl)-L-glutamine (9b)**	
	^{1}H-NMR (600 MHz, $CDCl_3$)	**^{13}C-NMR** (150 MHz, CD_3OD)
	δ ^{1}H (ppm)	δ ^{13}C (ppm)
1	8.08 (1H, m, CON – *H*)	n.d.
2	1.91 – 2.31 (2H, m)	36.3 (t)
3	1.53 – 1.66 (2H, m)	24.1 (t)
4	1.23 – 1.31 (2H, m)	29.0 – 29.9 (t)
5	1.23 – 1.31 (2H, m)	29.0 – 29.9 (t)
6	1.23 – 1.31 (2H, m)	29.0 – 29.9 (t)
7	1.39 – 1.43 (2H, m)	29.0 – 29.9 (t)
8	1.91 – 2.31 (2H, m)	32.3 (t)
9	5.45 – 5.51 (1H, m)	135.1 (d)
10	5.45 – 5.51 (1H, m)	121.9 (d)
11	3.07 – 3.10 (2H, m)	46.9 (t)
12	-	n.d.
13	2.38 – 2.42 (2H, m)	42.5 (t)
14	1.53 – 1.66 (2H, m)	24.0 (t)
15 - 26	1.23 – 1.31 (24H, m)	29.0 – 29.9 (t)
27	1.23 – 1.31 (2H, m)	32.1 (t)
28	1.23 – 1.31 (2H, m)	22.9 (t)
29	0.86 (3H, t, J = 6.9 Hz)	14.3 (q)
1′	-	n.d.
2′	4.17 – 4.23 (1H, m)	57.0 (d)
3′	1.91 – 2.31 (2H, m)	32.4 (t)
4′	2.32 – 2.34 (2H, m)	36.4 (t)
5′	-	n.d.

6.10. (S)-*N*-α-Octanoyl-L-glutamine (10b)

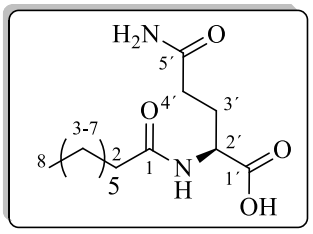

Isolated yield: 347 mg (26%).

Table 22: HRMS (ESI) of (S)-*N*-α-octanoyl-L-glutamine (**10b**).

molecular ion	calculated m/z	found m/z
$[M+H+K]^{2+}$	156.0720	156.0679
$[M+H]^{+}$	273.1809	273.1809
$[M+Na]^{+}$	295.1628	295.1630
$[2M+Na]^{+}$	567.3364	567.3361

Table 23: NMR data of (S)-*N*-α-octanoyl-L-glutamine (**10b**).

position	**(S)-*N*-α-octanoyl-L-glutamine (10b)**	
	^{1}H-NMR (600 MHz, CD_3OD)	**^{13}C-NMR** (150 MHz, CD_3OD)
	δ ^{1}H (ppm)	δ ^{13}C (ppm)
1	8.20 (1H, d, *J* = 8.2 Hz, CON – *H*)	176.6 (s)
2	2.25 (2H, t, *J* = 7.5 Hz)	37.0 (t)
3	1.57 – 1.65 (2H, m)	27.0 (t)
4	1.26 – 1.37 (2H, m)	30.3 (t)
5	1.26 – 1.37 (2H, m)	30.4 (t)
6	1.26 – 1.37 (2H, m)	32.9 (t)
7	1.26 – 1.37 (2H, m)	23.8 (t)
8	0.90 (3H, t, *J* = 7.1 Hz)	14.5 (q)
1′	-	175.1 (s)
2′	4.39 (1H, dd, *J* = 9.1, 5.0 Hz)	53.4 (d)
3′a	1.94 (1H, dtd, *J* = 13.8, 8.4, 5.7 Hz)	28.6 (t)
3′b	2.16 (1H, dtd, *J* = 13.8, 8.4, 5.7 Hz)	
4′	2.31 (2H, dd, *J* = 6.8, 4.7 Hz)	33.0 (t)
5′	6.80 (1H, s, CON – H_2)	177.8 (s)
	7.57 (1H, s, CON – H_2)	

6.11. *N*-(12-Hydroxynonadec-9-enoyl)-L-glutamine (11e), *N*-(12-Oxononadec-10-enoyl)-L-glutamine (11f) and *N*-(12-Hydroxynonadec-10-enoyl)-L-glutamine (11g)

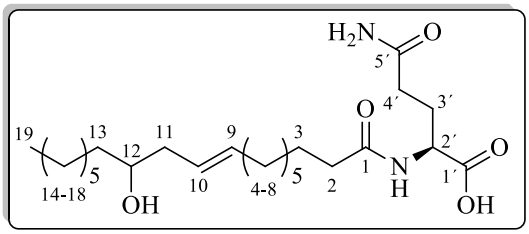

11e

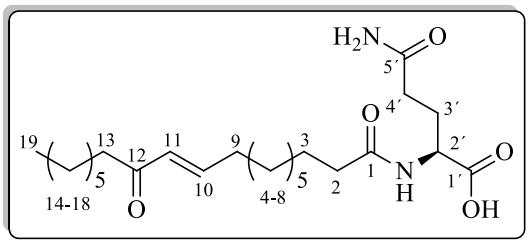

11f

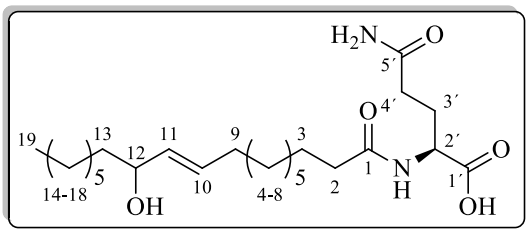

11g

Isolated yield: 412 mg (9% in 3 steps).

Table 24: HRMS (ESI) of *N*-(12-hydroxynonadec-9-enoyl)- L-glutamine (**11e**) or *N*-(12-hydroxynonadec-10-enoyl)-L-glutamine (**11g**).

molecular ion	calculated m/z	found m/z
$[M+Na]^+$	463.3148	463.3141
$[M+H]^+$	441.3328	441.3315

Table 25: NMR data of *N*-(12-hydroxynonadec-9-enoyl)-L-glutamine (**11e**), *N*-(12-oxononadec-10-enoyl)-L-glutamine (**11f**) and *N*-(12-hydroxynonadec-10-enoyl)-L-glutamine (**11g**). Unless otherwise noted, the shifts refer to all three compounds. Abbreviation "n.d." means "not defined".

position	***N*-(12-Hydroxynonadec-9-enoyl)-L-glutamine (11e), *N*-(12-Oxononadec-10-enoyl)-L-glutamine (11f) and *N*-(12-Hydroxynonadec-10-enoyl)-L-glutamine (11g)**	
	^{1}H-NMR (600 MHz, CD_3OD)	**^{13}C-NMR** (150 MHz, CD_3OD)
	δ ^{1}H (ppm)	δ ^{13}C (ppm)
1	-	178.0 (s)
2	2.24 (3×2H, t, *J* =7.5)	38.6 (t)
3	1.57 – 1.66 (3×2H, m)	26.7 (t)
4	1.34 (3×2H, m)	30.03 – 31.01 (t)
5 – 6	1.31 - 1.34 (3×4H, m)	30.03 – 31.01 (t)
7	1.31 - 1.34 (for **11f** & **11g**, 2×2H, m),	30.03 – 31.01 (t)
	1.43 – 1.52 (for **11e**, 2H, m)	30.03 – 31.01 (t)
8	1.49 (for **11f** & **11g**, 2×2H, m)	30.03 – 31.01 (t)
	2.01 (for **11e**, 2H, m)	29.4 (t)
9	2.03 (for **11g**, 2H, m)	29.4 (t)
	2.26 (for **11f**, 2H, m)	32.9 (t)
	5.44 (for **11e**, 1H, m)	134.6 (d)
10	5.45 (for **11e**, 1H, m)	127.8 (d)
	5.59 (for **11g**, 1H, m)	135.5 (d)
	6.92 (for **11f**, 1H, m)	150.7 (d)
11	2.14 (for **11e**, 2H, m)	41.6 (t)
	5.40 (for **11g**, 1H, m)	134.7 (d)
	6.13 (for **11f**, 1H, m)	131.7 (d)
12	3.52 (for **11e**, 1H, m)	72.9 (d)
	3.94 (for **11g**, 1H, m)	73.9 (d)
	-	n.d.
13	1.37 (for **11e**, 2H, m)	37.8 (t)
	1.47 (for **11g**, 2H, m)	37.8 (t)
	2.58 (for **11f**, 2H, m)	40.7 (t)
14	1.43 – 1.52 (3×2H, m)	23.9 (t)
15	1.31 - 1.34 (3×2H, m)	28.9 (t)
16	1.31 - 1.34 (3×2H, m)	30.0 – 31.0 (t)
17	1.31 - 1.34 (3×2H, m)	33.0 (t)
18	1.31 - 1.34 (3×2H, m)	23.8 (t)
19	0.90 (3×3H, t, *J* = 6.9 Hz)	14.6 (q)
1′	-	175.3 (s)
2′	4.37 (3×1H, dd, *J* = 8.8, 5.0 Hz)	53.6 (d)
3′a	1.94 (3×1H, m)	28.9 (t)
3′b	2.16 (3×1H, m)	
4′	2.32 (3×2H, m)	33.2 (t)
5′	-	176.52 (s)

7. List of figures

8. List of tables

9. References

[1] D. J. Ballhorn, S. Kautz, M. Heil, and A. D. Hegeman, "Analyzing plant defenses in nature," *Plant Signaling & Behavior*, vol. 4, no. 8, pp. 743–745, Aug. 2009, doi: 10.4161/psb.4.8.9088.

[2] C. E. Lovelock, M. C. Ball, K. C. Martin, and I. C. Feller, "Nutrient enrichment increases mortality of mangroves," *PLOS ONE*, vol. 4, no. 5, p. e5600, May 2009, doi: 10.1371/journal.pone.0005600.

[3] A. Mithöfer and W. Boland, "Plant defense against herbivores: Chemical aspects," *Annual Review of Plant Biology*, vol. 63, no. 1, pp. 431–450, 2012, doi: 10.1146/annurev-arplant-042110-103854.

[4] P. W. Lucas, I. M. Turner, N. J. Dominy, and N. Yamashita, "Mechanical defences to herbivory," *Annals of Botany*, vol. 86, no. 5, pp. 913–920, Nov. 2000, doi: 10.1006/anbo.2000.1261.

[5] B. Freeman and G. Beattie, "An overview of plant defenses against pathogens and herbivores," 2008, doi: 10.1094/PHI-I-2008-0226-01.

[6] E. Pichersky and E. Lewinsohn, "Convergent evolution in plant specialized metabolism," *Annual Review of Plant Biology*, vol. 62, no. 1, pp. 549–566, 2011, doi: 10.1146/annurev-arplant-042110-103814.

[7] U. Wittstock and J. Gershenzon, "Constitutive plant toxins and their role in defense against herbivores and pathogens," *Current Opinion in Plant Biology*, vol. 5, no. 4, pp. 300–307, Aug. 2002, doi: 10.1016/s1369-5266(02)00264-9.

[8] U. Wittstock, K. H. Lichtnow, and E. Teuscher, "Effects of cicutoxin and related polyacetylenes from *Cicuta virosa* on neuronal action potentials: A comparative study on the mechanism of the convulsive action," *Planta Medica*, vol. 63, no. 2, pp. 120–124, Apr. 1997, doi: 10.1055/s-2006-957626.

[9] P. J. Facchini and V. De Luca, "Opium poppy and Madagascar periwinkle: Model non-model systems to investigate alkaloid biosynthesis in plants," *The Plant Journal*, vol. 54, no. 4, pp. 763–784, 2008, doi: 10.1111/j.1365-313X.2008.03438.x.

[10] A. Osbourn, "Saponins and plant defence — a soap story," *Trends in Plant Science*, vol. 1, no. 1, pp. 4–9, Jan. 1996, doi: 10.1016/S1360-1385(96)80016-1.

[11] W. F. Morris, M. B. Traw, and J. Bergelson, "On testing for a tradeoff between constitutive and induced resistance," *Oikos*, vol. 112, no. 1, pp. 102–110, 2006, doi: 10.1111/j.0030-1299.2006.14253.x.

[12] G. Arimura, C. Kost, and W. Boland, "Herbivore-induced, indirect plant defences," *Biochimica et Biophysica Acta (BBA) - Molecular and Cell Biology of Lipids*, vol. 1734, no. 2, pp. 91–111, May 2005, doi: 10.1016/j.bbalip.2005.03.001.

[13] N. Yoshinaga, "Physiological function and ecological aspects of fatty acid-amino acid conjugates in insects," *Bioscience, Biotechnology, and Biochemistry*, vol. 80, no. 7, pp. 1274–1282, Jul. 2016, doi: 10.1080/09168451.2016.1153956.

[14] M. Loivamäki, R. Mumm, M. Dicke, and J.-P. Schnitzler, "Isoprene interferes with the attraction of bodyguards by herbaceous plants," *Proceedings of the National Academy of Sciences of the United States of America*, vol. 105, no. 45, pp. 17430–17435, Nov. 2008, doi: 10.1073/pnas.0804488105.

[15] J. Laothawornkitkul, P. D. Nigel, C. E. Vickers, M. Possell, J. E. Taylor, P. M. Mullineaux, and N. C. Hewitt, "Isoprene emissions influence herbivore feeding decisions," *Plant, Cell & Environment*, vol. 31, no. 10, pp. 1410–1415, Oct. 2008, doi: 10.1111/j.1365-3040.2008.01849.x.

[16] H. Xu, D. Lybrand, S. Bennewitz, A. Tissier, R. L. Last, and E. Pichersky, "Production of trans-chrysanthemic acid, the monoterpene acid moiety of natural pyrethrin insecticides, in tomato fruit," *Metabolic Engineering*, vol. 47, pp. 271–278, May 2018, doi: 10.1016/j.ymben.2018.04.004.

[17] A. Aharoni, A. P. Giri, S. Deuerlein, F. Griepink, W.-J. de Kogel, F. W. A. Verstappen, H. A. Verhoeven, M. A. Jongsma, W. Schwab, and H. J. Bouwmeester, "Terpenoid metabolism in wild-type and transgenic *Arabidopsis* plants," *The Plant Cell*, vol. 15, no. 12, pp. 2866–2884, Dec. 2003, doi: 10.1105/tpc.016253.

[18] R. M. Van Poecke, M. A. Posthumus, and M. Dicke, "Herbivore-induced volatile production by *Arabidopsis thaliana* leads to attraction of the parasitoid *Cotesia rubecula*: Chemical, behavioral, and gene-expression analysis," *Journal of Chemical Ecology*, vol. 27, no. 10, pp. 1911–1928, Oct. 2001, doi: 10.1023/a:1012213116515.

[19] J. Fäldt, G. Arimura, J. Gershenzon, J. Takabayashi, and J. Bohlmann, "Functional identification of AtTPS03 as (*E*)-β-ocimene synthase: Monoterpene synthase catalyzing jasmonate- and wound-induced volatile formation in *Arabidopsis thaliana*," *Planta*, vol. 216, no. 5, pp. 745–751, Mar. 2003, doi: 10.1007/s00425-002-0924-0.

[20] G. Arimura, R. Ozawa, S. Kugimiya, J. Takabayashi, and J. Bohlmann, "Herbivore-induced defense response in a model legume. Two-spotted spider mites induce emission of (*E*)-β-ocimene and transcript accumulation of (*E*)-β-ocimene synthase in *Lotus japonicus*," *Plant Physiology*, vol. 135, no. 4, pp. 1976–1983, Aug. 2004, doi: 10.1104/pp.104.042929.

[21] K. Raffa and A. A. Berryman, "The role of host plant resistance in the colonization behavior and ecology of bark beetles (Coleoptera: Scolytidae)," *The Bark Beetles, Fuels, and Fire Bibliography*, vol. 53, Mar. 1983, doi: 10.2307/1942586.

[22] M. Phillips and R. Croteau, "Resin-based defenses in conifers," *Trends in Plant Science*, vol. 4, no. 5, pp. 184–190, May 1999, doi: 10.1016/s1360-1385(99)01401-6.

[23] A. Bhattacharya, P. Sood, and V. Citovsky, “The roles of plant phenolics in defence and communication during *Agrobacterium* and *Rhizobium* infection,” *Molecular Plant Pathology*, vol. 11, no. 5, pp. 705–719, 2010, doi: 10.1111/j.1364-3703.2010.00625.x.

[24] P. Thomas and M. B. Ravindra, “Shoot tip culture in mango: Influence of medium, genotype, explant factors, season and decontamination treatments on phenolic exudation, explant survival and axenic culture establishment,” *Journal of Horticultural Science*, vol. 72, no. 5, pp. 713–722, Jan. 1997, doi: 10.1080/14620316.1997.11515563.

[25] D. G. Lynn and M. Chang, “Phenolic signals in cohabitation: Implications for plant development,” *Annual Review of Plant Physiology and Plant Molecular Biology*, vol. 41, no. 1, pp. 497–526, 1990, doi: 10.1146/annurev.pp.41.060190.002433.

[26] I. I. Ozyigit, “Relation between explant age, total phenols and regeneration response in tissue cultured cotton (*Gossypium hirsutum* L.),” Jan. 2007.

[27] V. Lattanzio, V. M. T. Lattanzino, and A. Cardinali, “Role of phenolics in the resistance mechanisms of plants against fungal pathogens and insects,” vol. 661, pp. 23–67, Jan. 2006.

[28] M. N. Zaprometov, “The formation of phenolic compounds in plant cell and tissue cultures and the possibility of its regulation,” in *Advances in Cell Culture*, vol. 7, K. Maramorosch and G. H. Sato, Eds. Elsevier, 1989, pp. 201–260. doi: 10.1016/B978-0-12-007907-0.50014-1.

[29] V. I. Kefeli, M. V. Kalevitch, and B. Borsari, “Phenolic cycle in plants and environment,” *Journal of Cell and Molecular Biology*, p. 13, 2003.

[30] R. Dixon and N. Paiva, “Stress-induced phenylpropanoid metabolism,” *The Plant Cell*, vol. 7, no. 7, pp. 1085–1097, Jul. 1995.

[31] C. Clé, L. M. Hill, R. Niggeweg, C. R. Martin, Y. Guisez, E. Prinsen, and M. A. K. Jansen, “Modulation of chlorogenic acid biosynthesis in *Solanum lycopersicum;* consequences for phenolic accumulation and UV-tolerance,” *Phytochemistry*, vol. 69, no. 11, pp. 2149–2156, Aug. 2008, doi: 10.1016/j.phytochem.2008.04.024.

[32] G. W. Todd, A. Getahun, and D. C. Cress, “Resistance in Barley to the Greenbug, *Schizaphis graminum*. Toxicity of phenolic and flavonoid compounds and related substances.,” *Annals of the Entomological Society of America*, vol. 64, no. 3, pp. 718–722, May 1971, doi: 10.1093/aesa/64.3.718.

[33] L. J. Corcuera, “Biochemical basis for the resistance of barley to aphids,” *Phytochemistry*, vol. 33, no. 4, pp. 741–747, Jul. 1993, doi: 10.1016/0031-9422(93)85267-U.

[34] C. A. Elliger, B. C. Chan, and A. C. Waiss, “Flavonoids as larval growth inhibitors,” *Naturwissenschaften*, vol. 67, no. 7, pp. 358–360, Jul. 1980, doi: 10.1007/BF01106595.

[35] M. S. J. Simmonds, “Flavonoid–insect interactions: Recent advances in our knowledge,” *Phytochemistry*, vol. 64, no. 1, pp. 21–30, Sep. 2003, doi: 10.1016/S0031-9422(03)00293-0.

[36] I. Castellanos and F. J. Espinosa-García, “Plant secondary metabolite diversity as a resistance trait against insects: a test with *Sitophilus granarius* (Coleoptera: Curculionidae) and seed

secondary metabolites," *Biochemical Systematics and Ecology*, vol. 25, no. 7, pp. 591–602, Oct. 1997, doi: 10.1016/S0305-1978(97)00045-8.

[37] J. B. Harborne, "Twenty-five years of chemical ecology," *Natural Product Reports*, vol. 18, no. 4, pp. 361–379, Jan. 2001, doi: 10.1039/B005311M.

[38] A. Urbanska, W. F. Tjallingii, A. F. G. Dixon, and B. Leszczynski, "Phenol oxidising enzymes in the grain aphid's saliva," *Entomologia Experimentalis et Applicata*, vol. 86, no. 2, pp. 197–203, 1998, doi: 10.1046/j.1570-7458.1998.00281.x.

[39] C. P. Constabel, L. Yip, J. J. Patton, and M. E. Christopher, "Polyphenol oxidase from hybrid poplar. Cloning and expression in response to wounding and herbivory.," *Plant Physiology*, vol. 124, no. 1, pp. 285–296, Sep. 2000, doi: 10.1104/pp.124.1.285.

[40] M. Haruta, J. A. Pedersen, and C. P. Constabel, "Polyphenol oxidase and herbivore defense in trembling aspen (*Populus tremuloides*): cDNA cloning, expression, and potential substrates," *Physiologia Plantarum*, vol. 112, no. 4, pp. 552–558, 2001, doi: 10.1034/j.1399-3054.2001.1120413.x.

[41] S. Bhambhani, K. R. Kondhare, and A. P. Giri, "Diversity in chemical structures and biological properties of plant alkaloids," *Molecules*, vol. 26, no. 11, Art. no. 11, Jan. 2021, doi: 10.3390/molecules26113374.

[42] L. Bush and F. F. Fannin, "Alkaloids," in *Tall Fescue for the Twenty-first Century*, John Wiley & Sons, Ltd, 2009, pp. 229–249. doi: 10.2134/agronmonogr53.c13.

[43] M. Morita, N. Shitan, K. Sawada, M. C. E. Van Montagu, D. Inzé, H. Rischer, A. Goossens, K.-M. Oksman-Caldentey, Y. Moriyama, and K. Yazaki, "Vacuolar transport of nicotine is mediated by a multidrug and toxic compound extrusion (MATE) transporter in *Nicotiana tabacum*," *Proceedings of the National Academy of Sciences of the United States of America*, vol. 106, no. 7, pp. 2447–2452, Feb. 2009, doi: 10.1073/pnas.0812512106.

[44] S. B. Soloway, "Naturally occurring insecticides," *Environmental Health Perspectives*, vol. 14, pp. 109–117, Apr. 1976, doi: 10.1289/ehp.7614109.

[45] D. B. Sattelle, "Acetylcholine receptors of insects," in *Advances in Insect Physiology*, vol. 15, M. J. Berridge, J. E. Treherne, and V. B. Wigglesworth, Eds. Academic Press, 1980, pp. 215–315. doi: 10.1016/S0065-2806(08)60142-3.

[46] J. A. Nathanson, "Caffeine and related methylxanthines: Possible naturally occurring pesticides," *Science (New York, N.Y.)*, vol. 226, no. 4671, pp. 184–187, Oct. 1984, doi: 10.1126/science.6207592.

[47] Y.-S. Kim, Y.-E. Choi, and H. Sano, "Plant vaccination: Stimulation of defense system by caffeine production in planta," *Plant Signaling & Behavior*, vol. 5, no. 5, pp. 489–493, May 2010, doi: 10.4161/psb.11087.

[48] T. Hartmann, “Plant-derived secondary metabolites as defensive chemicals in herbivorous insects: A case study in chemical ecology,” *Planta*, vol. 219, no. 1, pp. 1–4, May 2004, doi: 10.1007/s00425-004-1249-y.

[49] H. T. Alborn, T. C. J. Turlings, T. H. Jones, G. Stenhagen, J. H. Loughrin, and J. H. Tumlinson, “An elicitor of plant volatiles from beet armyworm oral secretion,” *Science*, May 1997, doi: 10.1126/science.276.5314.945.

[50] T. C. J. Turlings, P. J. McCall, H. T. Alborn, and J. H. Tumlinson, “An elicitor in caterpillar oral secretions that induces corn seedlings to emit chemical signals attractive to parasitic wasps,” *Journal of Chemical Ecology*, vol. 19, no. 3, pp. 411–425, Mar. 1993, doi: 10.1007/BF00994314.

[51] T. C. J. Turlings, J. H. Tumlinson, and W. J. Lewis, “Exploitation of herbivore-induced plant odors by host-seeking parasitic wasps,” *Science*, Nov. 1990, doi: 10.1126/science.250.4985.1251.

[52] H. T. Alborn, T. H. Jones, G. S. Stenhagen, and J. H. Tumlinson, “Identification and synthesis of volicitin and related components from beet armyworm oral secretions,” *Journal of Chemical Ecology*, vol. 26, no. 1, pp. 203–220, Jan. 2000, doi: 10.1023/A:1005401814122.

[53] N. Yoshinaga, C. Ishikawa, I. Seidl-Adams, E. Bosak, T. Aboshi, J. Tumlinson, and N. Mori, “*N*-(18-Hydroxylinolenoyl)-L-lutamine: A newly discovered analog of volicitin in *Manduca sexta* and its elicitor activity in plants,” *Journal of chemical ecology*, vol. 40, May 2014, doi: 10.1007/s10886-014-0436-y.

[54] G. Pohnert, V. Jung, E. Haukioja, K. Lempa, and W. Boland, “New fatty acid amides from regurgitant of Lepidopteran (Noctuidae, Geometridae) caterpillars,” *Tetrahedron*, vol. 55, no. 37, pp. 11275–11280, Sep. 1999, doi: 10.1016/S0040-4020(99)00639-0.

[55] J. C. Sheehan, J. Preston, and P. A. Cruickshank, “A rapid synthesis of oligopeptide derivatives without isolation of intermediates,” *Journal of the American Chemical Society*, vol. 87, no. 11, pp. 2492–2493, Jun. 1965, doi: 10.1021/ja01089a034.

[56] S. Itoh, S. Kuwahara, M. Hasegawa, and O. Kodama, “Synthesis of the (17R)- and (17S)-isomers of volicitin, an elicitor of plant volatiles contained in the oral secretion of the beet armyworm,” *Bioscience, Biotechnology, and Biochemistry*, vol. 66, no. 7, pp. 1591–1596, Jan. 2002, doi: 10.1271/bbb.66.1591.

[57] G. Pohnert, T. Koch, and W. Boland, “Synthesis of volicitin: A novel three-component Wittig approach to chiral 17-hydroxylinolenic acid,” *Chemical Communications*, no. 12, pp. 1087–1088, Jan. 1999, doi: 10.1039/A902020I.

[58] P. Verma, A. K. Mathur, and K. Shanker, “Enhanced vincamine production in selected tryptophan-overproducing shoots of *Vinca minor*,” *Plant Cell, Tissue and Organ Culture (PCTOC)*, vol. 111, no. 2, pp. 239–245, Nov. 2012, doi: 10.1007/s11240-012-0185-y.

[59] N. Tanaka, M. Takao, and T. Matsumoto, “Vincamine production in multiple shoot culture derived from hairy roots of *Vinca minor*,” *Plant Cell, Tissue and Organ Culture*, vol. 41, no. 1, pp. 61–64, Apr. 1995, doi: 10.1007/BF00124087.

[60] F. Fard, A. Moieni, and R. Omidbaigi, “Effects of different concentrations of α-naphthaleneacetic acid and 6-benzylaminopurine on shoot regeneration of *Vinca minor* L.,” *Journal of Agricultural Science and Technology (JAST)*, 2008.

[61] J. Murata, J. Roepke, H. Gordon, and V. De Luca, “The leaf epidermome of *Catharanthus roseus* reveals its biochemical specialization,” *The Plant Cell*, vol. 20, no. 3, pp. 524–542, Mar. 2008, doi: 10.1105/tpc.107.056630.

[62] J. Murata and V. D. Luca, “Localization of tabersonine 16-hydroxylase and 16-OH tabersonine-16-*O*-methyltransferase to leaf epidermal cells defines them as a major site of precursor biosynthesis in the vindoline pathway in *Catharanthus roseus*,” *The Plant Journal*, vol. 44, no. 4, pp. 581–594, 2005, doi: 10.1111/j.1365-313X.2005.02557.x.

[63] D. Levac, J. Murata, W. S. Kim, and V. De Luca, “Application of carborundum abrasion for investigating the leaf epidermis: Molecular cloning of *Catharanthus roseus* 16-hydroxytabersonine-16-*O*-methyltransferase,” *The Plant Journal*, vol. 53, no. 2, pp. 225–236, 2008, doi: 10.1111/j.1365-313X.2007.03337.x.

[64] B. Proksa and E. Grossmann, “High performance liquid chromatographic determination of alkaloids from *Vinca minor* L.,” *Phytochemical Analysis*, vol. 2, no. 2, pp. 74–76, 1991, doi: 10.1002/pca.2800020206.

[65] K. Miettinen, L. Dong, N. Navrot, T. Schneider, V. Burlat, J. Pollier, L. Woittiez, S. van der Krol, R. Lugan, T. Ilc, R. Verpoorte, K.-M. Oksman-Caldentey, E. Martinoia, H. Bouwmeester, A. Goossens, J. Memelink, and D. Werck-Reichhart, “The seco-iridoid pathway from *Catharanthus roseus*,” *Nature Communications*, vol. 5, no. 1, p. 3606, Apr. 2014, doi: 10.1038/ncomms4606.

[66] V. Tzin and G. Galili, “The biosynthetic pathways for shikimate and aromatic amino acids in *Arabidopsis thaliana*,” *The Arabidopsis Book / American Society of Plant Biologists*, vol. 8, p. e0132, May 2010, doi: 10.1199/tab.0132.

[67] K. M. Herrmann, “The shikimate pathway as an entry to aromatic secondary metabolism,” *Plant Physiology*, vol. 107, no. 1, pp. 7–12, Jan. 1995.

[68] E. A. Stander, L. J. Sepúlveda, T. Dugé de Bernonville, I. Carqueijeiro, K. Koudounas, P. Lemos Cruz, S. Besseau, A. Lanoue, N. Papon, N. Giglioli-Guivarc’h, R. Dirks, S. E. O’Connor, L. Atehortùa, A. Oudin, and V. Courdavault, “Identifying genes involved in alkaloid biosynthesis in *Vinca minor* through transcriptomics and gene co-expression analysis,” *Biomolecules*, vol. 10, no. 12, Art. no. 12, Dec. 2020, doi: 10.3390/biom10121595.

[69] P. Verma, A. K. Mathur, N. Masood, S. Luqman, and K. Shanker, “Tryptophan over-producing cell suspensions of *Catharanthus roseus* (L) G. Don and their up-scaling in stirred tank

bioreactor: Detection of a phenolic compound with antioxidant potential," *Protoplasma*, vol. 250, no. 1, pp. 371–380, Feb. 2013, doi: 10.1007/s00709-012-0423-5.

[70] F. Kellner, F. Geu-Flores, N. H. Sherden, S. Brown, E. Foureau, V. Courdavault, and S. E. O'Connor, "Discovery of a P450-catalyzed step in vindoline biosynthesis: A link between the aspidosperma and eburnamine alkaloids," *Chemical Communications*, vol. 51, no. 36, pp. 7626–7628, Apr. 2015, doi: 10.1039/C5CC01309G.

[71] P. Verma, N. Singh, S. A. Khan, A. K. Mathur, A. Sharma, and F. Jamal, "TIAs pathway genes and associated miRNA identification in *Vinca minor*: Supporting aspidosperma and eburnamine alkaloids linkage via transcriptomic analysis," *Physiology and Molecular Biology of Plants*, vol. 26, no. 8, pp. 1695–1711, Aug. 2020, doi: 10.1007/s12298-020-00842-x.

[72] T. Dugé de Bernonville, I. Carqueijeiro, A. Lanoue, F. Lafontaine, P. Sánchez Bel, F. Liesecke, K. Musset, A. Oudin, G. Glévarec, O. Pichon, S. Besseau, M. Clastre, B. St-Pierre, V. Flors, S. Maury, E. Huguet, S. E. O'Connor, and V. Courdavault, "Folivory elicits a strong defense reaction in *Catharanthus roseus*: Metabolomic and transcriptomic analyses reveal distinct local and systemic responses," *Scientific Reports*, vol. 7, no. 1, p. 40453, Jan. 2017, doi: 10.1038/srep40453.

[73] V. J. Nikiforova, M. Bielecka, B. Gakière, S. Krueger, J. Rinder, S. Kempa, R. Morcuende, W.-R. Scheible, H. Hesse, and R. Hoefgen "Effect of sulfur availability on the integrity of amino acid biosynthesis in plants," *Amino Acids*, vol. 30, no. 2, pp. 173–183, Mar. 2006, doi: 10.1007/s00726-005-0251-4.

[74] X. Guo, L. Yang, J. Yu, Z. Tang, and Y. Zu, "Alkaloid variations in *Catharanthus roseus* seedlings treated by different temperatures in short term and long term," *Journal of Forestry Research*, vol. 18, no. 4, pp. 313–315, Dec. 2007, doi: 10.1007/s11676-007-0063-3.

[75] Y. Liu, Q. Meng, X. Duan, Z. Zhang, and D. Li, "Effects of PEG-induced drought stress on regulation of indole alkaloid biosynthesis in *Catharanthus roseus*," *Journal of Plant Interactions*, vol. 12, no. 1, pp. 87–91, Jan. 2017, doi: 10.1080/17429145.2017.1293852.

[76] A. Dutta, J. Sen, and R. Deswal, "New evidences about strictosidine synthase (Str) regulation by salinity, cold stress and nitric oxide in *Catharanthus roseus*," *Journal of Plant Biochemistry and Biotechnology*, vol. 22, no. 1, pp. 124–131, Jan. 2013, doi: 10.1007/s13562-012-0118-1.

[77] R. J. Aerts, D. Gisi, E. De Carolis, V. De Luca, and T. W. Baumann, "Methyl jasmonate vapor increases the developmentally controlled synthesis of alkaloids in *Catharanthus* and *Cinchona* seedlings," *The Plant Journal*, vol. 5, no. 5, pp. 635–643, 1994, doi: 10.1111/j.1365-313X.1994.00635.x.

[78] P. Zhou, J. Yang, J. Zhu, S. He, W. Zhang, R. Yu, J. Zi, L. Song, and X. Huang, "Effects of β-cyclodextrin and methyl jasmonate on the production of vindoline, catharanthine, and ajmalicine in *Catharanthus roseus* cambial meristematic cell cultures," *Applied Microbiology*

and Biotechnology, vol. 99, no. 17, pp. 7035–7045, Sep. 2015, doi: 10.1007/s00253-015-6651-9.

[79] S. K. Raina, D. P. Wankhede, M. Jaggi, P. Singh, S. K. Jalmi, B. Raghuram, A. H. Sinha, and A. K. Sheikh, "CrMPK3, a mitogen activated protein kinase from *Catharanthus roseus* and its possible role in stress induced biosynthesis of monoterpenoid indole alkaloids," *BMC Plant Biology*, vol. 12, no. 1, p. 134, Aug. 2012, doi: 10.1186/1471-2229-12-134.

[80] A. A. AL-Huqail and E. F. Ali, "Effect of jasmonic acid on alkaloids content and salinity tolerance of *Catharanthus roseus* based on morpho-physiological evaluation," *South African Journal of Botany*, vol. 141, pp. 440–446, Sep. 2021, doi: 10.1016/j.sajb.2021.05.029.

[81] R. L. Lindroth and S.-Y. Hwang, "Clonal variation in foliar chemistry of quaking aspen (*Populus tremuloides* Michx.)," *Biochemical Systematics and Ecology*, vol. 24, no. 5, pp. 357–364, Jul. 1996, doi: 10.1016/0305-1978(96)00043-9.

[82] I. N. Abreu, M. Ahnlund, T. Moritz, and B. R. Albrectsen, "UHPLC-ESI/TOFMS determination of salicylate-like phenolic glycosides in *Populus tremula* leaves," *Journal of Chemical Ecology*, vol. 37, no. 8, p. 857, Jul. 2011, doi: 10.1007/s10886-011-9991-7.

[83] C. Fellenberg, O. Corea, L.-H. Yan, F. Archinuk, E.-M. Piirtola, H. Gordon, M. Reichelt, W. Brandt, J. Wulff, J., Ehlting, and C. Peter Constabel, "Discovery of salicyl benzoate UDP-glycosyltransferase, a central enzyme in poplar salicinoid phenolic glycoside biosynthesis," *The Plant Journal*, vol. 102, no. 1, pp. 99–115, 2020, doi: 10.1111/tpj.14615.

[84] G. A. Boeckler, J. Gershenzon, and S. B. Unsicker, "Phenolic glycosides of the Salicaceae and their role as anti-herbivore defenses," *Phytochemistry*, vol. 72, no. 13, pp. 1497–1509, Sep. 2011, doi: 10.1016/j.phytochem.2011.01.038.

[85] T. P. Clausen, P. B. Reichardt, J. P. Bryant, R. A. Werner, K. Post, and K. Frisby, "Chemical model for short-term induction in quaking aspen (*Populus tremuloides*) foliage against herbivores," *Journal of Chemical Ecology*, vol. 15, no. 9, pp. 2335–2346, Sep. 1989, doi: 10.1007/BF01012085.

[86] I. A. Pearl and S. F. Darling, "The structures of salicortin and tremulacin," *Phytochemistry*, vol. 10, no. 12, pp. 3161–3166, Dec. 1971, doi: 10.1016/S0031-9422(00)97369-2.

[87] T. Ruuhola, R. Julkunen-Tiitto, and P. Vainiotalo, "In vitro degradation of willow salicylates," *Journal of Chemical Ecology*, vol. 29, no. 5, pp. 1083–1097, May 2003, doi: 10.1023/A:1023821304656.

[88] R. N. Philippe and J. Bohlmann, "Poplar defense against insect herbivores," *Canadian Journal of Botany*, vol. 85, no. 12, pp. 1111–1126, Dec. 2007, doi: 10.1139/B07-109.

[89] R. T. Palo, "Distribution of birch (*Betula* SPP.), willow (*Salix* SPP.), and poplar (*Populus* SPP.) secondary metabolites and their potential role as chemical defense against herbivores," *Journal of Chemical Ecology*, vol. 10, no. 3, pp. 499–520, Mar. 1984, doi: 10.1007/BF00988096.

[90] W. Greenaway, S. English, J. May, and F. R. Whatley, “Chemotaxonomy of section *Leuce* poplars by GC-MS of bud exudate,” *Biochemical Systematics and Ecology*, vol. 19, no. 6, pp. 507–518, Jan. 1991, doi: 10.1016/0305-1978(91)90071-7.

[91] T. Osier and R. Lindroth, “Long-term effects of defoliation on quaking aspen in relation to genotype and nutrient availability: Plant growth, phytochemistry and insect performance,” *Oecologia*, vol. 139, pp. 55–65, Apr. 2004, doi: 10.1007/s00442-003-1481-3.

[92] T. L. Osier and R. L. Lindroth, “Genotype and environment determine allocation to and costs of resistance in quaking aspen,” *Oecologia*, vol. 148, no. 2, pp. 293–303, Jun. 2006, doi: 10.1007/s00442-006-0373-8.

[93] M. T. Stevens and R. L. Lindroth, “Induced resistance in the indeterminate growth of aspen (*Populus tremuloides*),” *Oecologia*, vol. 145, no. 2, pp. 297–305, Sep. 2005, doi: 10.1007/s00442-005-0128-y.

[94] I. T. Major and C. P. Constabel, “Molecular analysis of poplar defense against herbivory: Comparison of wound- and insect elicitor-induced gene expression,” *New Phytologist*, vol. 172, no. 4, pp. 617–635, 2006, doi: 10.1111/j.1469-8137.2006.01877.x.

[95] T. L. Osier, S. Y. Hwang, and R. L. Lindroth, “Effects of phytochemical variation in quaking aspen *Populus tremuloides* clones on gypsy moth *Lymantria dispar* performance in the field and laboratory.,” *Ecological Entomology*, vol. 25, no. 2, pp. 197–207, 2000.

[96] A. T. Szeredi, “Investigation of chemical defenses of plants against herbivore-produced elicitors,” *Master´s thesis*, Vienna, Austria, 2021.

[97] J. Clayden, Ed., *Organic chemistry*. Oxford ; New York: Oxford University Press, 2001.

[98] F. A. Carey and R. J. Sundberg, *Advanced organic chemistry*, 5th ed. New York: Springer, 2007.

[99] J. O. Metzger and U. Biermann, “Alkylaluminium dichloride induced Friedel-Crafts acylation of unsaturated carboxylic acids and alcohols,” *Liebigs Annalen der Chemie*, vol. 1993, no. 6, pp. 645–650, 1993, doi: 10.1002/jlac.1993199301105.

[100] K. P. C. Vollhardt and N. E. Schore, *Organische Chemie. Hauptbd.*, 5. Aufl. Weinheim: Wiley-VCH, 2011.

[101] R. A. Valiulin, *Organic chemistry: 100 must-know mechanisms*. Berlin ; Boston: Walter de Gruyter GmbH, 2020.

[102] K. Bowden, I. M. Heilbron, E. R. H. Jones, and B. C. L. Weedon, “13. Researches on acetylenic compounds. Part I. The preparation of acetylenic ketones by oxidation of acetylenic carbinols and glycols,” *Journal of the Chemical Society (Resumed)*, no. 0, pp. 39–45, Jan. 1946, doi: 10.1039/JR9460000039.

[103] A. M. Pembere and Z. Luo, “Jones oxidation of glycerol catalysed by small gold clusters,” *Physical Chemistry Chemical Physics*, vol. 19, no. 9, pp. 6620–6625, 2017, doi: 10.1039/C6CP07941E.

[104] J. A. Soderquist and K. L. Thompson, “The oxymercuration-demercuration of alkenylsilanes in aqueous tetrahydrofuran,” *Journal of Organometallic Chemistry*, vol. 159, no. 3, pp. 237–249, Oct. 1978, doi: 10.1016/S0022-328X(00)93802-6.

[105] H. C. Brown and P. J. Geoghegan, “Solvomercuration-demercuration. I. Oxymercuration-demercuration of representative olefins in an aqueous system. Mild procedure for the Markovnikov hydration of the carbon-carbon double bond,” *The Journal of Organic Chemistry*, vol. 35, no. 6, pp. 1844–1850, Jun. 1970, doi: 10.1021/jo00831a028.

[106] M. Elyashberg, “Identification and structure elucidation by NMR spectroscopy,” *TrAC Trends in Analytical Chemistry*, vol. 69, pp. 88–97, Jun. 2015, doi: 10.1016/j.trac.2015.02.014.

[107] N. E. Jacobsen, *NMR spectroscopy explained: simplified theory, applications and examples for organic chemistry and structural biology*. Hoboken, N.J: Wiley-Interscience, 2007.

[108] J. Keeler, *Understanding NMR spectroscopy*. Chichester, England ; Hoboken, NJ: Wiley, 2005.

[109] R. R. Ernst and W. A. Anderson, “Application of fourier transform spectroscopy to magnetic resonance,” *Review of Scientific Instruments*, vol. 37, no. 1, pp. 93–102, Jan. 1966, doi: 10.1063/1.1719961.

[110] W. P. Aue, E. Bartholdi, and R. R. Ernst, “Two-dimensional spectroscopy. Application to nuclear magnetic resonance,” *The Journal of Chemical Physics*, vol. 64, no. 5, pp. 2229–2246, Mar. 1976, doi: 10.1063/1.432450.

[111] E. de Hoffmann and V. Stroobant, *Mass spectrometry: principles and applications*, 3rd ed. Chichester, West Sussex, England; Hoboken, NJ: J. Wiley, 2007.

[112] N. L. Stock, “Introducing graduate students to High-Resolution Mass Spectrometry (HRMS) using a hands-on approach,” *Journal of Chemical Education*, vol. 94, no. 12, pp. 1978–1982, Dec. 2017, doi: 10.1021/acs.jchemed.7b00569.

[113] J. H. Gross, *Mass spectrometry: A textbook*, 3rd edition. New York, NY: Springer Berlin Heidelberg, 2017.

[114] J. W. Robinson, E. M. Skelly Frame, and G. M. Frame II, *Undergraduate instrumental analysis*. New York, N.Y.: Dekker, 2005.

[115] F. Hufsky and S. Böcker, “Mining molecular structure databases: Identification of small molecules based on fragmentation mass spectrometry data: MINING MOLECULAR STRUCTURE DATABASES,” *Mass Spectrometry Reviews*, vol. 36, no. 5, pp. 624–633, Sep. 2017, doi: 10.1002/mas.21489.

[116] F. Lemière, “Interfaces for LC–MS,” *Guide to LC–MS*, University of Antwerp, Belgium, Dec. 2001.

[117] J. T. Watson and O. D. Sparkman, *Introduction to mass spectrometry: Instrumentation, applications and strategies for data interpretation*, 4th ed. Chichester, England ; Hoboken, NJ: John Wiley & Sons, 2007.

[118] B. A. Mamyrin, “Laser assisted reflectron time-of-flight mass spectrometry,” *International Journal of Mass Spectrometry and Ion Processes*, vol. 131, pp. 1–19, Feb. 1994, doi: 10.1016/0168-1176(93)03891-O.

[119] P. E. Miller and M. B. Denton, “The quadrupole mass filter: Basic operating concepts,” *Journal of Chemical Education*, vol. 63, no. 7, p. 617, Jul. 1986, doi: 10.1021/ed063p617.

[120] J. V. Johnson, R. A. Yost, P. E. Kelley, and D. C. Bradford, “Tandem-in-space and tandem-in-time mass spectrometry: Triple quadrupoles and quadrupole ion traps,” *Analytical Chemistry*, vol. 62, no. 20, pp. 2162–2172, Oct. 1990, doi: 10.1021/ac00219a003.

[121] M. Smoluch, G. Grasso, P. Suder, and J. Silberring, Eds., *Mass Spectrometry: An applied approach*, 1st ed. Wiley, 2019. doi: 10.1002/9781119377368.

[122] J. H. Gross, *Massenspektrometrie: Spektroskopiekurs kompakt*. Berlin: Springer Spektrum, 2019. doi: 10.1007/978-3-662-58635-8.

[123] L. S. Ettre, “Chromatography: The separation technique of the 20th century,” *Chromatographia*, vol. 51, no. 1–2, pp. 7–17, Jan. 2000, doi: 10.1007/BF02490689.

[124] M. W. Dong, *Modern HPLC for practicing scientists*. Hoboken, N.J: Wiley-Interscience, 2006.

[125] M. C. McMaster, *LC/MS: A practical user’s guide*. Hoboken, N.J: John Wiley, 2005.

[126] R. Majors, “Developments in HPLC column packing design,” *LCGC North America*, vol. 24, Apr. 2006.

[127] F. Gritti and G. Guiochon, “The van Deemter equation: Assumptions, limits, and adjustment to modern high performance liquid chromatography,” *Journal of Chromatography A*, vol. 1302, pp. 1–13, Aug. 2013, doi: 10.1016/j.chroma.2013.06.032.

[128] M. C. McMaster, *HPLC, a practical user’s guide*, 2nd ed. Hoboken, N.J: Wiley-Interscience, 2007.

[129] M. R. Siddiqui, Z. A. AlOthman, and N. Rahman, “Analytical techniques in pharmaceutical analysis: A review,” *Arabian Journal of Chemistry*, vol. 10, pp. S1409–S1421, Feb. 2017, doi: 10.1016/j.arabjc.2013.04.016.

[130] D. J. Fox, J. Reckless, S. G. Warren, and D. J. Grainger, “Design, synthesis, and preliminary pharmacological evaluation of *N*-acyl-3-aminoglutarimides as broad-spectrum chemokine inhibitors in vitro and anti-inflammatory agents in vivo,” *Journal of Medicinal Chemistry*, vol. 45, no. 2, pp. 360–370, Jan. 2002, doi: 10.1021/jm010984i.

[131] A. Kruve, K. Kaupmees, J. Liigand, M. Oss, and I. Leito, “Sodium adduct formation efficiency in ESI source,” *Journal of Mass Spectrometry*, vol. 48, no. 6, pp. 695–702, 2013, doi: 10.1002/jms.3218.

[132] A. Kruve and K. Kaupmees, “Adduct formation in ESI/MS by mobile phase additives,” *Journal of The American Society for Mass Spectrometry*, vol. 28, no. 5, pp. 887–894, May 2017, doi: 10.1007/s13361-017-1626-y.

[133] S. Ghosh, P. Challamalla, and D. Banji, “Negative ion mode mass spectrometry- an overview,” *Journal of Chemical, Biological and Physical Sciences*, vol. 2, pp. 1462–1471, May 2012.

[134] A. J. Tsetegho Sokeng, A. P. Sobolev, A. Di Lorenzo, J. Xiao, L. Mannina, D. Capitani, and M. Daglia, “Metabolite characterization of powdered fruits and leaves from *Adansonia digitata* L. (baobab): A multi-methodological approach,” *Food Chemistry*, vol. 272, pp. 93–108, Jan. 2019, doi: 10.1016/j.foodchem.2018.08.030.

[135] D. A. S. Grahame, C. Olauson, R. H. Lam, T. Pedersen, F. Borondics, S. Abraham, R. G. Weiss, and M. A. Rogers, “Influence of chirality on the modes of self-assembly of 12-hydroxystearic acid in molecular gels of mineral oil,” *Soft Matter*, vol. 7, no. 16, p. 7359, 2011, doi: 10.1039/c1sm05757j.

[136] L. Boyadzhiev, D. Mecheva, and B. Yordanov, “Extraction of vincamine from periwinkle (*Vinca minor* L.): I. Obtaining of total extract,” *Comptes Rendus de l’Academie Bulgare des Sciences*, vol. 55, p. 49, Jan. 2002.

[137] A. Akhgari, I. Laakso, T. Seppänen-Laakso, T. Yrjönen, H. Vuorela, K.-M. Oksman-Caldentey, and H. Rischer, “Analysis of indole alkaloids from *Rhazya stricta* hairy roots by Ultra-Performance Liquid Chromatography-Mass Spectrometry,” *Molecules*, vol. 20, no. 12, pp. 22621–22634, Dec. 2015, doi: 10.3390/molecules201219873.

[138] S. Kumar, A. Singh, V. Bajpai, M. Srivastava, B. P. Singh, S. Ojha, and B. Kumar, “Simultaneous determination of bioactive monoterpene indole alkaloids in ethanolic extract of seven *Rauvolfia* species using UHPLC with hybrid triple quadrupole linear ion trap mass spectrometry: Phytochemical analysis of Rauvolfia species,” *Phytochemical Analysis*, vol. 27, no. 5, pp. 296–303, Sep. 2016, doi: 10.1002/pca.2631.

[139] S. A. A. Abouzeid, “Modulation of indole alkaloid composition in *Vinca minor*,” Dissertation, Technische Universität Carolo-Wilhelmina zu Braunschweig, Braunschweig, Germany, 2018.

[140] I. Mathe, “Effect of shade on the total alkaloid and vincamine contents of *Vinca minor*,” *Herba Hungarica*, pp. 47–60, 1965.

[141] F. Kaczmarek and J. Lutomski, “Alkaloid content in *Vinca minor* during growth,” *Farmacja Polska*, pp. 444–450, 1965.

[142] Y. Liu, B. Patra, S. K. Singh. P. Paul, Y. Zhou, Y. Li, Y. Wang, S. Pattanaik, and L. Yuan, “Terpenoid indole alkaloid biosynthesis in *Catharanthus roseus*: Effects and prospects of environmental factors in metabolic engineering,” *Biotechnology Letters*, vol. 43, no. 11, pp. 2085–2103, Nov. 2021, doi: 10.1007/s10529-021-03179-x.

[143] B. Thines, L. Katsir, M. Melotto, Y. Niu, A. Mandaokar, G. Liu, K. Nomura, S. Y. He, G. A. Howe, and J. Browse, “JAZ repressor proteins are targets of the SCF^{COI1} complex during jasmonate signalling,” *Nature*, vol. 448, no. 7154, pp. 661–665, Aug. 2007, doi: 10.1038/nature05960.

[144] G. A. Howe, “Metabolic end run to jasmonate,” *Nature Chemical Biology*, vol. 14, no. 2, Art. no. 2, Feb. 2018, doi: 10.1038/nchembio.2553.

[145] C. Delker, I. Stenzel, B. Hause, O. Miersch, I. Feussner, and C. Wasternack, “Jasmonate biosynthesis in *Arabidopsis thaliana*-enzymes, products, regulation,” *Plant Biology (Stuttgart, Germany)*, vol. 8, no. 3, pp. 297–306, May 2006, doi: 10.1055/s-2006-923935.

[146] S. Wei, “Methyl jasmonic acid induced expression pattern of terpenoid indole alkaloid pathway genes in *Catharanthus roseus* seedlings,” *Plant Growth Regulation*, vol. 61, no. 3, pp. 243–251, Jul. 2010, doi: 10.1007/s10725-010-9468-7.

[147] G. Montiel, A. Zarei, A. P. Körbes, and J. Memelink, “The jasmonate-responsive element from the ORCA3 promoter from *Catharanthus roseus* is active in Arabidopsis and is controlled by the transcription factor AtMYC2,” *Plant and Cell Physiology*, vol. 52, no. 3, pp. 578–587, Mar. 2011, doi: 10.1093/pcp/pcr016.

[148] K. Okada, H. Abe, and G. Arimura, “Jasmonates induce both defense responses and communication in Monocotyledonous and Dicotyledonous plants,” *Plant and Cell Physiology*, vol. 56, no. 1, pp. 16–27, Jan. 2015, doi: 10.1093/pcp/pcu158.

[149] Q. Pan, Y. Chen, Q. Wang, F. Yuan, S. Xing, Y. Tian, J. Zhao, X. Sun, and K. Tang, “Effect of plant growth regulators on the biosynthesis of vinblastine, vindoline and catharanthine in *Catharanthus roseus*,” *Plant Growth Regulation*, vol. 60, no. 2, pp. 133–141, Mar. 2010, doi: 10.1007/s10725-009-9429-1.

[150] S. Rodriguez, V. Compagnon, N. P. Crouch, B. St-Pierre, and V. De Luca, “Jasmonate-induced epoxidation of tabersonine by a cytochrome P-450 in hairy root cultures of *Catharanthus roseus*,” *Phytochemistry*, vol. 64, no. 2, pp. 401–409, Sep. 2003, doi: 10.1016/S0031-9422(03)00269-3.

[151] S. K. Rijhwani and J. V. Shanks, “Effect of elicitor dosage and exposure time on biosynthesis of indole alkaloids by *Catharanthus roseus* hairy root cultures,” *Biotechnology Progress*, vol. 14, no. 3, pp. 442–449, Jun. 1998, doi: 10.1021/bp980029v.

[152] S. Abouzeid, U. Beutling, and D. Selmar, “Stress-induced modification of indole alkaloids: Phytomodificines as a new category of specialized metabolites,” *Phytochemistry*, vol. 159, pp. 102–107, Mar. 2019, doi: 10.1016/j.phytochem.2018.12.015.

[153] K. Keefover-Ring, M. Ahnlund, I. N. Abreu, S. Jansson, T. Moritz, and B. R. Albrectsen, “No evidence of geographical structure of salicinoid chemotypes within *Populus tremula*,” *PLOS ONE*, vol. 9, no. 10, p. e107189, Oct. 2014, doi: 10.1371/journal.pone.0107189.

[154] B. J. Rehill, T. G. Whitham, G. D. Martinsen, J. A. Schweitzer, J. K. Bailey, and R. L. Lindroth, “Developmental trajectories in cottonwood phytochemistry,” *Journal of Chemical Ecology*, vol. 32, no. 10, pp. 2269–2285, Oct. 2006, doi: 10.1007/s10886-006-9141-9.

[155] N. Förster, C. Ulrichs, M. Zander, R. Kätzel, and I. Mewis, "Factors influencing the variability of antioxidative phenolic glycosides in *Salix* species," *Journal of Agricultural and Food Chemistry*, vol. 58, no. 14, pp. 8205–8210, Jul. 2010, doi: 10.1021/jf100887v.

[156] H. Thieme and R. Benecke, "Untersuchungen über die Glykosidakkumulation in einigen mitteleuropäischen *Populus*-Arten," *Pharmazie 26*, pp. 227–231, 1971.

[157] J. Tahvanainen, E. Helle, R. Julkunen-Tiitto, and A. Lavola, "Phenolic compounds of willow bark as deterrents against feeding by mountain hare," *Oecologia*, vol. 65, no. 3, pp. 319–323, Feb. 1985, doi: 10.1007/BF00378905.

[158] B. Young, D. Wagner, P. Doak, and T. Clausen, "Induction of phenolic glycosides by quaking aspen (*Populus tremuloides*) leaves in relation to extrafloral nectaries and epidermal leaf mining," *Journal of Chemical Ecology*, vol. 36, no. 4, pp. 369–377, Apr. 2010, doi: 10.1007/s10886-010-9763-9.

[159] M. J. Fields and C. M. Orians, "Specificity of phenolic glycoside induction in willow seedlings (*Salix sericea*) in response to herbivory," *Journal of Chemical Ecology*, vol. 32, no. 12, pp. 2647–2656, Dec. 2006, doi: 10.1007/s10886-006-9188-7.

[160] L. Bresadola, C. Caseys, S. Castiglione, C. A. Buerkle, D. Wegmann, and C. Lexer, "Admixture mapping in interspecific *Populus* hybrids identifies classes of genomic architectures for phytochemical, morphological and growth traits," *New Phytologist*, vol. 223, no. 4, pp. 2076–2089, Sep. 2019, doi: 10.1111/nph.15930.

[161] R. L. Lindroth, J. M. Scriber, and M. T. S. Hsia, "Chemical ecology of the tiger swallowtail: Mediation of host use by phenolic glycosides," *Ecology*, vol. 69, no. 3, pp. 814–822, 1988, doi: 10.2307/1941031.

[162] E. Fattorusso and O. Taglialatela-Scafati, *Modern alkaloids: structure, isolation, synthesis and biology*. Weinheim; Chichester: Wiley-VCH, 2008.

[163] J. Hemming and R. Lindroth, "Effects of light and nutrient availability on aspen: Growth, phytochemistry, and insect performance," *Journal of Chemical Ecology*, vol. 28, no. 7, pp. 1687–1714, Jan. 1999.

[164] J. R. Donaldson, E. L. Kruger, and R. L. Lindroth, "Competition- and resource-mediated tradeoffs between growth and defensive chemistry in trembling aspen (*Populus tremuloides*)," *New phytologist*, 2006.

[165] E. L. Kruger, K. Keefover-Ring, L. M. Holeski, and R. L. Lindroth, "To compete or defend: Linking functional trait variation with life-history tradeoffs in a foundation tree species," *Oecologia*, vol. 192, no. 4, pp. 893–907, Apr. 2020, doi: 10.1007/s00442-020-04622-y.